



THE UNIVERSITY OF
WAIKATO
Te Whare Wānanga o Waikato

Research Commons

<http://researchcommons.waikato.ac.nz/>

Research Commons at the University of Waikato

Copyright Statement:

The digital copy of this thesis is protected by the Copyright Act 1994 (New Zealand).

The thesis may be consulted by you, provided you comply with the provisions of the Act and the following conditions of use:

- Any use you make of these documents or images must be for research or private study purposes only, and you may not make them available to any other person.
- Authors control the copyright of their thesis. You will recognise the author's right to be identified as the author of the thesis, and due acknowledgement will be made to the author where appropriate.
- You will obtain the author's permission before publishing any material from the thesis.

Is There a Salty Solution to Sensitive Soil Sliding in the Bay of Plenty, New Zealand?

A thesis
submitted in partial fulfilment
of the requirements for the degree
of
Master of Science (Earth Sciences)
at
The University of Waikato
by
Thomas Robertson



THE UNIVERSITY OF
WAIKATO
Te Whare Wānanga o Waikato

2017

Abstract

Found globally, sensitive soils are widely regarded as a key cause of slope instability. These sensitive soils often contribute to the production of large retrogressive landslides that pose significant danger to a people and infrastructure. Within the Bay of Plenty region, sensitive soil based landslides are widespread and numerous Moun *et al* (1970) successfully trialled remediation of a sensitive soil landslide in Scandinavia by application of potassium chloride via leaching columns. The aim of this study is to determine whether salt treatment of sensitive soils formed in halloysite rich soils of the Bay of Plenty provides a viable means of improving soil behaviour.

Soil collected from the base of the landslide at Bramley Drive, Omokoroa, was treated with 3 differing potassium based salts (KCl, KOH and K₂CO₃) to observe which would produce the greatest positive rheological effect. Results indicated that treatment with KCl and KOH had a negative rheological effect on the soil reducing the liquid limit of the soil from a baseline of 92.3 to 79.3 and 83.5 respectively. Only K₂CO₃ did not have a negative effect on the soil, maintaining the liquid limit at 92.6. Soil kept within soil cores was then soaked in K₂CO₃ solution for a period of three weeks before being subjected to tri-axial testing at three confining pressures of 205 kPa, 280 kPa and 355 kPa; untreated soil cores were tested at the same stress conditions

Tri-axial testing of the soil showed a significant increase in the peak deviator stress measured when comparing the untreated and treated soils at its point of failure, with increases in peak deviator stress measured for the treated soils in the order of 227% at 205 kPa, 187% at 280 kPa and 124% increase at 355 kPa. Strain softening for treated soil was also measured to be less than that of the untreated soil at all confining pressures, a trait reflected in pore pressures measured at point of failure also. Stress path plots indicated that untreated samples underwent contraction rapidly as deviator stress increased, with no clear failure point observed as would be expected from an over consolidated clay. In contrast, stress paths for the treated samples showed the soils dilating before reaching point of failure and undergoing contraction following failure. Differences in friction angle and cohesion were also measured between treated and untreated samples, with untreated soil indicating friction angle and cohesion of $\Phi'=19.3^\circ$, $C'=26.6$ kPa. These results were consistent with those given in literature and fell within the range expected for ii

halloysite rich clays (Mills, 2016; Moon, 2016). Both friction angle and cohesion values increased in treated soils ($\Phi'=28.2$ and $C'=58.4$).

Based upon the results gathered during this study I infer that stabilisation of the sensitive layer of soil found within Omokoroa is possible, in particular when treated with K_2CO_3 . It is my belief that this occurs due to the successful intercalation of the K_2CO_3 ion into the halloysite basal space, displacing the water found in the space originally, and causing an expansion of the crystal lattice. The expansion of the halloysite crystal lattices in turn increases the particle contact areas, which as a result causes a rise in the cohesion and friction angle as a result of increased energy required to overcome the grain to grain friction when stress is applied. Increased basal spacing in the halloysite crystals accommodates pore fluid and thus allows for reduced pore water pressure during stress application.

Though further research is warranted, results produced from this study show that treatment increases the effective strength of the soil to a significant and noticeable degree, and provides the impetus to warrant further research into the subject in the near future, as the potential engineering impacts in being able to effectively stabilise soil rich in halloysite holds significant value both in New Zealand and on a global scale.

Acknowledgements

Firstly, I would like to thank my chief supervisor Dr Vicki Moon for her unwavering support throughout this thesis, for putting up with my constant questions and arm waving explanations. Not only this but for taking me on initially as a student and for having a belief in me that I would be able to complete this masters, even whether I was even capable.

Secondly, I would like to thank Professor David Lowe, my secondary supervisor, your expertise on soil and clays has been indispensable during the course of this thesis and without your instruction I doubt I would have progressed to the level.

A thank you to the New Zealand Geotechnical Society for awarding me the NZGS scholarship to assist in the completion of this Masters thesis as well as the University of Waikato for awarding me the Broad Memorial scholarship.

A further thank you must be made to the Western Bay of Plenty council for providing access to landslide sites and drone footage of the recent failures.

To Dr Adam Hartland, Professor Bill Henderson, Dr Willem de Lange and Dr Adrian Pitari for your assistance throughout the course of this thesis across a wide range of subjects,

A thanks to Annette Rogers, Renat, Helen Turner and Janine Ryburn thank you for all your assistance in the labs.

To my Mum, Dad and little sister your support throughout the course of my thesis has been unwavering and invaluable. Your constant support standing by and challenging me to be the best person I could, and determination in ensuring that I back and believe in myself and the work I have conducted has been irreplaceable.

To my partner Lauren, thank you for your untiring care throughout the year, you've stuck with me through all the nitty gritty and put up with me even when tired and grumpy from writing, I wouldn't have been able to do it without you. A thank you must be made to you Caitlin and Calum, the two of you have been there helping me for so long now words cannot express what I owe the pair of you. All the things you've done for me over the years, I know without you two I never would have made it here. And finally, a thank you to Ben Campbell for his moral support and field assistance throughout this thesis, your company shall be sorely missed.

Table of Contents

Abstract	i
Acknowledgements	iii
Table of Contents	v
List of Figures	xi
List of Tables.....	xvii
1 CHAPTER 1	1
Introduction	1
1.1 Background and Motivation	1
1.2 Aims.....	3
1.3 Thesis layout	3
2 Chapter 2	5
Literature Review	5
2.1 Chapter framework	5
2.2 Sensitive Soils.....	5
2.3 Global Sensitive Soils	6
2.3.1 Glacially Sourced Sensitive Soils	6
2.3.2 Sensitive Soils in New Zealand.....	7
2.4 Halloysite background	8
2.5 Structure.....	9
2.6 Morphology	10
2.6.1 Spherical Halloysite	11
2.6.2 Tubular Halloysite.....	12
2.7 Halloysite reactivity	12
2.7.1 Basal spacing.....	13
2.7.2 Cation Exchange Capacity	13
2.7.3 Isomorphous Substitution.....	13
2.7.4 Hydrogen Replacement	14

2.7.5	Broken Bond edges.....	14
2.8	Dehydration Behaviour	15
2.9	K Selectivity.....	15
2.10	Clay Cation Manipulation with Salts	16
2.11	Landslide evolution in sensitive soils.....	17
2.12	Strain Localisation in Clays	19
2.12.1	Riedel Shears	20
3	CHAPTER 3	23
	METHODS.....	23
3.1	INTRODUCTION.....	23
3.2	SOIL TREATMENT STUDY	23
3.3	Field Methods.....	23
3.3.1	Soil Coring driving and extraction methodology	25
3.3.2	Soil core transport and storage	25
3.4	Laboratory Methods	26
3.4.1	Atterberg limits and treatment methods	26
3.4.2	Soil core treatment.....	27
3.4.3	Tri-axial testing.....	28
3.4.4	Triaxial apparatus	28
3.4.5	Test Procedure	31
3.4.6	Saturation.....	31
3.4.7	Consolidation.....	31
3.5	Soil core failure analysis	32
4	CHAPTER 4	33
	GEOMECHANICAL PROPERTIES- ATTERBERG LIMITS & TREATMENTS	
	33
4.1	Chapter Outline	33
4.2	Atterberg Limits	33
4.2.1	Distilled Water- Baseline Test.....	34

4.2.2	Atterberg Limits- Potassium Chloride Treatment (KCl).....	35
4.2.3	Atterberg Limits- Potassium Hydroxide treatment (KOH).....	35
4.2.4	Atterberg Limits- Potassium Carbonate treatment (K ₂ CO ₃).....	36
4.2.5	Atterberg Limits- A line chart.....	37
4.2.6	Atterberg Limit pH changes.....	38
4.3	Soil core treatment.....	39
4.4	Atterberg and treatment summary.....	40
5	CHAPTER 5.....	41
	GEOMECHANICAL PROPERTIES – Tri-axial testing & Shear Fracture properties.....	41
5.1	Introduction.....	41
5.2	Tri-axial plots and tables.....	41
5.2.1	Results summary.....	41
5.2.2	Tri-axial Stress/Strain plots.....	43
5.3	Stress Path Characteristics.....	47
5.3.1	Stress Path Characteristics - Background.....	47
5.3.2	Stress Path Plots.....	49
5.4	Post Failure Strain Surfaces - Failure Types.....	51
5.4.1	Untreated Soil Cores.....	51
5.4.2	Treated Samples.....	53
5.5	Thin Sections.....	59
5.5.1	Component abundances and characteristics.....	59
5.5.2	205 kPa confining pressure Thin Section.....	60
5.5.3	280 kPa confining pressure Thin Section.....	64
5.5.4	355 kPa confining stress thin Section.....	67
5.6	Summary of Chapter.....	70
6	CHAPTER 6.....	71
	Scanning Electron Microscope Imagery.....	71
6.1	Introduction.....	71

6.2	General Thin Section.....	71
6.3	Mineral Specifics (180x Magnification)	72
6.3.1	Mineral 1.....	72
6.3.2	Mineral 2.....	73
6.3.3	Minerals 3 & 4.....	73
6.4	Infilling in Shears (180x magnification)	75
6.5	Shear Zone Alignment	79
6.6	Surface Nodules	82
6.7	Nodules.....	82
6.8	Fractured Crystals	86
6.9	Crystal identification	87
6.9.1	Unidentified crystal	89
6.10	Summary	91
7	Chapter 7.....	93
	Discussion.....	93
7.1	Chapter Outline	93
7.2	Geo-mechanical properties.....	93
7.2.1	Atterberg Limits.....	94
7.2.2	Atterberg Limits - Treatments How they Worked out	95
7.2.3	Ion Uptake Curves	106
7.2.4	Concluding.....	107
7.3	Tri-axial data	107
7.3.1	Comparison of Treated and Untreated.....	109
7.3.2	Shear Strength Increase	109
7.3.3	Stress Paths	111
7.4	Failure Types, Thin Sections and SEM.....	113
7.5	Thin Sections.....	113
7.5.1	Riedel Shears	114

7.6 Scanning Electron Microscopy	115
8 CHAPTER 8	117
Conclusion	117
References	121

List of Figures

Figure 2.1. Salt precipitates in the pore spaces, allowing a ‘house of cards’ structure. Upon leaching, salts dissolve and this structure is lost. Figure source: http://www.toulane.edu	7
Figure 2.2A. A profile image of the proposed arrangement of a pair of halloysite units in its dehydrated form, with a basal space of 7.2Å identified. The halloysite unit is made up of a aluminol sheet, denoted with the letter G, with an overlying silanol sheet on top of it. 2.2B. An image idea of the shape of a hydrated halloysite unit, with the silanol sheet stretching to accommodate the water present in the intra-clay basal space source Joussein et al (2005).	10
Figure 2.3. SEM imagery of spherical halloysite, with some tubular halloysite present within the image at a high magnification. Image sourced form http://www.minersoc.org	12
Figure 2.4. Three of the four main types of failure that occur in sensitive clays; (a) multiple regressive slide/flows, (b) translational progressive slides, (c) spreads (Locat et al., 2011).....	18
Figure 2.5. Progressive failure along a circular failure surface, related to the shear stress/strain curve. At points 1 and 2, the soil is becoming fully remoulded as a result of local failure, at point 3 there is a sharp strain increase, and at point 4 strain gradually increases from loss of underlying strength (Locat et al. 2011).....	19
Figure 2.6. An idealised diagram of Thakur’s strain modelling, showing a shear band with decrease with increasing deformation rate. The shear bands thickness is dependent on post-peak strain softening of sensitive clays (Thakur, 2011).	20
Figure 2.7. The relationship between the orientation of Riedel shears and thrust shears to the friction angle (Φ) of the material (Ahlgren, 2001 after Skempton, 1966).....	21
Figure 3.1. (A) The Bramley Drive landslide as seen from the edge of the shore platform via drone. The image highlights the former location of the sampling bench, indicated by the red circle, of which has since been covered by material from the upper slope. Image used with permission from the Western Bay of Plenty Council (WBOP, 2017). (B) After a bench was dug into the slope face at a sufficient distance to ensure that material would contain as little dehydrated halloysite possible soil cores were driven into the soil in a pattern as shown in the image, note large iron pans passing through the bench were avoided. Source Robertson, 2017.	24
Figure 3.2. (A) The VJ Technology Triplex Multitester Tri-axial apparatus shown in use in the image above, was used during the course of this study. Bladders controlling cell pressure and water still are	

not shown in this image. (B) A simplified view of the tri-axial apparatus used during the course of this study Source: Cunningham, 2012..... 30

Figure 4.1. Results for the degree of cone penetration in mm at differing moisture contents for soil treated with distilled water. The orange line represents the point of cone penetration that is regarded as the liquid limit. A line of best fit (dashed blue) was applied to the results, with the equation for this line and R^2 value displayed on the graph. 34

Figure 4.2 Results for the degree of cone penetration in mm at differing moisture contents for soil treated with KCL. The orange line represents the point of cone penetration that is regarded as the liquid limit. A line of best fit (dashed blue) was applied to the results, with the equation for this line and R^2 value displayed on the graph. 35

Figure 4.3. Results for the degree of cone penetration in mm at differing moisture contents for soil treated with KOH. The orange line represents the point of cone penetration that is regarded as the liquid limit. A line of best fit (dashed blue) was applied to the results, with the equation for this line and R^2 value displayed on the graph. 36

Figure 4.4. Results for the degree of cone penetration in mm at differing moisture contents for soil treated with K_2CO_3 . The orange line represents the point of cone penetration that is regarded as the liquid limit. A line of best fit (dashed blue) was applied to the results, with the equation for this line and R^2 value displayed on the graph. 37

Figure 4.5. Adapted from Skempton & Northey (1952), the A-line chart above plots the relative Liquid Limit and Plasticity Indexes of the results gathered in this study, Mills (2016) study and Moons (2016) review. The colour of the dots correspond to the respective treatments as indicated on the left hand side of the diagram..... 38

Figure 4.6. The chart above shows the changing conductivity of two separate sets of soil cores that were being treated independently, with each treatment having 4 soil cores within the solution. The conductivity was measured once a week every week prior to testing of the samples..... 40

Figure 5.1. A stress versus strain plot derived for untreated soil core samples following tri-axial failure. Deviator stress (Q) is represented as the solid blue line, while pore water pressure (U) is represented by the dashed blue line. The results for specific confining pressures are presented on the graph. 44

Figure 5.2. A stress versus strain plot derived for treated soil core samples following tri-axial failure. Deviator stress (Q) is represented as the solid orange line, while pore water pressure (U) is represented

by the dashed orange line. The results for specific confining pressures are presented on the graph.....	45
Figure 5.3. The graph above shows the stress versus strain plot for both untreated (blue) and treated (orange) samples plotted together on the same chart to allow for comparison of the results directly on the chart. Pore pressure (U) and deviator stress (Q) are shown by the dashed and solid lines respectively with respective confining pressures labelled.	46
Figure 5.4. a-d (top to bottom). Schematics of the different behaviours expected for over consolidated sand (pink), over consolidated clays (green), and normally consolidated material (orange) for both q (deviator stress) vs axial, and p' vs q' (effective stress). Schematics are sourced from Mills (2016).	48
Figure 5.5. Stress path plots (p'-q') for our untreated soil sample at 280 and 355 kPa.	49
Figure 5.6. Stress path (p'-q') plots for treated samples at all 3 confining pressures.	50
Figure 5.7. (A & B) Failed triaxial specimens for the untreated soil at 355 kPa, where grey denotes PSZ, Orange secondary shear zones, Red representing micro shears and blue depressions in the surface. (D &C) Failed tri-axial specimen sketches showing the drawn features with no overlying picture.....	52
Figure 5.8(A & B) Failed triaxial specimens for the treated soil at 205 kPa, where grey denotes PSZ, Orange secondary shear zones, Red representing micro shears and blue depressions in the surface. (D &C) Failed tri-axial specimen sketches showing the drawn features	54
Figure 5.9(A & B) Failed triaxial specimens for the treated soil at 280 kPa, where grey denotes PSZ, Orange secondary shear zones, Red representing micro shears and blue depressions in the surface. (D &C) Failed tri-axial specimen sketches showing the drawn features	56
Figure 5.10(A & B) Failed triaxial specimens for the treated soil at 205 kPa, where grey denotes PSZ, Orange secondary shear zones, Red representing micro shears and blue depressions in the surface. (D &C) Failed tri-axial specimen sketches showing the drawn features	58
Figure 5.11. An amorphous unidentified object observed on the 205 kPa thin section, with inclusions within the crystal thought to be either quartz or zircon crystals.	61
Figure 5.12. (A)Thin section at 205kPa with shears denoted on the sample. PSZ is represented as the green line, R'shear as blue, secondary conjugate shear as red and yellow as additional R shears.(B) Shears and shear direction overlain on thin section image.	63

Figure 5.13(A) Relict or infilled fractures present in the 280 kPa thin section (B)Hypersthene crystal present in the 280 kPa thin section with shears passing through the crystal. (C)Infilling by an unidentified black substance in the shear zone of the 280 kPa thin section. (D) shear fracture passing directly through what is thought to be a magnetite crystal.....	65
Figure 5.14 (A)Thin section at 280kPa with shears denoted on the sample. PSZ is represented as the green line, R'shear as blue, secondary conjugate shear as red and yellow as additional R shears. (B)Shears overlain on the slide are shown above.	66
Figure 5.15. (A) Quartz crystals present in the 355 kPa thin section, crystals were much more distinct throughout the groundmass as this higher confining pressure. (B) A snapshot of the intersection of two shear fractures passing through an apparent weak point of a crystal, the intersection appears to have an indistinct black mass in the middle. (C) A higher magnification view of the fracture intersection shown in 5.15B shows a lithic wedged into the shear space between the two fracture. (D)Further dark infillings present in the 355 kPa thin section.....	68
Figure 5.16. (A)Thin section at 355kPa with shears denoted on the sample. PSZ is represented as the green line, R'shear as blue, secondary conjugate shear as red. (B)Shears overlain on the slide image.....	69
Figure 6.1. A normal SEM image of the 280 kPa thin section at the lowest possible magnification, desiccation cracks are denoted as circled in orange and indeterminate crystal circled in red.....	72
Figure 6.2. A BSE image taken of the 355 kPa thin section of 4 separate key features, each labelled in red for separate identification.	73
Figure 6.3. Element distribution graphs showing distribution of elements on the image of figure 6.2, elements are identified as points in differing colours with particular element identified in the top left of each image.	74
Figure 6.4. (A)An SEM image of the 280 kPa image showing infilled shears present within the thin section at 179 times magnification(B) A BSE image of infilled shears present on the 280 kPa thin section at 179 times magnification.....	76
Figure 6.5. Element distribution maps for the images used in figure 6.4, with particular element for each distribution identified above each distribution box in the top left.	77
Figure 6.6. Point element distribution on the 280 kPa thin section, where specific points had element volumes graphed. Each point has its own graph produced as shown above, with particular point indicated in the title of each graph.....	78

Figure 6.7. Taken at 710 times magnification of the 280 kPa thin section shear zone, propagation of alignments and fractures within the shear zone is indicated in the image above by the red lines.	80
Figure 6.8. Element distribution maps for the image above taken for the shear zone of the 280 kPa thin section at 710 times magnification. Concentrations of calcium (middle image) can be seen above by the grey dots on a black background.	81
Figure 6.9(A) Taken at 1500 times magnification of the 280 kPa thin section in regular SEM bright circular nodules can be observed propagating on the clay shear surface, with plate like flecks present. (B) A BSE taken at 15,000 times magnification of one of the nodules, at this higher magnification it can be seen that these nodules are connected to each other and made up of numerous smaller nodules that have bonded together. (C & D) Taken as a BSE image at 40,000 times magnification an extreme close up of the nodule reveals the circular concave shape of the nodules, with dessication cracks evident, the right hand image shows the points at which point element measurements have been mad	84
Figure 6.10. Point element analysis graphs for points 1,4,6 and 7 for image 6.9D. Points 1 and 7 show typic treated halloysite clay measurements with peaks measured for silicon and aluminium, whereas points 4 and 6 show peaks similarly for halloysite for silicon and aluminium, but differences are observed as there is a significant peak in potassium for these two points, with potassium measured as the highest proportion of element present at these points.	85
Figure 6.11. A possible orthoclase crystal with fracture propagating through the crystal at 200 times magnification taken in normal SEM	86
Figure 6.12. An element distribution graph for the crystal present in figure 6.14 with peaks measured for multiple elements.	87
Figure 6.13. An element distribution map for titanium, iron and silicon present for the image shown in the top left corner.	88
Figure 6.14(A) A BSE image of what is thought to be a weathered NaCl crystal found in the 355 kPa thin section. (B) An SEM image at 4500 times magnificaiton of what is thought to be a NaCl crystal.	90
Figure 6.15. An element distribution chart for a variety of elements detected on the image of figure 6.14. Concentrations of Na and Cl are heavily evident on the crystal itself.	91
Figure 7.1. A concept sketch of how water intercalates into the halloysite crystal basal space. The H ₂ O unit forms temporary hydrogen bonds with the hydrogen deficient hydroxyl groups on the aluminol sheets and actively intercalates.	96

Figure 7.2. Sourced from Theng & Wells (1995), showing how the Aluminol sheet in halloysite changes its charge dependant on the soil pH. 97

Figure 7.3. Sourced from Tan (2010), the diagram above represents the hypothetical inner and outer hemholtz layers that ions have to overcome to bond. 99

Figure 7.4. A hypothetical concept sketch of the chemical bonding and ionic bonding that will occur when KOH interacts with the aluminol sheet of halloysite. 101

Figure 7.5. A hypothetical concept sketch of the way in which K_2CO_3 intercalates into the halloysite crystal lattice, and subsequently forms temporary ionic bonds with the hydrogen deficient aluminol oxygens..... 103

Figure 7.6. Sourced from Tan (2010), the figure above indicates whether pore pressures will become positive or negative under axial strain conditions forclays..... 112

List of Tables

Table 2.1. A revised sensitivity scale produced by Rosenqvist (1953) to include both sensitive clays and the clays of a highly sensitive nature, named quick clays.	5
Table 2.2. Sourced from Torrances (1992) review of Jacquets (1990) paper on the development of sensitivity in New Zealand soils, the factors relevant to the production of a high undisturbed strength of a soil and factors relevant to the production of low remoulded strength are presented.	8
Table 2.3. Sourced from Joussein et al., (2005) morphologies of the various forms of Halloysite are displayed along with the source material and locations that the particular morphologies have been found.	11
Table 4.1. The table below details the various Atterberg limit results that were measured during this study. These include the results for treatment of the soil with Distilled water, KOH, K ₂ CO ₃ and KCL. Also included in this table are the results produced by Mills (2016) in her study as well as the results given in Moons (2016) review paper.	33
Table 4.2. pH's of the differing treatments applied to the soil are displayed in the table below. Two methods were applied due to the lack of consensus in literature of a clear method to use when measuring the soil pH of a remoulded clay paste.	38
Table 5.1. The table below presents a summary of the data collected during tri-axial testing of the untreated and treated soil cores collected from Bramley Drive at the three differing confining pressures.	41
Table 5.2. Mineral abundances observed across the thin sections produced for 205 and 280 kPa, mineral abundances have been estimated as point counting was not conducted due to the small size of the clay and silt minerals.	59
Table 7.1. Effective stresses measured for both untreated and treated soils, measuring effective friction angle, and effective cohesion.	110

CHAPTER 1

Introduction

1.1 Background and Motivation

Sensitive soils are found globally and have been widely regarded as a contributing to slope instability. Of all traits, sensitive soils most notably have been linked to causing large retrogressive landslides, resulting in serious hazards to infrastructure, local environments and human life (Quinn *et al.*, 2011). Sensitivity itself is recognised as the loss of strength within a soil upon remoulding and is defined in literature as the ratio of undisturbed strength to remoulded strength of a soil at similar moisture contents (Skempton & Northey, 1952).

Globally sensitive soils form in a wide range of environments and locations, with sensitive soils made up of differing clays and causing different issues depending on where in the world they are found. Generally sensitive soils are made up of young, clay rich deposits, that have been re-worked or been subject to a change in environment following deposition. The soils themselves can be sourced from deposits found from marine, lacustrine and pyroclastic (tephra) deposits. (Skempton & Northey, 1952; Rosenqvist, 1953, 1977; Torrance, 1983).

Research into these sensitive soil slides globally has been extensive, with historical research focussed on regions within North America and Europe being most dominant. Scandinavia and Canada in particular are regions that have had extensive and well documented research conducted into sensitive soils and the resultant failures that they induce, with the failures well documented. These regions are rich in sensitive soils due to their proximity to the upper polar regions and being strongly influenced by the recession of the ice-caps following the last ice age (Locat *et al.*, 2011; Locat & St-Gelais, 2014) During glacial period, the rocks present were ground into a fine powder which was deposited on the sea floor. Following isostatic rebound of these marine terraces this fine grained glacial flour had the salt present within the clay leached over a significant period of time resulting in the loss of flocculation and strength within these soils, producing a sensitive response. In the Quebec region of Canada where in 1971 a large retrogressive landslide in St Jean Vianney resulted in the death of 31 persons, as well as significant damage to properties (40 buildings), highways, local roads and infrastructure to the region

(Tavenas *et al.*, 1971). Outside of these regions other localities where sensitive soils have been identified include Japan, Indonesia, various African countries and New Zealand (Wesley, 1973; Joussein *et al.*, 2005)

Within New Zealand, sensitive soils are predominantly derived from rhyolitic and andesitic tephra and volcanic deposits (Jacquet, 1990). In some instances some sensitive soils are sourced from hydrothermal alteration to soils and rocks (Joussein *et al.*, 2005), but the bulk of the sensitive soil deposits have occurred as a result of the extensive volcanic activity across the central North Island of New Zealand in the last 2 million years. Within New Zealand sensitive soils have been studied extensively across Taranaki, the upper Waikato, Coromandel Peninsula and within the Bay of Plenty, in particular within the bounds of the Tauranga area (McCraw, 1967; Carr *et al.*, 1978; Gulliver & Houghton, 1980; Smalley *et al.*, 1980; Taylor, 1980; Jacquet, 1990; Theng & Wells, 1995; Churchman, 2000; Joussein *et al.*, 2005; Keam, 2008; Wyatt, 2009; Taylor, 2011; Cunningham, 2012; Moon *et al.*, 2013; Moon *et al.*, 2015; Lowe & Churchman, 2016; Mills, 2016; Moon, 2016; Kluger *et al.*, 2017; Manderson, 2017; Moon, 2017)

Within the Tauranga region recent and historic landslide events have been attributed to sensitivity within weathered, reworked pyroclastic soil deposits. Yet to date the failure behaviour of these soils, and in particular the interactions of the clays in causing sensitivity is not clearly understood. In recent times a number of significant landslide events that have been associated with sensitive soils within the Tauranga region, and these have caused significant costs and hazards to people. Some of these examples include the Ruahihi Canal failure in 1981 (Hatrack *et al.*, 1982), the Bramley Drive landslide in 1971 and its subsequent reactivations (Gulliver & Houghton, 1980) and finally the numerous landslides that occurred within Omokoroa and the wider Tauranga region in 2017 following the cyclone events of Cyclones Cook and Debbie.

Attempting to mitigate and stabilise landslides that have their sources in sensitive soil are an invaluable area of research, with considerable potential benefits of such studies. As such recent and historic research conducted in Norway has indicated a successful methodology of stabilising landslides based within sensitive soils. This was achieved by directly treating the soil *in-situ* with Potassium Chloride (KCl) solutions, with treatment achieved by filling large leaching columns at a regular spacing across the landslide in an attempt to cause re-flocculation of the sensitive soil and stabilisation of the slope (Moum *et al.*, 1970; Helle *et al.*, 2015;

Helle *et al.*, 2017). The study proved a success and the researcher successfully stabilised their slope. The methodology has subsequently been modified and used by scientists in Italy in an attempt to stabilise a slide with its basis in a sensitive soils, with results to date appearing promising, with sliding appearing to have been negated and flocculation of clay structure is re-occurring within the soil (De Rosa *et al.*, 2016)

1.2 Aims

The overarching aim of this thesis is to examine the use of salts in stabilising sensitive soil based landslides with the goal of producing a methodology in the BoP. Further aims of this thesis were to map the recent failures that occurred in the Autumn of 2017 on the Omokoroa peninsula in Tauranga, which will be added to the appendices of this thesis. To achieve this goal a number of objectives were proposed, these were developed in a fashion to allow for a comprehensive and detailed understanding of the results produced. These objectives were:

1. To determine which specific salt would be best to utilise for treatment of the sensitive soil of the BoP through literature searching and laboratory testing
2. To undertake consolidated, undrained triaxial tests at rates recommended by the British Standard 1377 (1990) Part 8: Shear Strength tests (effective stress) on both untreated soil cores to produce a baseline result, and on cores treated with a salt thus allowing for the comparison of the results; to determine the mechanisms and interactions of the clay and salt.
3. To undertake optical microscopy and Scanning Electron Microscopy to examine shear surfaces of the failed samples to observe any morphological and fabric differences present within treated soil samples.

1.3 Thesis layout

Chapter 2 of this thesis presents a literature review on the background and evolution of sensitivity within volcanic ash and glacial till soils both in New Zealand and globally. Furthermore, characteristics of halloysite are reviewed. Further reviews will be conducted on Tri-axial failure methods. Chapter 3 presents all laboratory and field methods used throughout the course of this study.

Results for the laboratory testing on the soil from Omokoroa will be presented in Chapters 4,5, and 6. Chapter 4 will outline the geomechanical properties with regards to Atterberg limits of the soil, with a focus on the various salts that can be

used throughout testing. Chapter 5 will include all data collected for Consolidated Undrained Tri-axial testing on both treated and untreated soil samples, with descriptions of failed specimens presented. Within this section thin sections of failed specimens will also be analysed. Chapter 6 will focus on the data collected on the soil using Scanning Electron Microscopy with a focus made on both images collected as well as the element detection for each area scanned. Chapter 7 will discuss the observations and results produced within the result chapters, with a focus on relevant literature. Halloysite morphology and chemical interactions will be discussed with an examination on tri-axial failure mechanisms highlighted.. Finally Chapter 8 will summarise all research finding and will provide comprehensive recommendations for future research topics derived from this study.

Chapter 2

Literature Review

2.1 Chapter framework

This chapter will explore the literature relevant to the subjects covered in this thesis. These subjects include an overview of research conducted on sensitive soils, how they are sourced globally and here in New Zealand. Focus will then be given to halloysite, its structure, morphology, dehydration behaviour, potassium selectivity and background on factors impacting on halloysite interaction with ions. Further research will be provided on clay cation manipulation, how landslides evolve in sensitive soils and the relevant literature on strain localisation in clays.

2.2 Sensitive Soils

Soil sensitivity is defined as the ratio of the undisturbed and remoulded shear strengths of a soil, at the same moisture content (Equation 2.1):

$$S_T = \frac{\text{Undisturbed Strength} - c}{\text{Remoulded Strength} - c_r} \quad (2-1)$$

where c is the undisturbed strength, c_r is remoulded strength and S_t gives the sensitivity ratio (Terzaghi, 1944; Skempton & Northey, 1952). Table 2.1 presents the classification of sensitivity values

Table 2.1. A revised sensitivity scale produced by Rosenqvist (1953) to include both sensitive clays and the clays of a highly sensitive nature, named quick clays.

St	Designation
1	Insensitive Clays
1-2	slightly sensitive clays
2-4	medium sensitive clays
4-8	very sensitive clays
8-16	slightly quick clays
16-32	medium quick clays
32-64	very quick clays
64+	extra quick clays

2.3 Global Sensitive Soils

Sensitive soils are found across the globe, varying in type and source. On a global scale, sensitive soils are sourced from a variety of environments and time periods. The sources of these sensitive soils include lacustrine, fluvial, marine and air fall (tephra) deposition (Skempton & Northey, 1952; Torrance, 1983; Joussein *et al.*, 2005; Torrance, 2014), with the countries affected by these sensitive soils including Canada, Norway, Sweden, France, Belgium, Indonesia, Japan and New Zealand. The best known sensitive soils are glacially derived in Scandinavia and Canada. These are discussed below.

2.3.1 Glacially Sourced Sensitive Soils

Within the Scandinavian regions of Europe and within certain areas of Canada glacially sourced sensitive soils have been linked to some of the largest and most damaging landslides attributed to sensitive soils (Moum *et al.*, 1970; Tavenas *et al.*, 1971), with these landslides having a significant impact on infrastructure, as well as posing real threats to human life.

Sensitive soils within these Northern Hemisphere regions are all young, recent deposits having formed within the period of the last ice age to today. The concept being that during the recession of the large polar ice sheets over the Northern Hemisphere during the last ice age, rocks trapped underneath the glacial sheets were ground into a fine almost 'flour'-like consistency, and were carried into a marine environment. Within the marine environment this rock flour was deposited in large deposits on the sea floor. These deposits, rich in illite clays flocculated as the pore spaces were rich in salt as a result of the sea water they were exposed to, with slow deposition through marine water columns allowing time for flocculation. The resultant edge to edge interactions of these deposits produced what has been defined as a 'house of cards' structure (Figure 2.1) (Skempton & Northey, 1952; Torrance, 1983; Locat & St-Gelais, 2014; Lowe & Churchman, 2016). As a result of the retreat of the large polar ice caps, the sea bed had a significant weight removed, incurring isostatic rebound of the sea floor. This exposed the illite flocculated deposits to sub-aerial environments. As a result, fresh water infiltrated these salt rich deposits, with the salt leached from the clay due to the osmotic difference between the salt rich clay, and salt deficient groundwater. The loss of the salts resulted in the edge to edge interactions of the clays losing their bonding

charges, producing a loss in structure with the clays essentially collapsing. This collapsed structure results in a loss of structural strength, producing a sensitive soil.

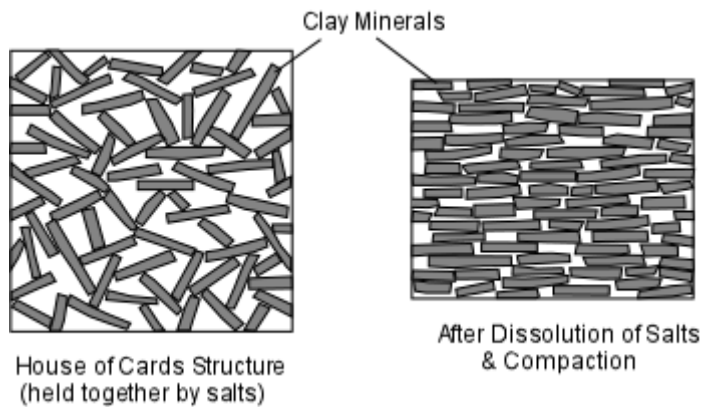


Figure 2.1. Salt precipitates in the pore spaces, allowing a ‘house of cards’ structure. Upon leaching, salts dissolve and this structure is lost. Figure source: <http://www.toulane.edu>

2.3.2 Sensitive Soils in New Zealand

Within New Zealand, unlike the soils of a sensitive nature within the Northern Hemisphere, the sensitive soils here are dominated by 1:1 clay minerals such as kaolinite, halloysite and allophane. These sensitive soils are for the most part sourced from deposits associated with some form of volcanic activity, ranging from soils developed from reworked air fall tephra deposits, such as those seen in the Tauranga region, to hydrothermally altered soils rich in kaolin within the Coromandel region of New Zealand (Torrance, 1983; Jacquet, 1990; Parfitt, 1990). How sensitivity develops within these samples has been examined by several researchers including Torrance (1983) and Jacquet (1990). The work undertaken indicates that sensitivity can be attributed to a number of factors that result in a low remoulded strength. Table 2.2 produced by Torrance in his 1992 review of Jacquet’s (1990) paper of sensitivity in remoulded volcanic ash soils indicates that the most likely cause for low remoulded strength can be linked to the high void ratio experienced by air fall deposits or removal of material during weathering and diagenesis removing any structure present within the soil. (Torrance, 1992).

Table 2.2. Sourced from Torrances (1992) review of Jacquets (1990) paper on the development of sensitivity in New Zealand soils, the factors relevant to the production of a high undisturbed strength of a soil and factors relevant to the production of low remoulded strength are presented.

Depositional	Post-depositional
<i>Factors producing a high undisturbed strength</i>	
Mineralogy —allophanic	Diagenesis and weathering —hydrothermal alteration to product halloysite —weathering to produce imogolite —weathering to produce ferrihydrite
<i>Factors producing a low remoulded strength</i>	
Air-fall origin —high void ratio	Void ratio increase by dissolution and removal of soluble material during weathering and diagenesis
Mineralogy —allophanic	Dispersing agents

2.4 Halloysite background

At the Bramley Drive slide site on the Omokoroa Peninsula previous studies conducted have indicated that the primary cause of sensitivity is the dominance of the low activity clay mineral halloysite, found in its hydrated form at the particular site (Smalley *et al.*, 1980; Wyatt, 2009; Cunningham, 2012; Kluger *et al.*, 2017). Halloysite is a dioctahedral 1:1 clay mineral of the kaolin group (Berthier, 1826; Joussein *et al.*, 2005). Many different forms of halloysite have been identified including ferro-halloysite, dehydrated halloysite, and hydrated halloysite (Joussein *et al.*, 2005). Some authors maintained that the description of halloysite should be reserved for halloysite in its hydrated form (Mehmel, 1935; Alexander *et al.*, 1943). Later, due to a number of authors using a wide variety of terms for the description of halloysite the AIPEA Nomenclature Committee, following consensus by a number of authors, determined that, halloysite should be referred to as halloysite (10.1Å) for its hydrated form and halloysite(7Å) for its dehydrated form (Douglas, 1947; Bridley, 1961; Churchman, 1973; Joussein *et al.*, 2005).

Halloysite as a clay mineral forms generally from alteration of a wide variety of weathered rocks and soils, though is widely prevalent in andisols and soils

derived from volcanic materials in some areas of the world. These include the formation of ferro-halloysites in volcanic soils within tropical areas, while also being the kinetically controlled end product of arid-zone basalt weathering (Churchman, 2000; Chadwick *et al.*, 2003; Ndayiragije & Delvaux, 2004). In New Zealand numerous deposits of halloysite rich deposits are derived from rhyolitic volcanic deposits that have undergone rapid, low temperature alteration. Halloysite is more prevalent in rhyolitic weathered deposits and kaolinite, its group sister is dominant in hydrothermal alteration of rhyolitic deposits (Harvey & Murray, 1990; Harvey, 1997)

2.5 Structure

Known to be in the kaolin group of clay minerals, halloysites 1:1 clay mineral structure is known to differ from its group counterparts in structural makeup. In its dehydrated form halloysite has the same kaolinite structure of a tetrahedral silica sheet with an octahedral alumina sheet sitting above it (Figure 2.2A). These features give halloysite a basal spacing of 7Å, with basal spacing defined as a measurement of the length between the base of the octahedral sheet and top of the tetrahedral sheet. Hydrated halloysite has the presence of an interlayer water layer between each sheet pairing (Figure 2.2A). This causes the clay to increase its basal spacing to 10Å, which is achieved by a stretching of sorts of the upper tetrahedral layer, causing it to bend as observed in Figure 2.2B (Mitchell, 1994; Tan & Bartlett, 1994; White, 2013). The tetrahedral layer has an alignment in such a fashion that it forms hexagonal recesses within the sheet. These hexagonal recesses allow active access to the octahedral sheet from two directions increasing chances of potential exchange between external ions if of correct size and charge. This also promotes the chances of isomorphous substitution occurring at each of the clay layers, causing a shift in possible charge. (Mitchell, 1994; Joussein *et al.*, 2005; White, 2013)

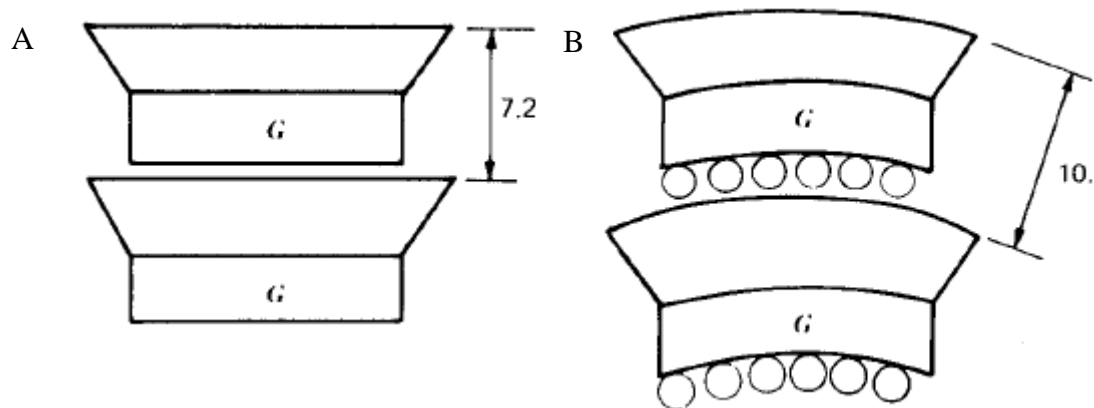


Figure 2.2A. A profile image of the proposed arrangement of a pair of halloysite units in its dehydrated form, with a basal space of 7.2\AA identified. The halloysite unit is made up of a aluminol sheet, denoted with the letter G, with an overlying silanol sheet on top of it. **2.2B.** An image idea of the shape of a hydrated halloysite unit, with the silanol sheet stretching to accommodate the water present in the intra-clay basal space source Joussein *et al* (2005).

2.6 Morphology

Morphology of halloysite refers to the structural make up and shape formed by the sheets of the halloysite mineral (Joussein *et al.*, 2005). Table 2.3 details the array of shapes the mineral can have depending on location and initial parent material. It has been indicated that at the Omokoroa site the main forms of halloysite present within the sensitive soil region are made up of small, similar sized spheroidal halloysite, stubby tubular and plate booklet halloysite morphologies (Lowe & Churchman, 2016).

Table 2.3. Sourced from Joussein *et al.*, (2005) morphologies of the various forms of Halloysite are displayed along with the source material and locations that the particular morphologies have been found.

Morphologies	Occurrences
Tubular, long and thin, short and stubby tubes	Cryptokarstic sediment, volcanic glass and pumice, feldspar and mica alteration
Pseudo spherical and spheroidal	Weathered volcanic ash and pumices, volcanic glass in marine environment, (e.g. Guatemala soils, New Zealand)
Platy or tabular	Volcanic ash soils, weathered pyroclastic, lateritic profiles, fissures within granite, hydrothermal alteration, tuff bed (e.g. Texas, Brazil, Guatemala)
Fibre	Lateritic soil, weathered granite (e.g. Australia, Brazil)
Prismatic, rolled, crinkly, walnut-meat	Volcanic ash soils, weathered granite (Japan)
Cylindrical, disk	Rhyolitic tephra (New Zealand)
Spherulitic, irregular lath with rolling edge	Weathered granite/gabbros, (Scotland)
Crumpled lamellar	Weathered pumices (Japan)
Lath, scroll	Altered volcanic glass (Japan)
Glomerular or 'onion-like'	Volcanic ash (Cameroon)

2.6.1 Spherical Halloysite

As observed in Table 2.3 spheroidal and pseudo spherical halloysite have been found to occur in a variety of environments with the primary source of these spheroidal halloysite forms a result of weathering of volcanic ashes and pumiceous deposits. The spheroidal shape occurs as a product of deposition of halloysite from super saturated solutions of weathered volcanic glass derivatives (Sudo, 1953; Nagasawa & Miyazaki, 1975; Kirkman, 1977; Tazaki, 1979; Noro, 1986; Joussein *et al.*, 2005). An example of this spheroidal halloysite can be seen in figure 2.3.

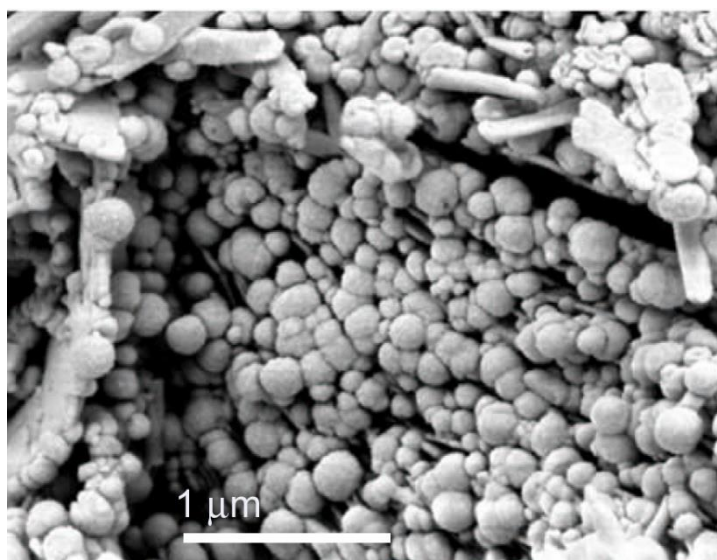


Figure 2.3. SEM imagery of spherical halloysite, with some tubular halloysite present within the image at a high magnification. Image sourced from <http://www.minersoc.org>.

2.6.2 Tubular Halloysite

Of all the forms of halloysite the dominant morphology that can be found for the mineral is in its tubular form, with there being a wide range of sizes that tubular halloysite can take, with tubules as small as 0.2 μm up to 30μm+ long tubules (Churchman, 1973; Nagasawa & Miyazaki, 1975; Robertson & Eggleton, 1991; Churchman *et al.*, 1995; Norrish, 1995). An important factor when observing tubular halloysite is the difference of pore space present within the central cylinder for the tubes, with small tubes being hollow, allowing for the infilling by external material, whereas larger tubules have infilled centres with no pore spaces present (Churchman *et al.*, 1995).

2.7 Halloysite reactivity

When examining halloysite it is imperative to distinguish and explore the size of the halloysite itself, how the basal spacing of the clay occurs and the clays cation exchange capacity. Furthermore, it is necessary to look over the literature present, of which all indicate halloysite selectivity for potassium, and to explore why this occurs.

2.7.1 Basal spacing

Two main forms of halloysite found, the 10Å hydrated form and 7Å dehydrated form (Joussein *et al.*, 2005). Figure 2.2B details an example of what the 10Å halloysite crystalline structure may be. Within the halloysite layers the interlayer water found is a key aspect that allows for the distinction and what makes halloysite unique within the kaolin group from other minerals (Churchman & Carr, 1975). Issues can arise when identifying dehydrated Halloysite in its 7Å form from kaolinite, of similar 7Å in size.

The 10Å size of halloysite in its hydrated form comes from a combination of the two 1:1 alumino silicate layers of halloysite itself, 7Å in size and a 3Å monolayer of water in between the two layers, as represented in figure 2.2B (Churchman & Carr, 1975; Joussein *et al.*, 2005). As a direct result of this interlayer, cations within the halloysite should be available for exchange from within the crystal lattice and externally (Garrett & Walker, 1959).

2.7.2 Cation Exchange Capacity

Cation exchange capacity (CEC) in clays is among the most important features when determining how a clay may interact and change under differing conditions. Cation exchange capacity is defined as the sum of the exchangeable cations found within a soil, whether they be from solution or from bonding sites (Chapman, 1965; White, 2013). Cation exchange is of importance in clay soils due to the net negative charge found on the colloidal surfaces of clays, with the negative charge attracting cations in an attempt to neutralise the surface charges and ensure the clay reaches a Point of Zero Charge (PZC) (Chapman, 1965; Tan & Bartlett, 1994; White, 2013). Cation exchange in soils and the development of cation exchange capacity can be sourced from 3 main methods: isomorphous substitution, hydrogen replacement, and broken particle edge charges (Mitchell, 1994).

2.7.3 Isomorphous Substitution

Isomorphous substitution is the term given to a method of cation exchange capacity promotion in which ions are substituted within the tetrahedral and octahedral sheets, with an ion of lesser charge substituting into the mineral structure and causing a net deficiency of cations, i.e. the substitution of Al^{3+} into a tetrahedral structure for Si^{4+} . The resulting loss of the additional positive charge results in a net

imbalance (Mitchell, 1994; White, 2013). A lot of debate occurs around whether isomorphous substitution does in fact occur in clay minerals of the kaolinite group, though it has been widely stated now that some isomorphous substitution must occur in halloysite to account for the net negative charge found on the clay surface in at pH values of 5 and lower, which for the bulk of clay minerals result in positive charges (Robertson *et al.*, 1954; Quantin *et al.*, 1988; Bailey, 1990; Joussein *et al.*, 2005).

2.7.4 Hydrogen Replacement

A further way of cation exchange capacity to develop and occur is via the replacement of the hydrogen on exposed hydroxyl bonds on the outer edges of the clay sheets. This method of cation exchange is seen as unlikely to occur for the most part due to the conditions required for exchange to occur (Grim, 1968). A key feature of this comes from issues surrounding the lyotropic series. The lyotropic series is a rule set which determines which cation's will be preferentially taken up by a negatively charged site, or will replace other ions, based on a cations valence. These are key as the salts in solution need to be of a sufficient valence to replace the strong ionic bond formed between the oxygen and hydrogen (Chapman, 1965; Grim, 1968; Mitchell, 1994; Tan & Bartlett, 1994). The likelihood of these hydrogen ions to be replaced can also be found to be pH and surface charge dependent - with a lower pH usually promoting the uptake of hydrogen from solution over other cations and increasing the strength of the bonding (White, 2013).

2.7.5 Broken Bond edges

A final method of cation exchange comes from broken bonds along particle edges and non-cleavage surfaces. These broken bonds allow for the exposure of open hydroxyl groups with a net negative charge to be exposed. Cations will preferentially seek out and seek to bond with open hydroxyl groups to attempt to reach a non-ionic state (White, 2013). Halloysite may have a large amount of these open hydroxyl groups due to the stretching of the tetrahedral layer as stated previously, this stretching causing strain on the hydroxyl group bonds, potentially causing them to weaken due to the larger distances between ions.

2.8 Dehydration Behaviour

The dehydration behaviour of halloysite is of importance as this can have a noticeable impact on the way in which soils containing halloysite may interact in the laboratory following transport as opposed to how they may act *in situ*. A key issue upon is that even under ambient conditions 10Å halloysite can rapidly dehydrate to its 7Å form, undergoing an irreversible change to its structure, with the 7Å form of halloysite being its favourable form (Giese, 1988; Joussein *et al.*, 2005). Extensive study has been undertaken to determine the changing points at which halloysite will dehydrate, with determinations for complete dehydration occurring where relative humidity was at 0% or the clay was heated to 200-300°C (Hughes, 1966). Studies conducted on certain halloysites determined that dehydration can occur at points as high as 90% humidity, with the 10Å peak of hydrated halloysite disappearing at 20% humidity (Harrison & Greenberg, 1962).

These features indicate that firstly for sampling, samples need to be taken at an appropriate distance from the soil face to ensure that as much halloysite as possible is still at its *in-situ* 10Å spacing, and furthermore during transport the sample is kept in conditions exceeding 90% humidity to prevent any dehydration occurring in the soil. Dehydration of a sample can have significant effects on laboratory experiments due to the change in crystalline structure, as the spacing between layers collapses. This collapse of layers then may have a direct effect on the clay's ability to uptake external cations (Joussein *et al.*, 2005).

2.9 K Selectivity

Halloysite as a clay mineral can be regarded as a low activity clay mineral, with a preferential selectivity for creating intercalated salts with low activity cations such as K⁺, Cs⁺ and NH₄⁺ (Garrett & Walker, 1959). The cause of this low activity cation selectivity is a mechanism which is the subject of much research and debate with a number of authors suggesting it is a result of interlayered zeolites or mica rich layers within the halloysite (Boettinger & Graham, 1995; Chorover *et al.*, 1999). Previously authors have examined the method by which intercalated salts are formed from the halloysite clays with some authors pointing to size of the voids formed by oxygen rings within the octahedral layer of the halloysite, with the cations required to fit snugly into these voids to ensure entry to the layers, while salt's anions hold the clay layers apart a distance equal to its own size. Garret and

Walker (1959) indicated that even though halloysite preferentially up took K^+ , other normally excluded cations such as Na^+ and Ca^{2+} , which on their own normally cannot enter the crystal lattice, are able to accompany the anion into the basal space.

2.10 Clay Cation Manipulation with Salts

Manipulation of cation content and the chemical aspects of a clay has been studied since early last century, beginning with Bradfield's potentiometric and conductometric titrations on acid clays in the early 1920's, whereupon he observed the dispersive and coagulation of clays under differing conditions (Bradfield, 1923; Marshall & Krinbill, 1942). As a result this had led to a large number of studies observing the effects of various chemicals and compounds on clays ranging from treatment of clays with various acids to treatment with various salts in attempts to manipulate various aspects of a clay's make-up (Panda *et al.*, 2010).

Halloysite itself has been subject to numerous studies examining the effects of manipulation of pore ion content, most notably that conducted by Garret and Walker (1959) examining the cation exchange capacity of the anomalously high reported values on the Djebel Debar halloysites, along with the hypothesis of an exchangeable interlayer of ions by Riviere (1950). Garret and Walker (1959) undertook a wide range of treatments with salts to attempt to determine whether this interlayer of ions was indeed present. Salts used included a wide range of potassium based salts, as well as a number of chloride rich metal based salts (i.e. lithium chloride). Of all samples they observed, only potassium carbonate and potassium acetate had an effect on the halloysite (Garrett & Walker, 1959). Wada (1959) undertook a similar study with halloysites from Japan and observed results similar to those of Garret and Walker (Wada, 1959).

In 1978 further research was undertaken to examine the potential reasons why halloysite formed these complexes, while also explaining newer complexes with new salt intercalation complexes. The study conducted provided a verification for the data collected and produced by Garret & Walker (1959) and Wada (1959), with the results produced in a differing halloysites, sourced from various areas around New Zealand (Carr *et al.*, 1978). Following this, Theng & Wells (1995) undertook detailed research on flow suspensions of halloysite to observe the changing traits of halloysite under treatment with salts and provided a comprehensive hypothesis to the observations made (Theng & Wells, 1995).

Outside of halloysite, usage of salts to influence shear strength has been used extensively in Norway, first by Moum *et al* (1970) who initiated an ongoing study to observe the increase in shear strength in a landslide over a long period of time (Moum *et al.*, 1970; Helle *et al.*, 2015; Helle *et al.*, 2017), and in more recent studies in Italy to achieve a similar goal (De Rosa *et al.*, 2016) with successful results observed all round. The studies all used potassium chloride to stabilise the landslides, with the theory being replenishment of a chloride based salt within the sensitive soil would cause flocculation of the illite clays and result in a strengthening of the soil. To date the treatment has successfully halted any further failure of the respective slopes and has been regarded a ‘success’.

2.11 Landslide evolution in sensitive soils

Landslides in sensitive soils and their evolution from first occurrence to continual failure is well established in literature. Of the failures that occur in soils of a sensitive nature there are 3 main forms that have been identified globally (Figure 2.4). The first is a flow style failure (Figure 2.4a), whereupon multiple retrogressive slides occur following the first failure, and the debris becomes strongly remoulded and flows out of the crater leaving an unstable scarp. As a result of this unstable scarp another failure surface will propagate within the remaining soil leading to a secondary failure of a similar size, resulting in more strongly remoulded material flowing out of the crater leaving a further unstable scarp, with failures occurring repeatedly in an attempt to return to a stable state (Tavenas, 1984; Locat *et al.*, 2011)

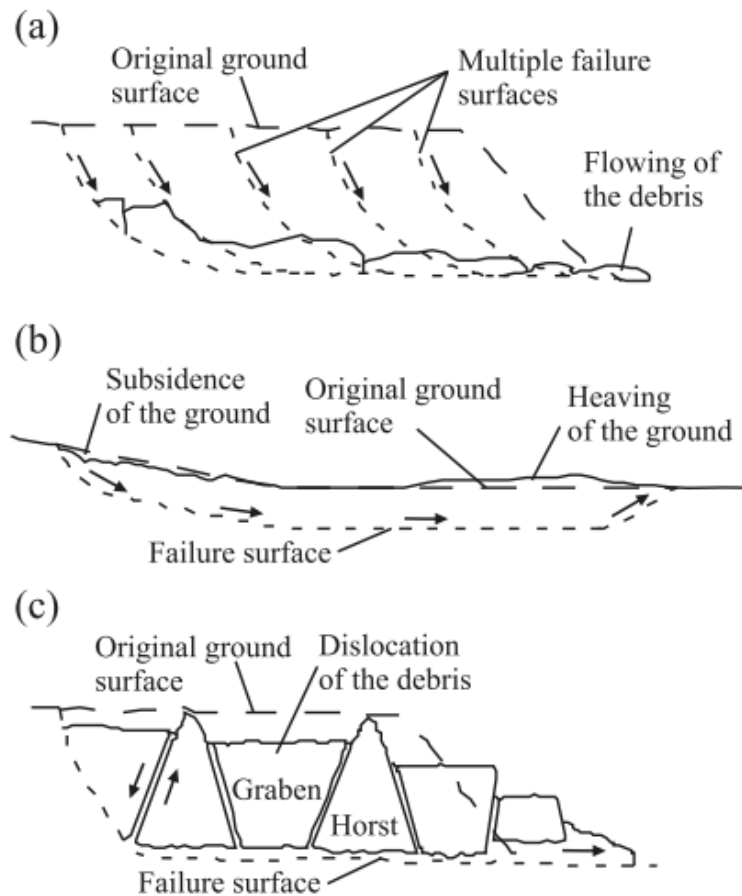


Figure 2.4. Three of the four main types of failure that occur in sensitive clays; (a) multiple regressive slide/flows, (b) translational progressive slides, (c) spreads (Locat *et al.*, 2011)

The second is a translational progressive landslide (Figure 2.4b). These landslides propagate from development of a shear surface parallel to the ground surface, above which the overburden soil is displaced downhill over a period of time. These landslides usually form as a result of excessive weight being placed on the head of the failure, resulting in a failure in attempting to accommodate this excess mass (Cruden & Varnes, 1996; Bernander, 2011; Locat *et al.*, 2011). The final form of these failures is spread failures (Figure 2.4c), with Cruden and Varnes (1996) describing these as a result of the extension and dislocation of a failure surface, which forms horsts and grabens within the sensitive clay, causing displacement of the overlying soil masses to a significant degree.

Of the failure types described above, the majority of failures observed in Omokoroa that have been attributed to sensitive soils are thought to be retrogressive landslides, evidence of this can be observed in Bramley Drive, with multiple failures occurring between the original failure in 1979 and to date, with large retrogressive failures causing the head-scarp to have retrogressed a significant

distance since original failure (Gulliver & Houghton, 1980; Moon *et al.*, 2013; Moon *et al.*, 2015; Mills, 2016; Moon, 2016; Kluger *et al.*, 2017). Though with this said, retrogression of the scarp head has been inconsistent and each failure has been of varying time scales.

The propagation of failure surfaces within large retrogressive landslides is a feature that has been studied extensively during the last century, with mobilised shear strength stated to be determined by the strain-softening behaviour of a soil (Skempton, 1964). Figure 2.5 displays this, with the figure drawing parallels between the stress-strain curve observed of a sample during tri-axial testing and the corresponding points of propagation during a shear failure (Locat *et al.*, 2011).

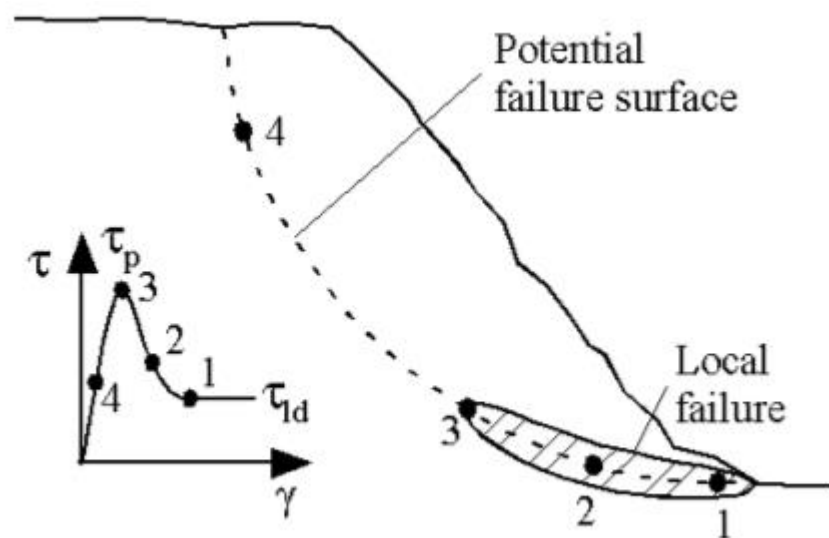


Figure 2.5. Progressive failure along a circular failure surface, related to the shear stress/strain curve. At points 1 and 2, the soil is becoming fully remoulded as a result of local failure, at point 3 there is a sharp strain increase, and at point 4 strain gradually increases from loss of underlying strength (Locat *et al.* 2011)

2.12 Strain Localisation in Clays

Tri-axial testing of clays is a feature that has been studied for a long period of time, with new discoveries on strain localisation and changes in propagation of shear failures being observed in recent studies (Thakur *et al.*, 2014). Strain localisation is a feature that occurs prior to strain softening where strain within a sample localises in one or two areas and the stress on the sample focuses along a specific plane (Gylland *et al.*, 2014; Thakur *et al.*, 2014). The degree of strain softening and degree of localised failure can often be attributed to failure type and rate of shearing, with higher rates of compression accounting for higher levels of

strain softening. Figure 2.6 below derived from Thakur (2011) shows this well. Though a key feature across all of this was identified that for any form of failure pore pressure migration and localisation in the sensitive samples is vital.

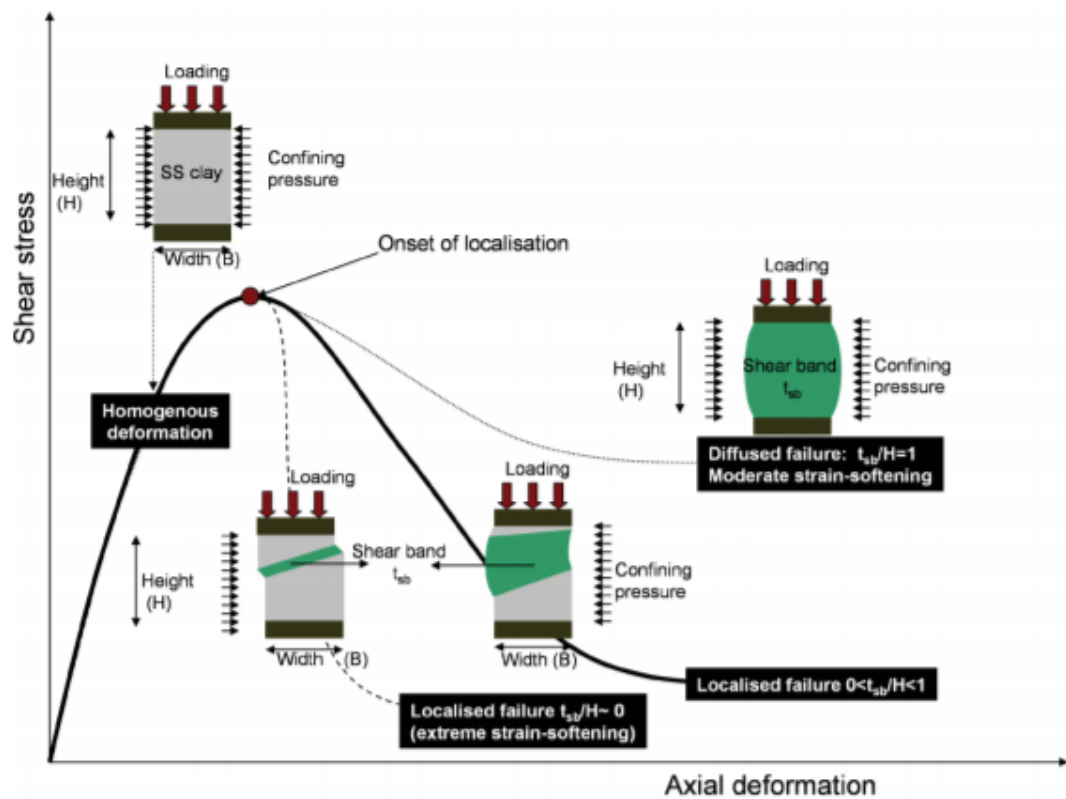


Figure 2.6. An idealised diagram of Thakur’s strain modelling, showing a shear band with decrease with increasing deformation rate. The shear bands thickness is dependent on post-peak strain softening of sensitive clays (Thakur, 2011).

When examining stress strain curves, the form of failure can be observed, with the brittleness of a failure being able to be defined accurately. Rapid strain softening follows failure, shifts to less brittle failure are associated with less localised strain, resulting in reduced strain softening of a sample (Gylland *et al.*, 2013; Gylland *et al.*, 2014; Thakur *et al.*, 2014)

2.12.1 Riedel Shears

During shear failure, shear bands are known to form along a specific axis, with shear propagating within a zone as pore pressures localise and spike, allowing deformation and shearing of a sample. During this process, several sets or types of shears occur in a well-defined pattern, though the sequential evolution of these shears is not well understood. First described on a much larger scale for features dealing with tectonic evolution and failure on a large scale (Skempton, 1966).

Morgenstern & Tchalenko (1967) adapted these large scale shear evolutions to a smaller scale, such that these concepts have been applied to tri-axial size testing. To date the most accepted model of the propagation of these shears is that first antithetic riedel shears (R and R') evolve during the early shearing process (Skempton, 1966). The orientation of these riedel shears is directly related to the friction angle (Φ) present within the soil or rock media that is being tested. The ideal angle of these R and R' shears proposed to be at 61° from the PDS (Figure 2.7), though in reality this is in ideal conditions (Morgenstern & Tchalenko, 1967). Thrust shears (P) form later during shearing, and are directly related to the primary displacement discontinuity (PDS), otherwise known as the first order shear. P shears are oriented at an angle of $45^\circ + \Phi/2$ to the PDS.

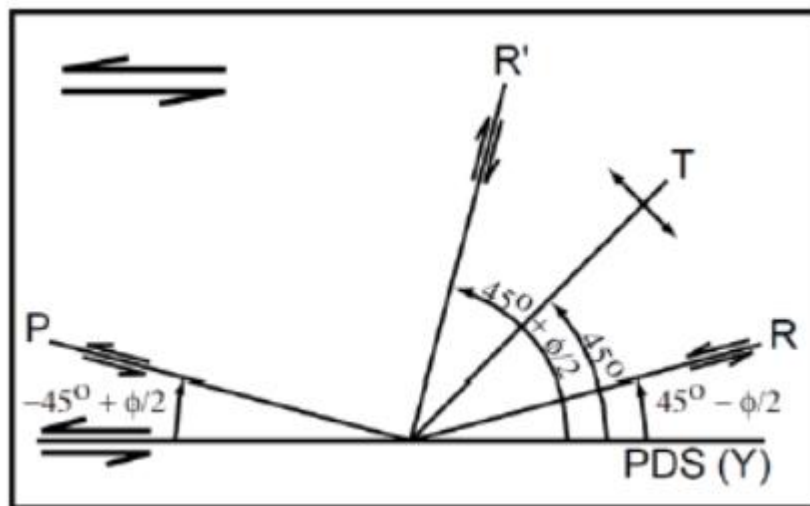


Figure 2.7. The relationship between the orientation of Riedel shears and thrust shears to the friction angle (Φ) of the material (Ahlgren, 2001 after Skempton, 1966)

CHAPTER 3

METHODS

3.1 INTRODUCTION

This chapter outlines the various field and laboratory methods utilised during this study. Where applicable, international standards were followed as closely as possible, and in a number of instances methods used by previous studies have been adapted. Methods described include all methods used during the collection of samples and experimentation on the resultant samples, as well as the field methods utilised during the mapping of failures within the peninsula that occurred during the study.

3.2 SOIL TREATMENT STUDY

The discussion of methods related to the soil treatment study have been split into a number of sections, including methods used for collection of samples in the field, the standards and adaptations used during measurement of Atterberg limits, and all methods used during triaxial testing of soil cores. Where possible ISO standards have been followed as closely as possible to ensure highest accuracy and replicability of results.

3.3 Field Methods

To ensure comparability between tests undertaken in this study and previously published results for the Bramley Drive site, soil cores were collected from the same ‘bench’ found at the base of the landslide upon which samples had been collected previously ((Wyatt, 2009; Cunningham, 2012; Mills, 2016; Kluger *et al.*, 2017). Figure 3.1A details the area that samples were taken from. When sampling was undertaken a smaller sub-bench was dug approximately 50-100 centimetres into the face of the slide, this was undertaken to ensure that the soil to be used in lab testing was as close in both make-up and moisture content to the soil that is found *in situ* deeper within the slope. Furthermore, due to the presence of halloysite as the dominant clay mineral present within the soil, it was vital that any potential sources of the dehydrated 7Å halloysite near the exposed surface were avoided as this could have a significant impact on the planned treatments. Soil cores

were spaced across the bench (Figure 3.1B), with the soil surrounding the cores taken as bulk sample to be utilised in Atterberg limit testing.

A



B



Figure 3.1. (A) The Bramley Drive landslide as seen from the edge of the shore platform via drone. The image highlights the former location of the sampling bench, indicated by the red circle, of which has since been covered by material from the upper slope. Image used with permission from the Western Bay of Plenty Council (WBOP, 2017). (B) After a bench was dug into the slope face at a sufficient distance to ensure that material would contain as little dehydrated halloysite possible soil cores were driven into the soil in a pattern as shown in the image, note large iron pans passing through the bench were avoided. Source Robertson, 2017.

3.3.1 Soil Coring driving and extraction methodology

12 samples were extracted from the bench with the soil extracted via 150 x 50 mm stainless steel soil core holders. Core holders were gently driven into the bench, with the area chosen for each core away from any visible cracks on the soil surface, or iron bands that were obvious on the soil surface. The cores were gently pushed into the soil to ensure that no air would be trapped in the corer and the soil was flush on the sides of the core, while avoiding compaction. Cores were driven in until the top of the soil within the core reached within 20 mm of the upper corer lip, with space left in the top of the core.

Following this soil was dug away from around the core, and the bottom end of the core was cut at the base to give an excess of approximately 30 mm of soil extending from the soil cores base, allowing for this to be trimmed before transport. Soil removed from around the core was taken for bulk soil storage to be utilised in Atterberg limit testing.

3.3.2 Soil core transport and storage

Regardless of how well sampled the soil may be or the high quality of the sample if the particular soil sample is stored in an improper manner following extraction it can lead to significant issues during lab testing as a result of drying of sample and loss of sensitivity. Lessard and Mitchell (1985) highlighted the importance of storing and transporting sensitive soil samples in a proper manner as improper storage and transport can lead to a drying of samples and a loss of sensitivity (Lessard & Mitchell, 1985; Rochelle *et al.*, 1986b). Furthermore, the importance of sensible storage is highlighted by the propensity of halloysite to dehydrate from its 10.1Å to its 7Å form, which has the potential to cause noticeable issues during further testing due to the resultant impact on restricting intercalation of products be it H₂O or salts (Hughes, 1966; Bailey, 1990; Joussein *et al.*, 2005). As a result, a specific storage method was developed for soil cores following extraction. The process for storing the soil cores from point of extraction was as follows:

1. Soil core was trimmed, with excess soil at base of core trimmed such that the soil on the base of the core was flush with the stainless-steel core holding it.

2. The entire sample was then sprayed extensively with distilled water so that the entire sample was moist. The top of the soil core was then covered with parafilm to ensure it was sealed.
3. The sample was then wrapped in 2 layers of cling film, ensuring that no air was present while wrapping.
4. Each cling film layer was sprayed once again with distilled water to ensure that it was sufficiently moist.
5. Steps 3 and 4 were repeated a minimum of 3 times, following this it was then wrapped 4 times with cling film to ensure that the soil core was unaffected by outside conditions.
6. The wrapped soil cores were then placed in a first sealable bag, which the air was then extracted from and sealed before being placed into a second larger bag with other samples.

This method was utilised as it was regarded as being the best method possible for ensuring that the soil within the core would remain at field moisture level and would not dry out in any way.

3.4 Laboratory Methods

3.4.1 Atterberg limits and treatment methods

Moisture content and bulk density were calculated from methods laid out in NZS 4402 (1986), with Atterberg limits determined through the usage of international standards (ISO/TS 17892-12:2004 (E)). Atterberg limits were determined using a cone penetrometer on homogenous soil pastes as opposed to Casagrande cup for determination of liquid limit, and rolled threads for plastic limits. This undertaken due to the high variability of results between operators that is known to occur when using Casagrande cup.

Initially a single large homogenous paste was created from the bulk samples collected using distilled water as the mixing medium. This homogenous paste was split into 7 smaller separate samples to be used with each treatment of salt and distilled water, while having an excess prepared in case of sampling error and specific tests requiring repetition. For the baseline tests, further distilled water was added at differing quantities such that an evident change in moisture content within the soil could be observed. The remaining sub-samples were tested in the same way but with appropriate salt solutions used to increase the moisture content of the paste. A minimum of 7 moisture content points was measured for each treatment. At each

moisture content, approximately 10 grams of soil was taken and placed into a prelabelled and weighed aluminium tin. The tin was then weighed with the soil inside of it and placed into an oven at a temperature of 105°C. The soil was then left in the oven for a period of 72 hours to ensure all moisture was removed before being taken out and placed in a desiccator for a period to cool down to room temperature and stabilise (24 hours). Following this they were weighed a first time, before being placed back in the oven for another 24 hours, cooled and re-weighed. Plastic limits were taken at the start of both tests for all samples, with a small sample taken initially before any treatment to ensure that initial plasticity for all samples was similar, and following the first treatment a section was taken and plasticity of this sample was measured. All salts were made up to 2 mol L⁻¹ by University of Waikato soil laboratory technicians in accordance with international standards.

During the course of testing further measurements were made of soil pH, two differing methods were used due to conflicting indications from literature of the appropriate method to measure soil pH on soil pastes. The first method was adapted from Torrance (1999) in which a pH probe is inserted directly into the soil paste and the pH is measured of the soil while undergoing treatment.

The second method was adapted from the soil science handbook, a method that is used as standard for a wide variety of agricultural applications in soils and measures pH by allowing a set amount of soil to dry till air-dry. Once air dry the soil is crushed and mixed vigorously with distilled water, with the approximate ratio of soil to distilled water at 1:4. Once mixed the soil water mixture is left for 24 hours to allow the settling of sediment such that the sediment and water mixtures are separate, with the intention that any pH changes that have occurred in the soil will be reflected in the water media. After the 24 hours has ended a pH probe is inserted into the mixture, with the end of the probe placed as close as possible to the sediment water interface without directly touching the sediment. Following this the pH is measured and recorded. The characteristics of the sediment mixtures were also recorded at time of pH measurement, with particular focus given to whether mixtures were still dispersive or coagulated.

3.4.2 Soil core treatment

Following identification of a solute that produced favourable results, this solute was then produced in larger quantities at the same concentration by Waikato University laboratory technicians. To achieve this soil cores were taken out of their

wrapping and placed into 30 litre UV protected plastic buckets. 4 cores were placed into the base of each bucket before being covered by approximately 2.5L of the solute, enough to ensure that cores would be completely covered, with approximately a 10cm buffer between the top of the soil core and the solution surface. After being covered with solution the conductivity of the solution shall be recorded to mark an initial conductivity measurement. This is undertaken as it provides a method of recording potential exchange between the clay within the soil and the solution of ions, with it expected that as time progresses conductivity within the solution will reduce as more ions are taken up by the clay. Following measurement of conductivity, a lid was placed on the buckets, forming an air-tight seal and the buckets were stored in a cool, dark place where temperature would be stable at approximately 20°C. Buckets were then opened once every week and conductivity was measured to determine the varying conductivity over time.

3.4.3 Tri-axial testing

When examining various soils effective strength and the formation of shear banding within certain soils, a variety of methods can be used. These include through biaxial direct shear testing (Thakur, 2007), static triaxial shearing (Gylland *et al.*, 2014) and dynamic triaxial shear testing (Mills, 2016).

In previous studies Mills utilised tri-axial tests to examine fracture development in soils of a similar nature and proximity. Within this study we replicated the conditions used by Mills to allow for comparability of results for untreated soil cores, and furthermore allow for a comparison to treated samples and how the fracture zones vary between them.

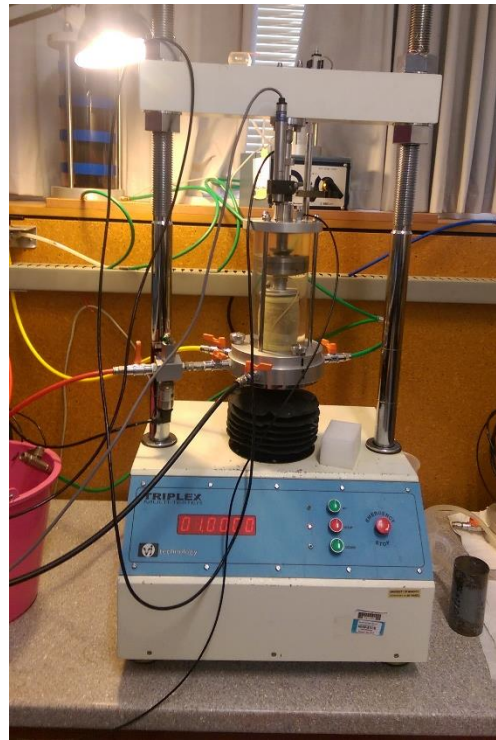
Three confining pressures were utilised during tri-axial testing, these derived from the estimated *in situ* pressures as described by Mills (2016). These were: 205 kPa; 280 kPa; and 355 kPa. These confining pressures were chosen as they best displayed conditions that a soil may be if under saturated, at field saturation and over-saturated during a storm rain event respectively. Consolidated, undrained (CU) tests were used, as these allowed for comparison with previous results.

3.4.4 Triaxial apparatus

A VJ Technology Triplex Multitester triaxial tester was used (Figure 3.2A). A simplified view of this set up can be observed in figure 3.2B below. The system was for the most part automated with cell strain, pore pressure and stress all

measured by electronic sensors within the apparatus. Cell and back pressure was manipulated manually by the increasing or decreasing of the pressure of air within two self-contained butyl air bladders. All water used during testing, whether in the cell with specimen or in the air bladders was initially de-aired to ensure no air bubbles would affect testing. Vertical strain was measured via a linear displacement sensor on top of the cell. Soil cores were extruded using a hydraulic soil core extractor, samples were extruded carefully while ensuring as little time as possible between extrusion and testing, this was done to ensure the samples had as little contact with the air as was possible to prevent any potential dehydration of the sample. Samples were trimmed and weighed prior to being placed into the apparatus, with trimming occurring to ensure the sample fits into the tri-axial tester and to ensure that the soil present is flush and fresh as possible.

A



B

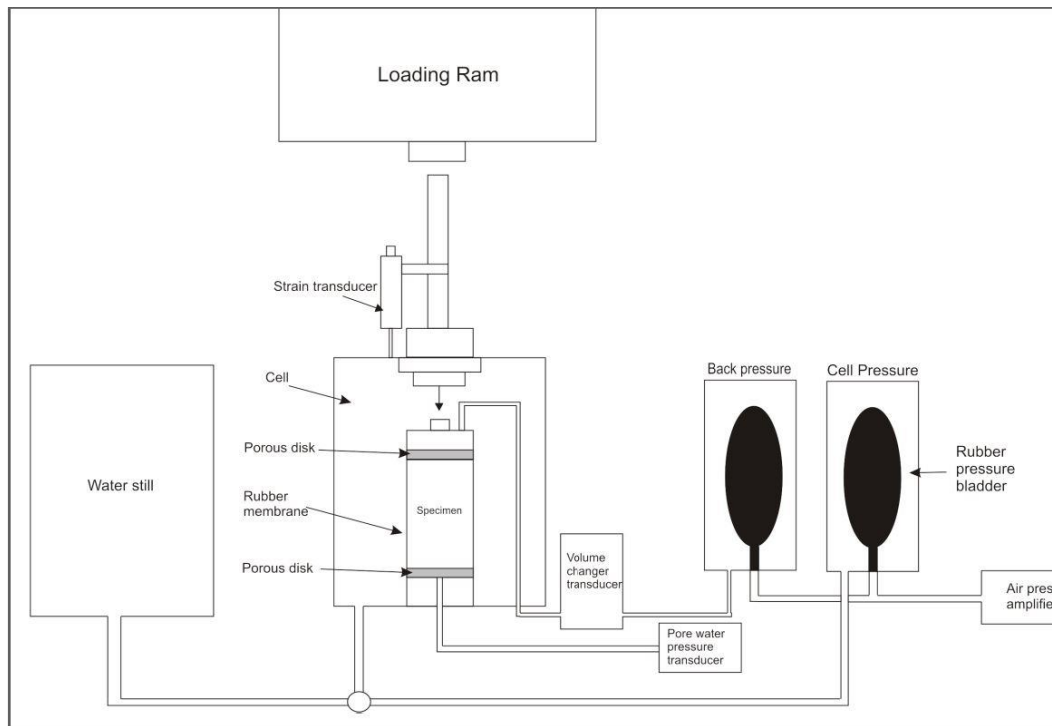


Figure 3.2. (A) The VJ Technology Triplex Multitester Tri-axial apparatus shown in use in the image above, was used during the course of this study. Bladders controlling cell pressure and water still are not shown in this image. (B) A simplified view of the tri-axial apparatus used during the course of this study Source: Cunningham, 2012.

3.4.5 Test Procedure

For each set of tests 3 samples were tested at the 3 differing confining pressures. Each sample took approximately 2 days to fully complete the test. Within each test approximately 5-8 hours was spent on sample consolidation, while 16-24 hours was taken to consolidate samples. In contrast samples only took 2-4 hours to shear. Data was recorded on a 16 Channel VJ Technology MPX 3000 data logger, with the data then transferred to WINCLISP software on a computer that displayed the raw data in graphical form. This data was then downloaded in raw CSV format before being converted to excel format where it was analysed for various geomechanical properties.

3.4.6 Saturation

Saturation of a sample is undertaken prior to consolidation so as to ensure all voids and pores within the soil specimen are filled with water. This is achieved by incrementally raising the pressure of both the cell and the pore pressure within the soil to a value that is greater than 300 kPa, which is the known pressure of the dissolution of air into water. During saturation, as stated in the BS 1377:8 (1990), cell pressure was incrementally raised by 50 kPa, followed by an increase of back pressure to a point such that the back pressure was 10 kPa less than that of cell pressure. After raising cell pressure, the pore water pressure within the sample was left to settle to a constant with back pressure between increments. Between increments the change in pore pressure was measured to calculate a B value (Equation 3-1). Pressure increments continued until the B value was $B \geq 95$, at which point the sample is considered saturated.

$$B = \frac{\partial u}{50} (\%) \quad (3-1)$$

3.4.7 Consolidation

Following saturation, the back-pressure valve was closed off. At this point cell pressure may be in the order of 450-500 kPa following saturation. To achieve consolidation the sample is required to be at a cell pressure reflecting confining effective stress. As a result, following saturation and closing of the back pressure, the internal cell pressure is regarded as being zero regardless of the measured value. As such the cell pressure is then raised by the relevant effective stress value i.e. 205kPa for the lowest range, meaning if cell pressure prior to consolidation was

500kPa it would be raised to 705kPa during consolidation. The back pressure was then opened and readings of volume change and pore pressure change were taken at increments laid out in the BS1377:8 (1990) until pore water pressure reached a value that was equilibrated to back pressure (pore pressure >95% dissipation). Volume change was plotted against square root of time to determine testing shear rate for the compressional stage.

3.5 Soil core failure analysis

Following the shear failure of samples during triaxial testing, soil cores were extracted and samples were sketched in detail while still moist from treatment. Focus was on failure surfaces and the various deformations and shear surfaces that were present on the surface of the specimen. Following sketching, pictures were taken of samples. The pictures of failed samples were manipulated in Adobe Illustrator CS7 to display in digital form the annotated failure surfaces and deformations on the samples. Following this samples were then trimmed down to expose the failure surface in a fashion such that thin section slides could be taken of the primary shear surface of the sample. By taking these thin sections, it allowed for the identification of key failure mechanisms along the primary shear surface as well as examining any potential propagated riedel shears that have, in previous studies (Mills, 2016) propagate along the primary shear zone. Furthermore, it allows for the identification of singular minerals and how these distribute and affect failure of a sample.

On top of this following identification through optical microscopy of thin sections, specific thin sections which contained minerals and conglomerates that were difficult to identify and features that under normal visible microscope were unable to identify the thin sections were run through a Scanning Electron Microscope at the University of Waikato. Standard Operating Procedures for SEM at the University were followed with the SEM gathering details pertaining to images at a variety of magnifications, single element identification of specific areas as well as element distribution on a specific area of thin section to allow for a higher degree of information on specific minerals.

CHAPTER 4

GEOMECHANICAL PROPERTIES- ATTERBERG LIMITS & TREATMENTS

4.1 Chapter Outline

This chapter will outline the first section of the results that were collected for this thesis. The focus of these results is the initial trials conducted on the soil of the Bramley Drive slide to first determine which salt is the best to use in attempting to raise soil shear strength. Atterberg limits for treated and untreated specimens are presented together to allow for a comparison of the varying results with consideration of the changing conductivity and ion uptake of the soil cores in solution.

4.2 Atterberg Limits

Table 4.1. The table below details the various Atterberg limit results that were measured during this study. These include the results for treatment of the soil with Distilled water, KOH, K₂CO₃ and KCL. Also included in this table are the results produced by Mills (2016) in her study as well as the results given in Moons (2016) review paper.

Sample	Liquid Limit (%)	Plastic Limit (%)	Plasticity Index (%)	Liquidity Index	Activity (%)
Distilled(Moon 2016)	100	53	47		1.2
Distilled (Mills, 2016)	66	41	25	2.9	0.4
Distilled	92.3	78.2	18.98	0.37	1.11
KOH	83.5	72.4	11.1	0.72	0.65
K ₂ CO ₃	92.6	73.4	19.2	0.42	1.13
KCL	79.3	74.5	4.8	1.22	0.28

Table 4.1 shows the results gathered for both the various treatments that were used during the course of testing as well as the ‘baseline’ test that was conducted for distilled water. The distilled water values that were derived during testing for Mills and Moons 2016 testing have been added to this table as points of reference to the results gathered in this test. As can be observed, Plastic Limits for

all soils tested in this instance were relatively high, with results produced ranging between 72 – 78%, noticeably higher than those measured in previous studies on the soil from Bramley Drive.

In contrast to this of the treatments conducted, Potassium Carbonate (K_2CO_3) was the only treatment on the soil that did not result in a net negative effect on the soils' liquid limit, with it slightly raising the liquid limit from the baseline value of 92.3 for distilled water to 92.6. Results gathered for liquid limits for this test were closer in similarity to those in previous studies with Moons' results producing a liquid limit of 100, similar to our distilled value of 92.3, with this said our liquid limit result was still markedly higher than that measured in Mills' 2016 study.

4.2.1 Distilled Water- Baseline Test

Figure 4.1 below plots the cone penetration versus moisture content for treatment of the soil paste with distilled water. The solid orange line represents the point at which a soil is determined to have reached its liquid limit. A trendline was fitted to the results gathered and the line equation and r^2 value were determined, and as can be observed the data points gathered fit well with the trendline fitted, with an r^2 value of 0.95 produced. The trend shows a relatively gentle net positive increase in penetration as moisture content increases ($y=0.7699x-51.123$). Standard errors were 2.7,1.4,4.5,3.6 and 1.3

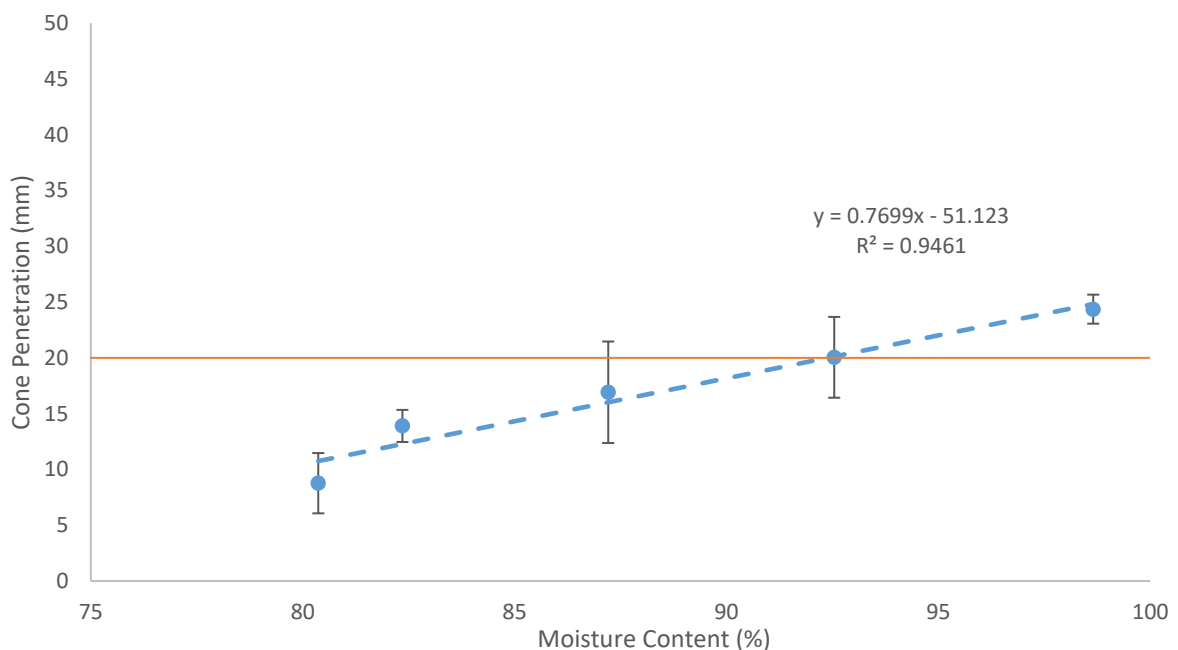


Figure 4.1. Results for the degree of cone penetration in mm at differing moisture contents for soil treated with distilled water. The orange line represents the point of

cone penetration that is regarded as the liquid limit. A line of best fit (dashed blue) was applied to the results, with the equation for this line and R^2 value displayed on the graph.

4.2.2 Atterberg Limits- Potassium Chloride Treatment (KCl)

The treatment of soil with KCl (Figure 4.2) produced a differing result to that derived by distilled water. As can be observed below, the orange line shows the point at which the liquid limit is expected in lieu of cone penetration of 20mm. All but the very first result for KCl were in excess of the liquid limit, with the results following a predictable trend with an r^2 value of 0.97. Furthermore the increase in penetration was somewhat sharper than that of distilled, with gradient being 1.2 as opposed to 0.8. Standard error was 0.4,6.6,0.6,2.7 and 4.6 respectively.

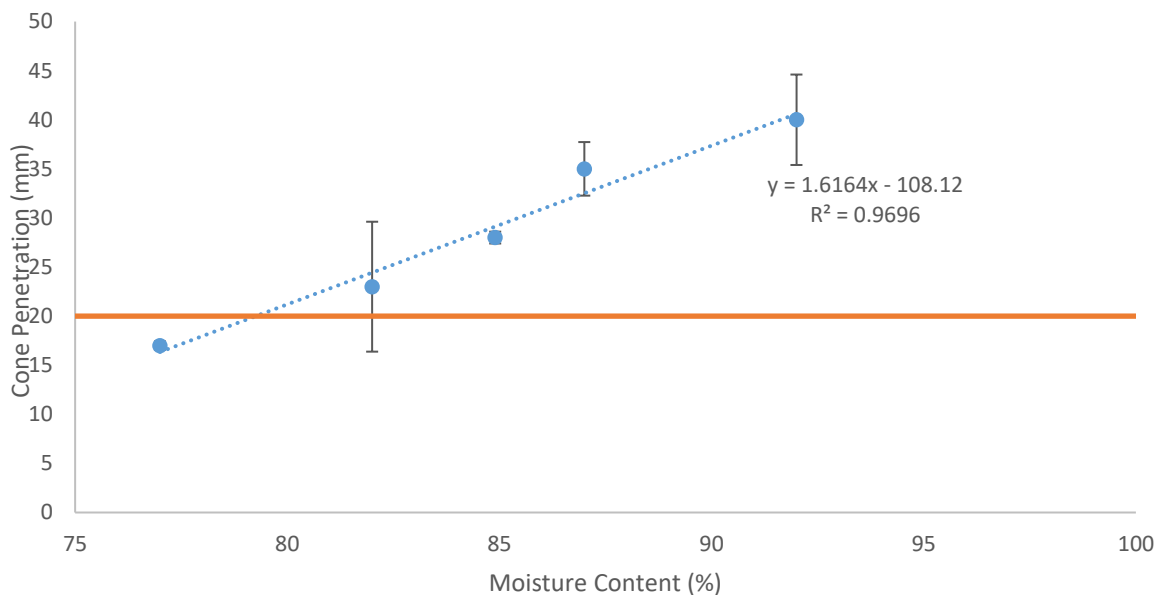


Figure 4.2 Results for the degree of cone penetration in mm at differing moisture contents for soil treated with KCL. The orange line represents the point of cone penetration that is regarded as the liquid limit. A line of best fit (dashed blue) was applied to the results, with the equation for this line and R^2 value displayed on the graph.

4.2.3 Atterberg Limits- Potassium Hydroxide treatment (KOH)

Treatment with KOH produced a result not overly dissimilar to that of KCl with 2 out of the 5 results collected for cone penetration falling below the point at which liquid limit is derived, the actual liquid limits relatively low at 83.5% moisture content. Figure 4.3 shows the general trend being shallower than that of

KCL with the gradient to failure being less than that of KCl, with this said the R^2 value was also lower at 0.83, showing considerably more variability.

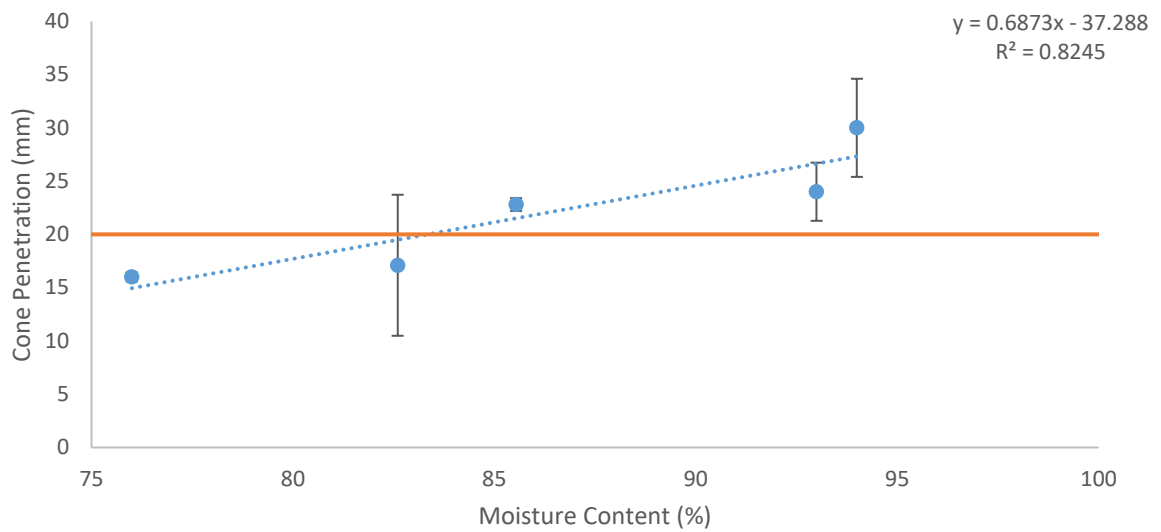


Figure 4.3. Results for the degree of cone penetration in mm at differing moisture contents for soil treated with KOH. The orange line represents the point of cone penetration that is regarded as the liquid limit. A line of best fit (dashed blue) was applied to the results, with the equation for this line and R^2 value displayed on the graph.

4.2.4 Atterberg Limits- Potassium Carbonate treatment (K_2CO_3)

Figure 4.4 below details the changing degree of penetration during testing for treatment of soil paste with Potassium Carbonate. The orange line on the graph represents the point at which liquid limit is usually derived on the basis of cone penetration. From the graph, it can be seen that the bulk of the results collected were below the point of liquid limit. The results were well correlated to forming a trend with an R^2 value of 0.93 produced, with one result falling below the trendline.

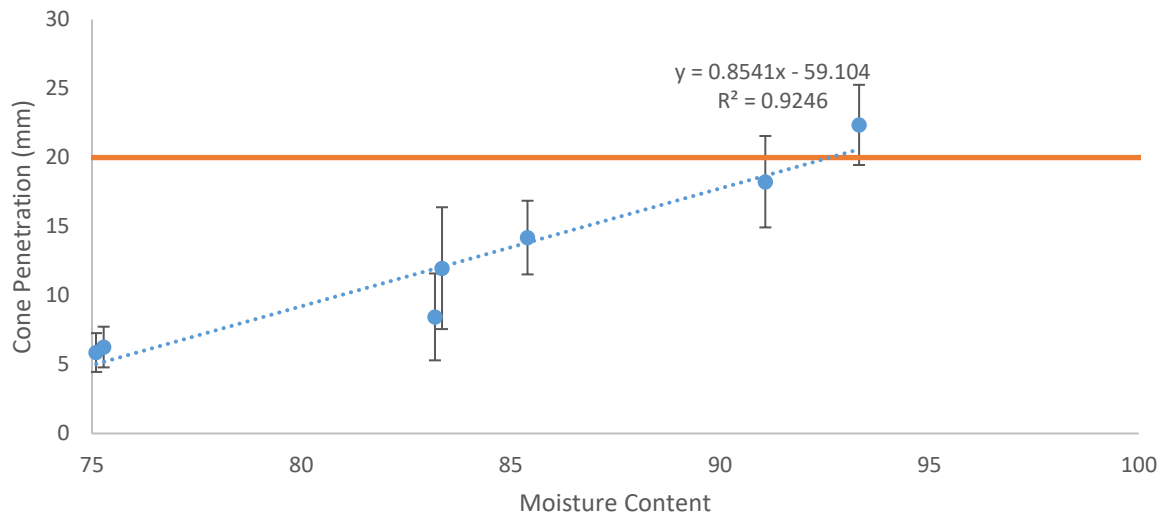


Figure 4.4. Results for the degree of cone penetration in mm at differing moisture contents for soil treated with K_2CO_3 . The orange line represents the point of cone penetration that is regarded as the liquid limit. A line of best fit (dashed blue) was applied to the results, with the equation for this line and R^2 value displayed on the graph.

4.2.5 Atterberg Limits- A line chart

A chart that was outlined in 1952 (Skempton & Northey, 1952), the A-line chart is a tool of comparing liquid limit of a soil to its plasticity index to determine characteristics of a soil, as to whether it is a clay, silt or sand along with the degree of compaction and potentially any organics. It is a useful tool to determine if any major changes in characteristics of the soil have occurred following a changing of a soils makeup. Figure 4.5 shows the A-line chart produced from the results collected during the course of this experiment as well as the results produced in Mills and Moons' (2016) investigations.

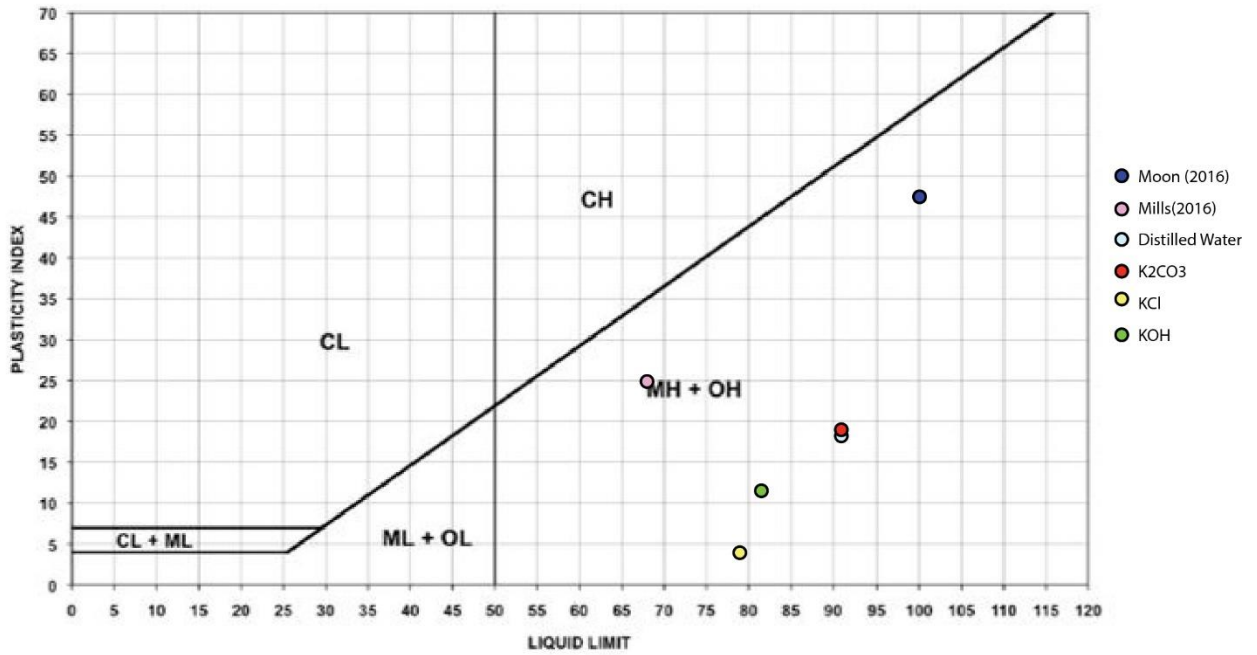


Figure 4.5. Adapted from Skempton & Northey (1952), the A-line chart above plots the relative Liquid Limit and Plasticity Indexes of the results gathered in this study, Mills (2016) study and Moons (2016) review. The colour of the dots correspond to the respective treatments as indicated on the left hand side of the diagram.

4.2.6 Atterberg Limit pH changes

Table 4.2. pH's of the differing treatments applied to the soil are displayed in the table below. Two methods were applied due to the lack of consensus in literature of a clear method to use when measuring the soil pH of a remoulded clay paste.

Sample	pH paste	pH air dry
Distilled	5.3	5.5
K ₂ CO ₃	10.3	10.4
KOH	8.03	8.32
KCL	5.02	4.85

Table 4.2 details the soils changing pH as the treatments occurred, through two methods, the results were averaged as can be observed and the results displayed below. There was little variance between the methods, with the natural pH of the soil being low at a pH of 5.3 and 5.5 measured. Of the treatments KCL had little effect on the pH (5.02,4.85), whereas KOH and K₂CO₃ both raised the pH to a point

where the soil could be considered neutral (pH=8.03 and 8.32) and alkaline (pH=10.3 and 10.4) respectively.

After observing all data collected it can be seen the treatment utilised that had a slight net positive effect when applied to the paste was that of K_2CO_3 , producing results that improved on that of distilled water, while all other treatments had a net negative effect on the rheology of the paste and weakened as opposed to stiffened the paste. As a direct result of this K_2CO_3 was chosen as the salt to apply as treatment.

4.3 Soil core treatment

Following the identification of an appropriate salt, which in this case was Potassium Carbonate, for the purpose of this research soil cores were submerged in the solute and left for a period of 3-4 weeks. As stated in the methods, the conductivity of the solute that 3 of the soil cores were placed in was measured once a week every week for the period of the cores soaking. Figure 4.6 below details the changing conductivity of the solute as time passed. During the first two weeks, there was evident significant uptake of ions from solution as conductivity of the solute dropped from 158 and 180 to 80 and 91 respectively, an average drop of 83.5 uS over the first week.

Following this there was a further noticeable drop from the 1st to 2nd week of treatment with a drop of 80 to 16, and 91 to 15, the average change around 70 u/s over the course of the second week of treatment. Following this there was a noticeable drop in the reduction of ion uptake by the cores with the change measured at the 3rd week only being drops of 6 u/s for each core treatment. Two lines can be observed on the figure below as two separate buckets of solute with 4 cores in were measured respectively to allow for both comparison the data produced as well as back up samples if issues were to arise during tri-axial testing of the samples.

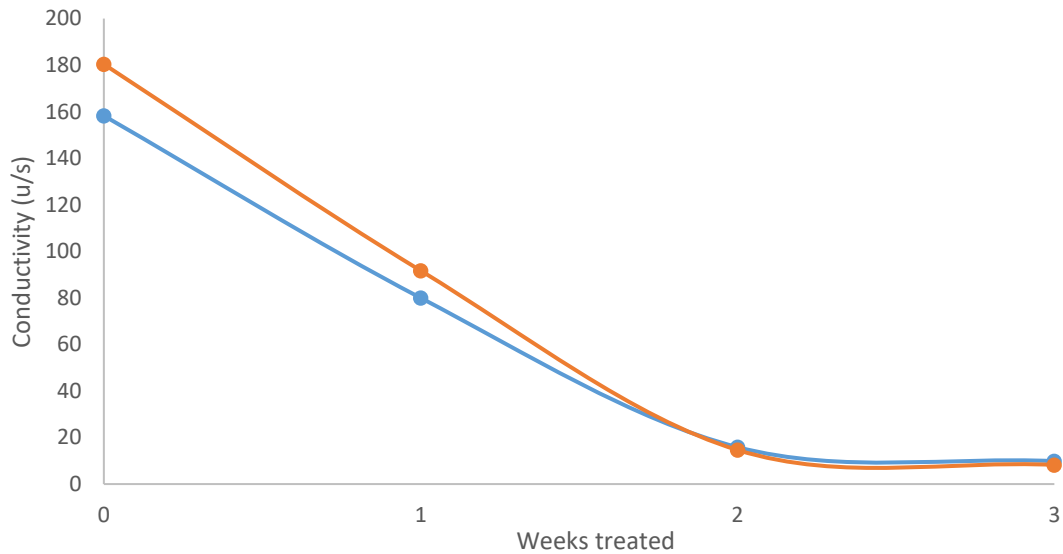


Figure 4.6. The chart above shows the changing conductivity of two separate sets of soil cores that were being treated independently, with each treatment having 4 soil cores within the solution. The conductivity was measured once a week every week prior to testing of the samples.

4.4 Atterberg and treatment summary

As can be seen from the data gathered during the course of treatment, though our results for plasticity did vary from those previously measured in literature (Mills, 2016; Moon, 2016), the liquid limit for our distilled baseline result was much closer to that of Moons 2016 study. It was of note that of the treatments both KOH and KCl had a negative effect, with the latter of the two treatments having a larger detrimental impact on the soils liquid limit. In contrast to this the soil paste treated with K_2CO_3 had a net positive effect on the soils rheology, where a positive effect can be regarded as a stiffening of the paste, by both lowering the soils plastic limit slightly from that measured for distilled as well as increasing the liquid limit, though only by a miniscule amount. A further point of notice is the changing pH of the soils as the treatments changed, with KOH and K_2CO_3 having greatest impact on the soil pH raising the pH to be neutral and alkaline respectively. From this it was determined that K_2CO_3 would be the solute of choice when treating the soil cores.

From this the soil cores were then treated with the solute and the changing uptake measured. From the measurements that were gathered the soil rapidly took on ions from solution during the first two weeks of treatment, with each week the solute conductivity dropping by approximately 75 micro-siemens a week.

CHAPTER 5

GEOMECHANICAL PROPERTIES – Tri-axial testing & Shear Fracture properties

5.1 Introduction

This chapter reports the main results produced by tri-axial shear testing. Failure paths (p' q') taken by the samples are presented together with consideration of strain and pore water pressure curves. Potential sources of error are also discussed. Furthermore, a final point will be examined in the post failure strain surfaces, with sketches presented of the various failed samples that were examined.

5.2 Tri-axial plots and tables

5.2.1 Results summary

Table 5.1. The table below presents a summary of the data collected during tri-axial testing of the untreated and treated soil cores collected from Bramley Drive at the three differing confining pressures.

Sample	Confining Pressure (kPa)	ϵ failure (%)	q failure (kPa)	u failure (kPa)	Strain Softening (%)
Un1	205	1.63	151	50	12
Un2	280	1.53	227	174	35
Un3	355	1.09	313	195	41
Tr1	205	0.78	343	123	24
Tr2	280	0.9	424	153	32
Tr3	355	1.11	386	170	25

Table 5.1 lists the key details of the tri-axial tests conducted on both the treated (Tr1-3) and untreated (Un1-3) soil core samples. A first key point to note is the (Hvorslev, 1961) reducing axial strain at point of failure as the confining pressure increased for untreated samples, with strain at failure falling from 1.63% to 1.09% as the confining pressure increased. For treated samples the strain at failure is typically

lower than for the untreated equivalents, and increases with confining pressure, with a shift from 0.78% to 1.11% evident.

There is also a marked increase in the peak stress measured across all samples following treatment at all confining pressures. We see a 227% increase in peak failure stress for lowest confining pressure, with a slight decrease in difference to 187% in peak failure stress for 280 kPa confining pressure, and only a 124% increase in peak failure stress achieved for the highest confining pressure at 355kPa. With this said, it is evident that as the confining pressure increased, the overall increase in peak failure stress decreased for the samples as it progressed.

Pore water pressure at point of failure showed an interesting trait, with the bulk of the treated samples showing a decreased pore pressure at point of failure compared with the untreated sample with the lowest confining pressure of 205kPa is the exception to this, with pore pressure decreased. Pore pressures in treated samples were 246% greater at 205kPa confining pressure, but markedly decreased with both 280 and 355kPa treated samples showing a decrease in pore water pressure at failure only exhibited 87% of the value derived for pore pressure at point of failure while treated.

Strain softening for untreated samples increased as the confining pressure increased (12-41%). In treated samples, strain softening was relatively consistent at ~24-32%, meaning that softening increased compared with untreated samples at low confining pressure, but decreased considerably at higher confining pressures.

When examining all the values together we can determine that at lower confining pressures the peak strength of the soil following treatment is more than doubled (227% increase), while strain softening is also doubled at these lower confining pressures also. This indicates that even following failure the remoulded strength of the treated soil will be greater than that of its untreated counterpart. As the confining pressures increase though, we can see that the degree to which peak failure stress is increased drops, with peak stress increases of only 187% and 124% measured for 280 and 355 kPa confining pressures. These can still be regarded as significant increases. Furthermore, the pore pressure at point of failure is noticeably reduced between untreated and treated samples at these points, with a relatively similar degree of strain softening measured for 280kPa across both samples, but a significantly decreased strain softening measured for 355kPa confining pressure. This indicates a potential for much greater residual strength within the soil.

5.2.2 Tri-axial Stress/Strain plots

Tri-axial stress versus strain plots are shown in figures 5.1 and 5.3 for untreated samples, defined by the blue coloured lines on the graph, and figure 5.2 and 5.3 for treated samples shown by the orange lines present on the graph. For untreated samples, it is vital to note that the pore water pressure transducer failed during the 205kPa untreated run, while also not recording data for a period during the 355kPa untreated run. No instrument errors occurred during the treated sample runs.

Figure 5.1 shows the untreated baseline value samples show an increase in both shear strain and pore water pressure. The pwp continues to rise following sample failure. In contrast, treated samples shown in figure 5.2 show a much more rapid peak failure point, though at a much higher value. The nature in which the PWP peak is reached and progression of the PWP during failure of the samples across both untreated and treated samples is similar. The comparison in figure 5.3 highlights this well, especially when regarding the PWP for both treated and untreated samples at 355kPa, with samples following an almost identical rise and fall progression as the measurements progress. This similarity is important as it indicates a consistency in the way in which the pores are acting within the samples, and indicates the water present in the sample, acts in an identical fashion regardless of the presence of the salt treatment.

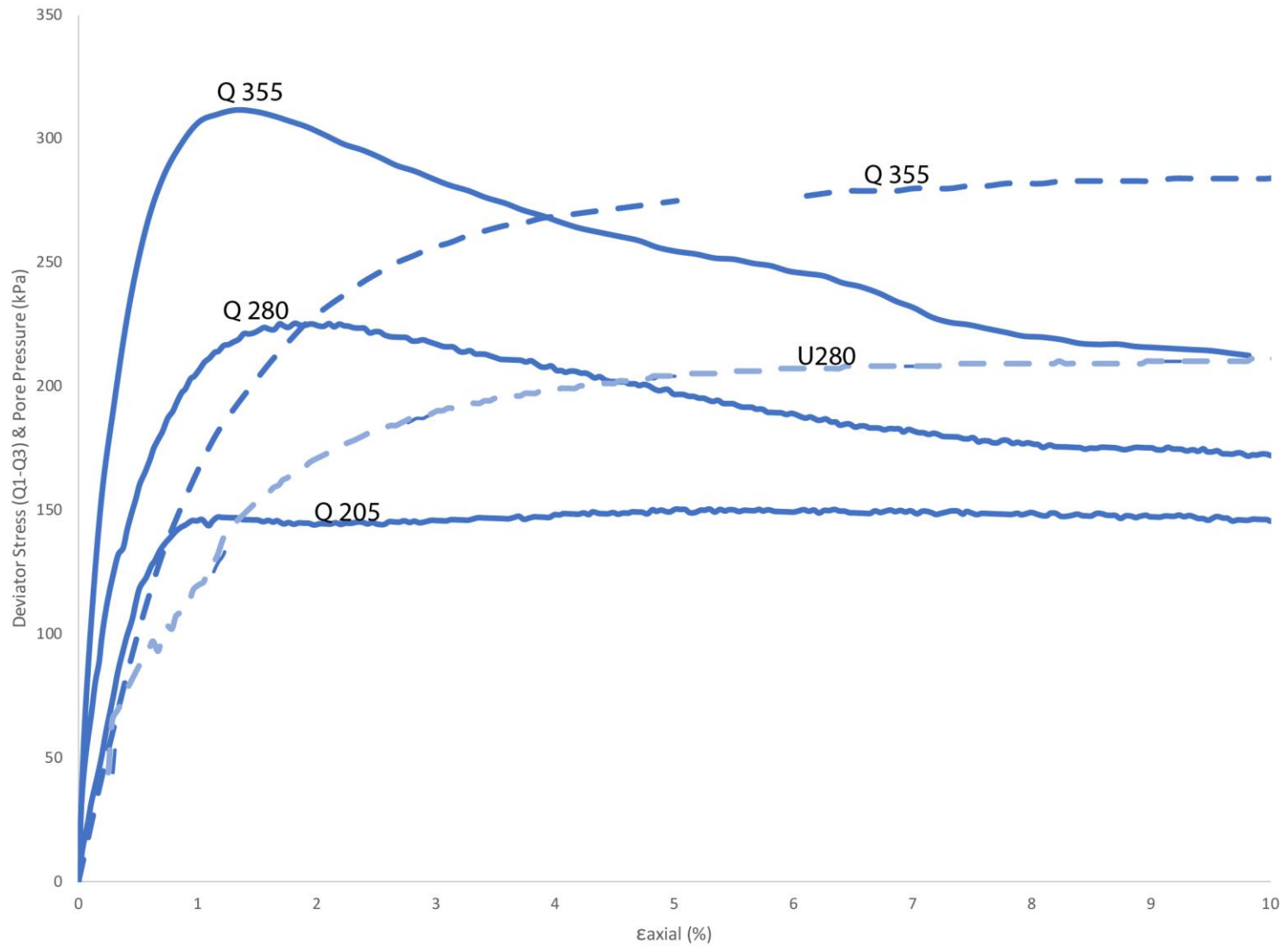


Figure 5.1. A stress versus strain plot derived for untreated soil core samples following tri-axial failure. Deviator stress (Q) is represented as the solid blue line, while pore water pressure (U) is represented by the dashed blue line. The results for specific confining pressures are presented on the graph.

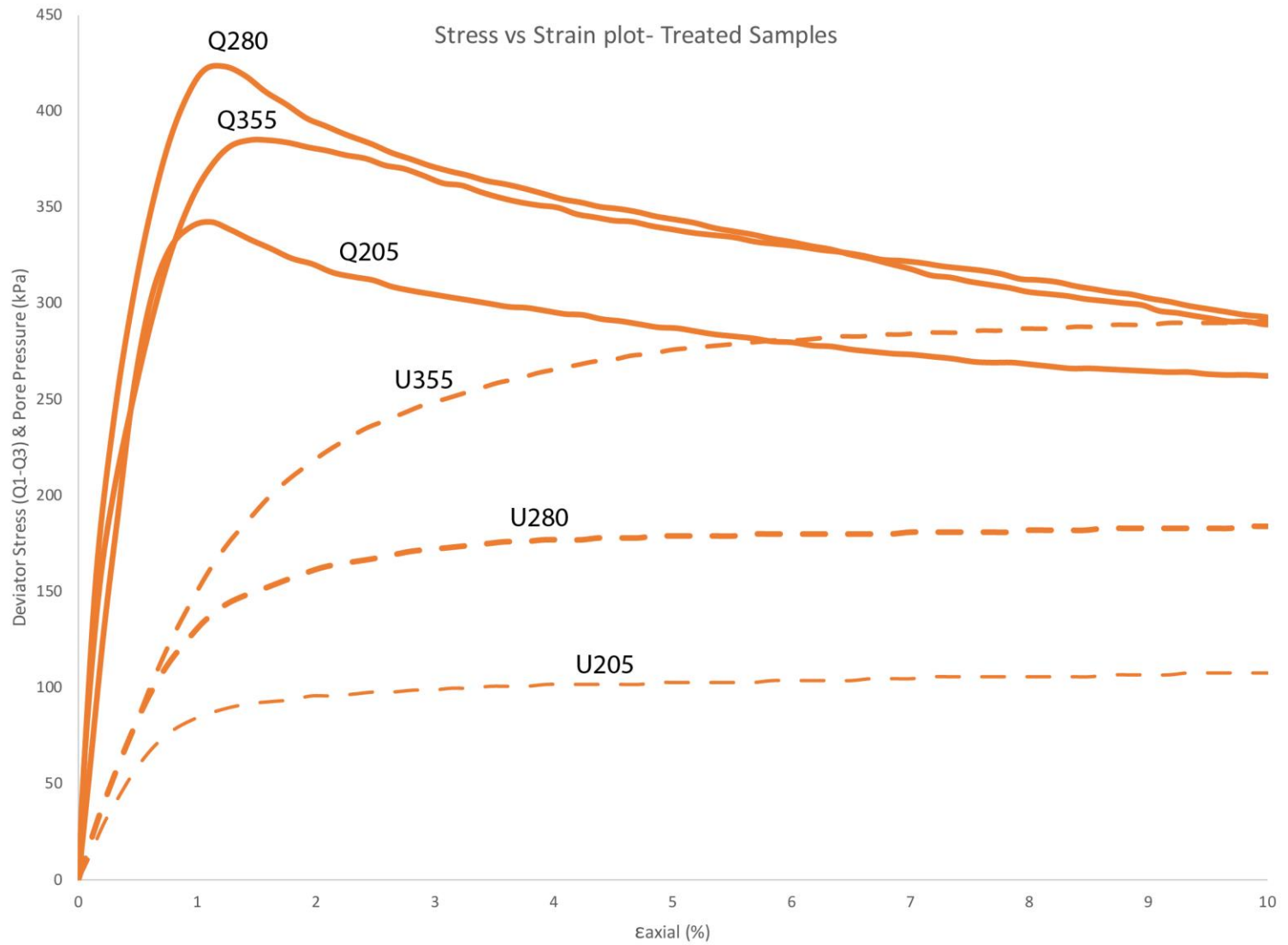


Figure 5.2. A stress versus strain plot derived for treated soil core samples following tri-axial failure. Deviator stress (Q) is represented as the solid orange line, while pore water pressure (U) is represented by the dashed orange line. The results for specific confining pressures are presented on the graph.

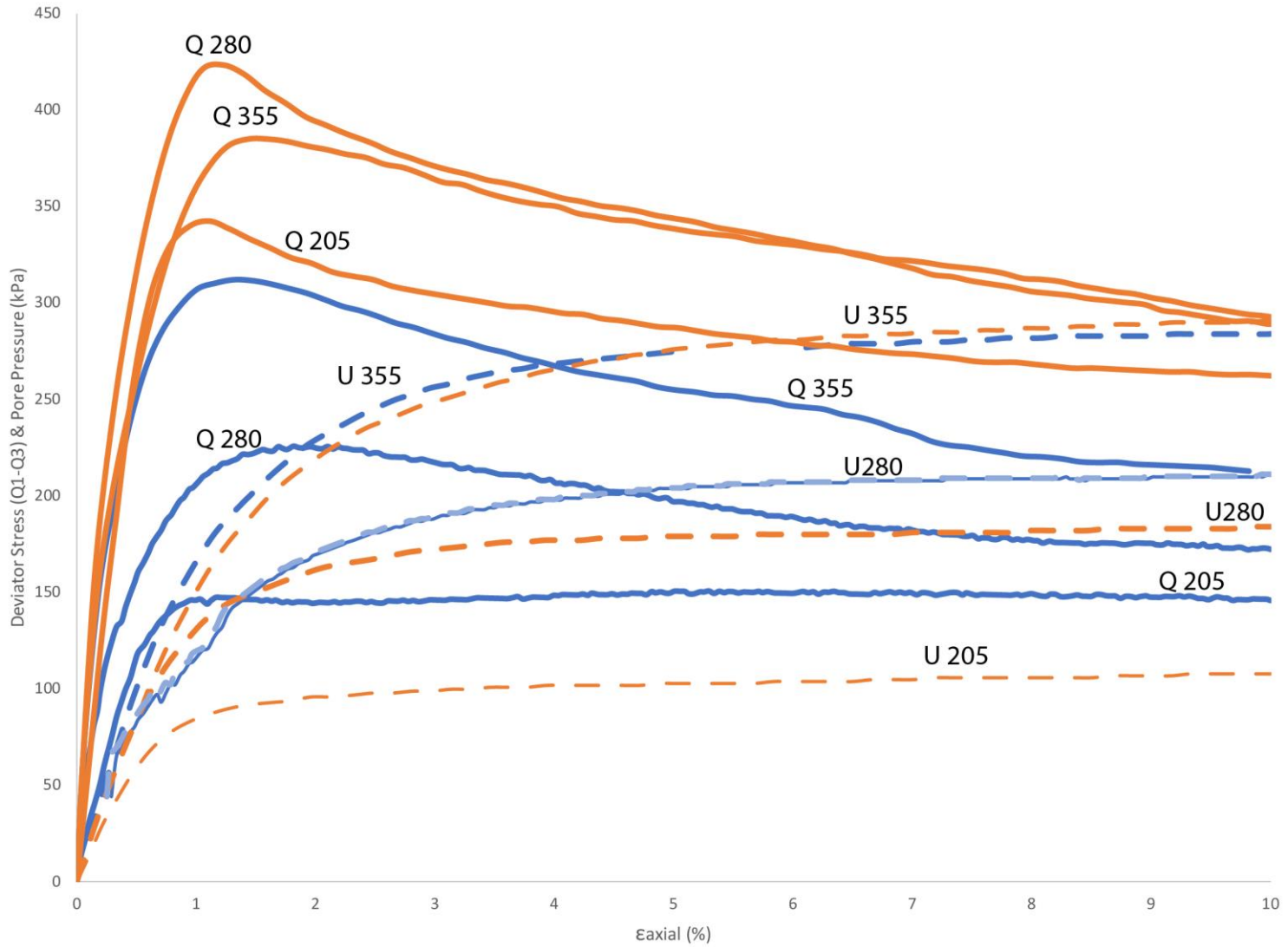


Figure 5.3. The graph above shows the stress versus strain plot for both untreated (blue) and treated (orange) samples plotted together on the same chart to allow for comparison of the results directly on the chart. Pore pressure (U) and deviator stress (Q) are shown by the dashed and solid lines respectively with respective confining pressures labelled.

5.3 Stress Path Characteristics

5.3.1 Stress Path Characteristics - Background

U

The use of stress paths in tri-axial testing is an effective method of measuring changes in behaviour of a material over time under differing effects, while also giving a strong indication as to the method of deformation the sample is undergoing. Prior to failure samples will undergo compression, causing samples to generally dilate and expand before reaching a peak failure value, with the sample undergoing what is known as strain hardening (Figure 5.4D). At the point of peak failure a sample reaches what is regarded as a critical state, whereupon following failure a sample will either contract, dilate or remain relatively stable dependant on the form of failure and materials that make-up the sample(Boulanger & Idriss, 2006; Briaud, 2013). Figure 5.4B details this for a sample undergoing contraction following failure, this form of failure is found generally in samples that are over-consolidated and have small grains (i.e clays and sensitive material). Failure in these instances is generally brittle with pore pressure increasing as the sample undergoes softening resulting in a net positive pressure being produced. In contrast if a sample undergoes ductile failure, usually found in over and normally consolidated sandy materials, the pore pressure acts inversely (Figure 5.4C), and produces a net negative pressure due to the drop in pressure, resulting in an increase in effective stress to accommodate this loss, with the sample dilating, resulting in further losses in pressure.

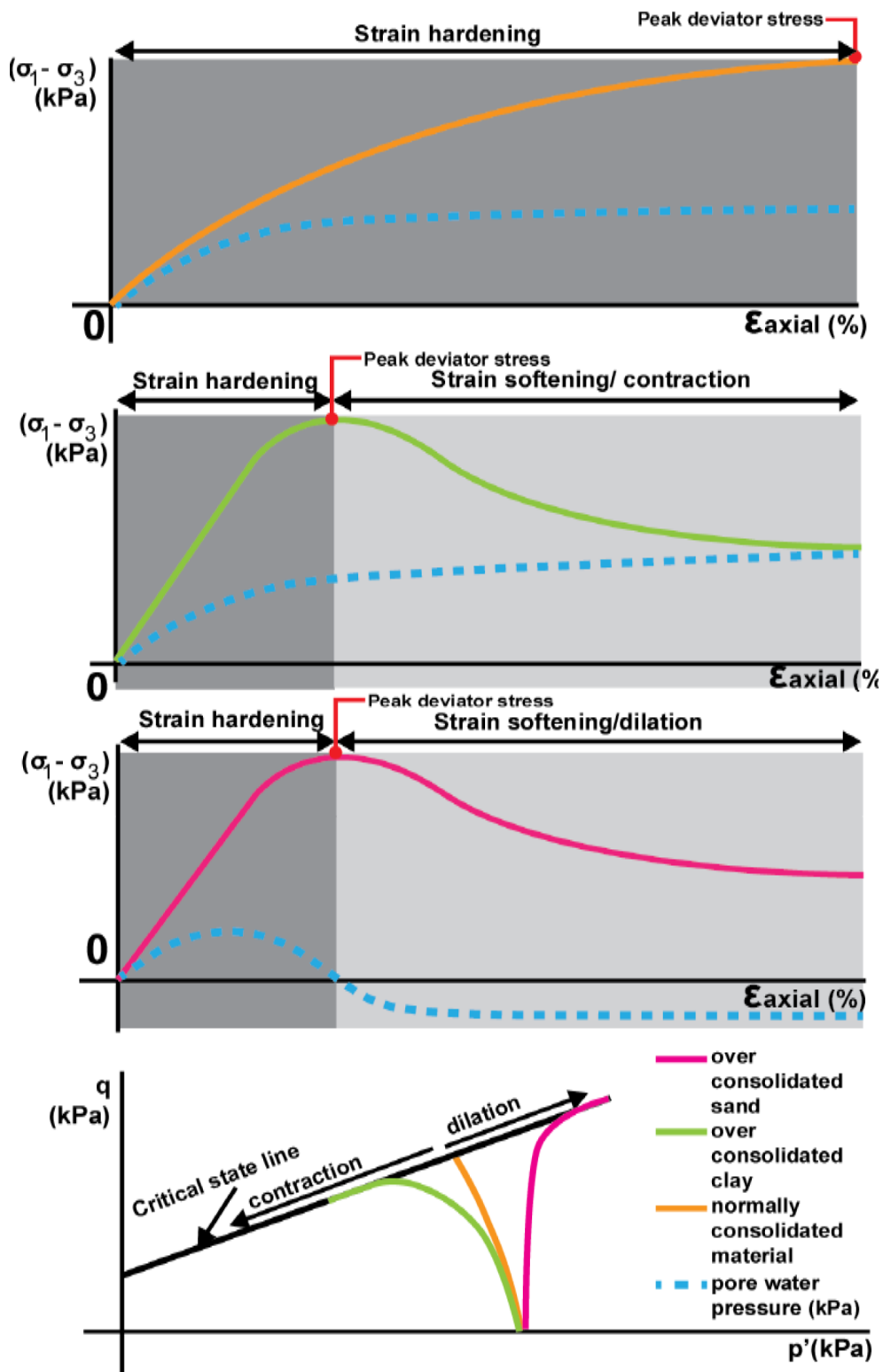


Figure 5.4. a-d (top to bottom). Schematics of the different behaviours expected for over consolidated sand (pink), over consolidated clays (green), and normally consolidated material (orange) for both q (deviator stress) vs axial, and p' vs q' (effective stress). Schematics are sourced from Mills (2016).

5.3.2 Stress Path Plots

5.3.2.1 Untreated Samples

Stress path plots for untreated samples were produced for only the 280 and 355 confining pressures (Figure 5.5) as the values produced during testing for the lowest confining pressure produced erroneous figures due to inaccurate pore pressure measurements made during sample testing for 205kPa. Furthermore, data was also omitted for the lower portion of the 280-confining pressure p' - q' plot due to the similar erroneous measurement made by sensors during testing. Both samples plotted in figure 5.5 show a very strong trend to the left following peak failure, indicating that samples for both 280 and 355 kPa confining pressures underwent significant contraction following evidently strongly brittle failure. The significant curvature of the p' - q' plots furthermore show no clear failure point, with contraction of samples occurring before reaching the critical state line.

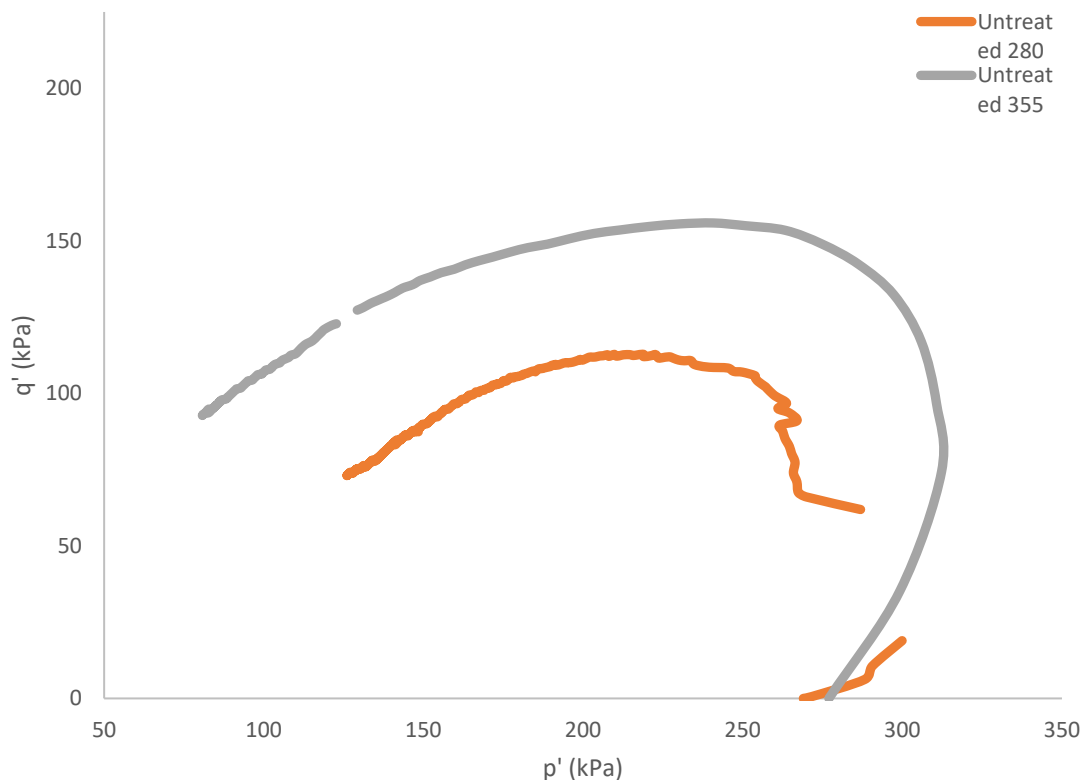


Figure 5.5. Stress path plots (p' - q') for our untreated soil sample at 280 and 355 kPa.

5.3.2.2 Treated Samples

In contrast to the stress path plots produced for untreated samples, p' - q' plots produced for samples that had undergone treatment with K_2CO_3 showed a much clearer, distinctive trend of contraction following failure, with the plots displaying a clear point at which samples reach the point of peak failure, and its progress along a critical line. Figure 5.6 displays the stress paths taken for samples following failure with samples at 205 and 280kPa confining pressure both tending to dilate as deviator stress increased, before reaching a point of failure and proceeding left, down the critical state line, with the pair trending left along similar contractile paths. In contrast, the 355 kPa confining stress sample underwent a failure like that observed for untreated samples with a less defined point of failure before looping, forming a boomerang style stress plot, with the sample undergoing significant contraction and reduction in effective stress following failure. The final measured point of effective stress is lower than that measured for 280kPa confining stress, though with a slightly higher deviator stress.

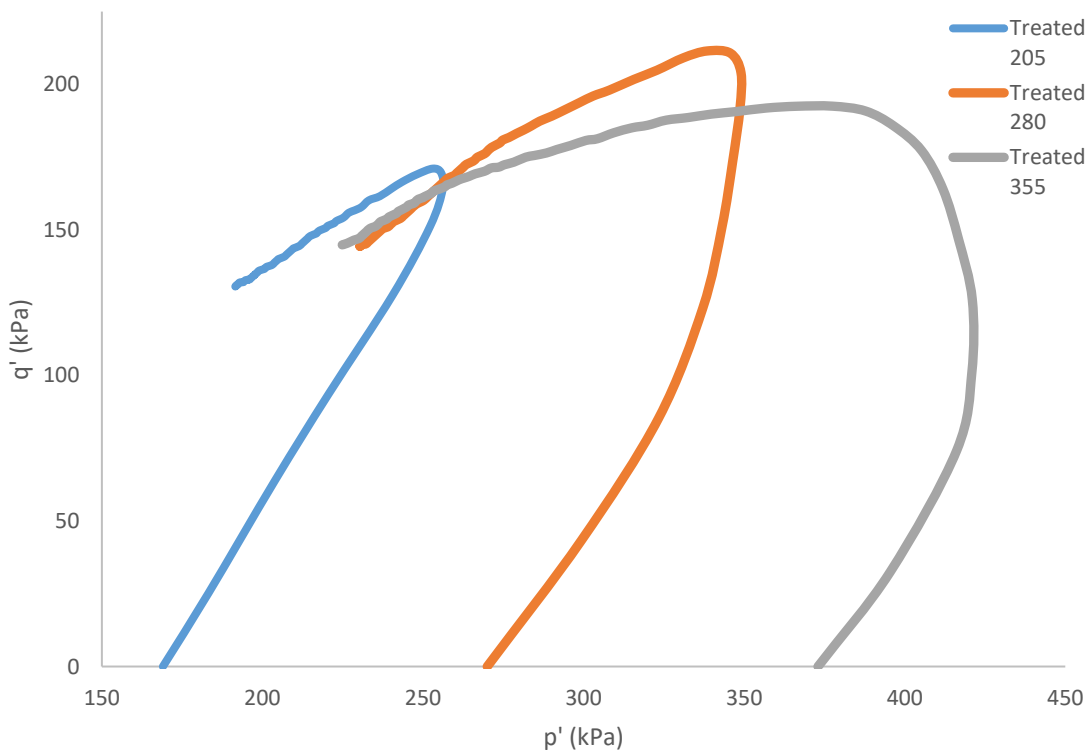


Figure 5.6. Stress path (p' - q') plots for treated samples at all 3 confining pressures.

5.4 Post Failure Strain Surfaces - Failure Types

Following failure of samples, it is important to examine the failed soil cores themselves as they can provide a valuable indication of the kinds of failure that occurred during the shearing process, allowing for a hypothesis to be formed as to how failure surfaces propagate during the shearing process of samples. Samples in this instance will be split between untreated and treated samples to give an indication of comparison between the two tests.

5.4.1 Untreated Soil Cores

Unfortunately, for the untreated soil cores only the sample tested at highest confining pressure was recoverable due to drainage issues for the lowest confining pressure following failure, and catastrophic failure of the pressure regulators following the end of the test at 280 kPa confining stress. The sample tested at 355 kPa confining pressure was recovered and sketches were made of the shear surfaces and failures that were evident on the soil core (Figures 5.7A-D). A key feature that is evident is the prominent primary shear surface, with evident brittle failure towards the base of the sample. This brittleness is apparent from the cracking occurring along the shear surface, as well as the single large distinctive shear surface. Furthermore, there are many secondary shear surfaces that have formed towards the base of the sample, the bulk of which are in noticeably close proximity to the primary shear zone (PSZ) and the cracks that are present, with some trending in a similar direction to the shear surface.

A secondary shear surface is present at the bottom left area of the sample, with a visible second shear surface forming during failure. On the opposite side of the sample where the primary shear surface tends from right to left of the sample (Figure 5.A,B) two further secondary shear surfaces can be observed forming towards the upper left area of the sample, with a distinctive banding forming below the secondary failures. On this converse side of the sample there is much more distinctive evidence of the brittle failure indicated, with numerous cracks propagating along the primary shear surface, and micro shears found along the length of the sample, highlighted by the smaller red coloured lines on both the pictures and sketches. It is also important to note the large concentration of manganese nodules that have formed in close proximity to the shear surface as can be seen in the pictures. This has not been highlighted in the

sketches due to the large number of them but can be observed towards the base of figure 5.7B, shown as noticeable black nodules.

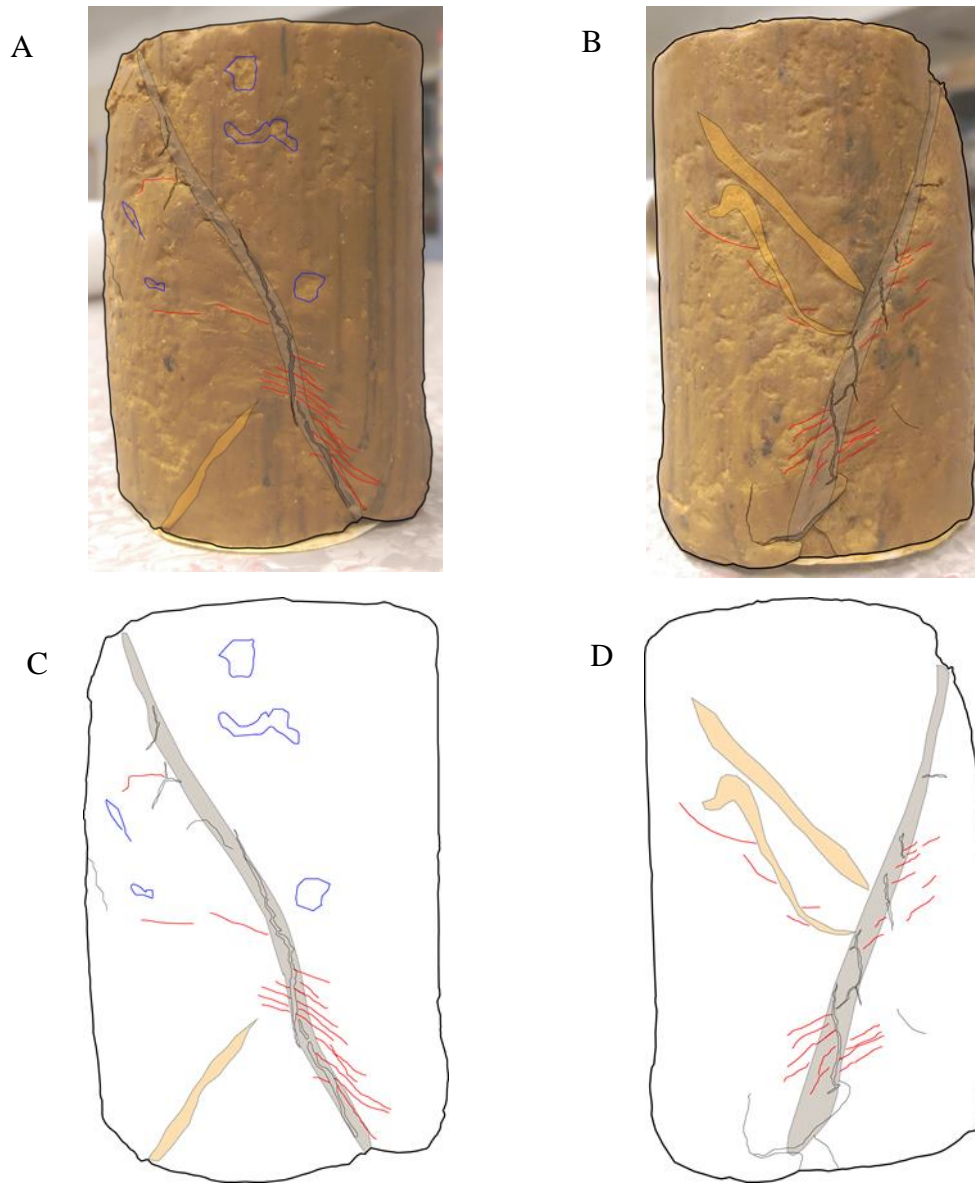


Figure 5.7. (A & B) Failed triaxial specimens for the untreated soil at 355 kPa, where grey denotes PSZ, Orange secondary shear zones, Red representing micro shears and blue depressions in the surface. (D & C) Failed tri-axial specimen sketches showing the drawn features with no overlying picture.

5.4.2 Treated Samples

205kPa confining pressure

Figure 5.8A,B shows the shear surfaces that develop for the treated soil core sheared at the lowest confining pressure. The sample developed a distinctive primary shear zone, trending from right to left (Figure 5.8A). There were a number of micro shears propagating throughout the sample, though not in large amounts. Furthermore, there were many secondary shear zones that visibly began to develop within the sample, indicating a complex failure either trending towards wedge or intermediate failure. Multiple streaked manganese stains were observed along the primary axis of the sample with smaller streaks present along edges of the sample, a trait not observed in the 355kPa untreated sample.

When observing the sample with shear trending left to right (Figure 5.8B), the micro-shears are significantly more evident, with the soil appearing to 'bunch' and accommodate some movement directly downward, while shear failure is much more distinctive. Another explanation as to this increase in micro-shears present could be that they propagated following failure as a form of relief following failure as the sample contracted after failure. Furthermore, there are fewer secondary failures evident, but the single significant failure indicates a secondary potential shear failure surface forming below the initial failure surface.

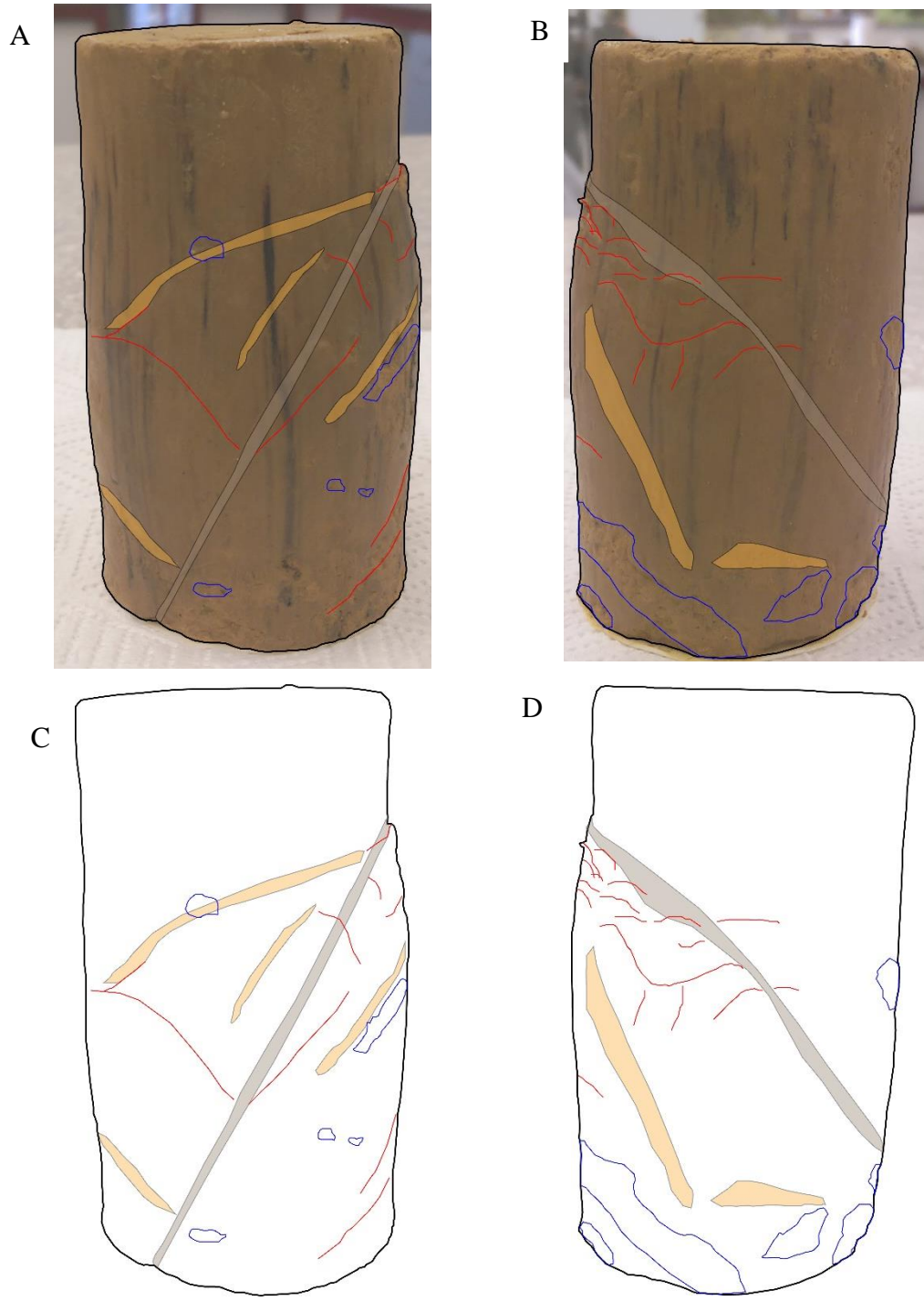


Figure 5.8(A & B) Failed triaxial specimens for the treated soil at 205 kPa, where grey denotes PSZ, Orange secondary shear zones, Red representing micro shears and blue depressions in the surface. (D & C) Failed tri-axial specimen sketches showing the drawn features

280kPa confining pressure

At 280 kPa confining pressure the primary shear is present without a uniform shear surface progressing from one edge of the sample to the next. Instead it can be observed to be discontinuous when observing shear surface from left to right, with the primary shear zone almost indistinguishable as can be observed in figure 5.9. Furthermore, within this failure there is a more prominent secondary shear zone that progresses across what is postulated to be the primary shear zone, and is more easily discernible. On top of this there is a significant reduction in micro-shears evident throughout the sample when compared to 205 kPa confining stress treated sample, with shearing becoming continually more discrete and difficult to distinguish as the shear progresses from left to right in figure 5.9A. Conversely when observed with shearing proceeding from right to left, the primary shear zone is more distinct, with a number of micro-shears propagating along the primary shear zone as failure has proceeded. A secondary shear zone is apparent at the base of the sample, forming a bulge to one side of the sample indicating the potential development of a further failure surface (Figure 5.9A, B,C and. D)

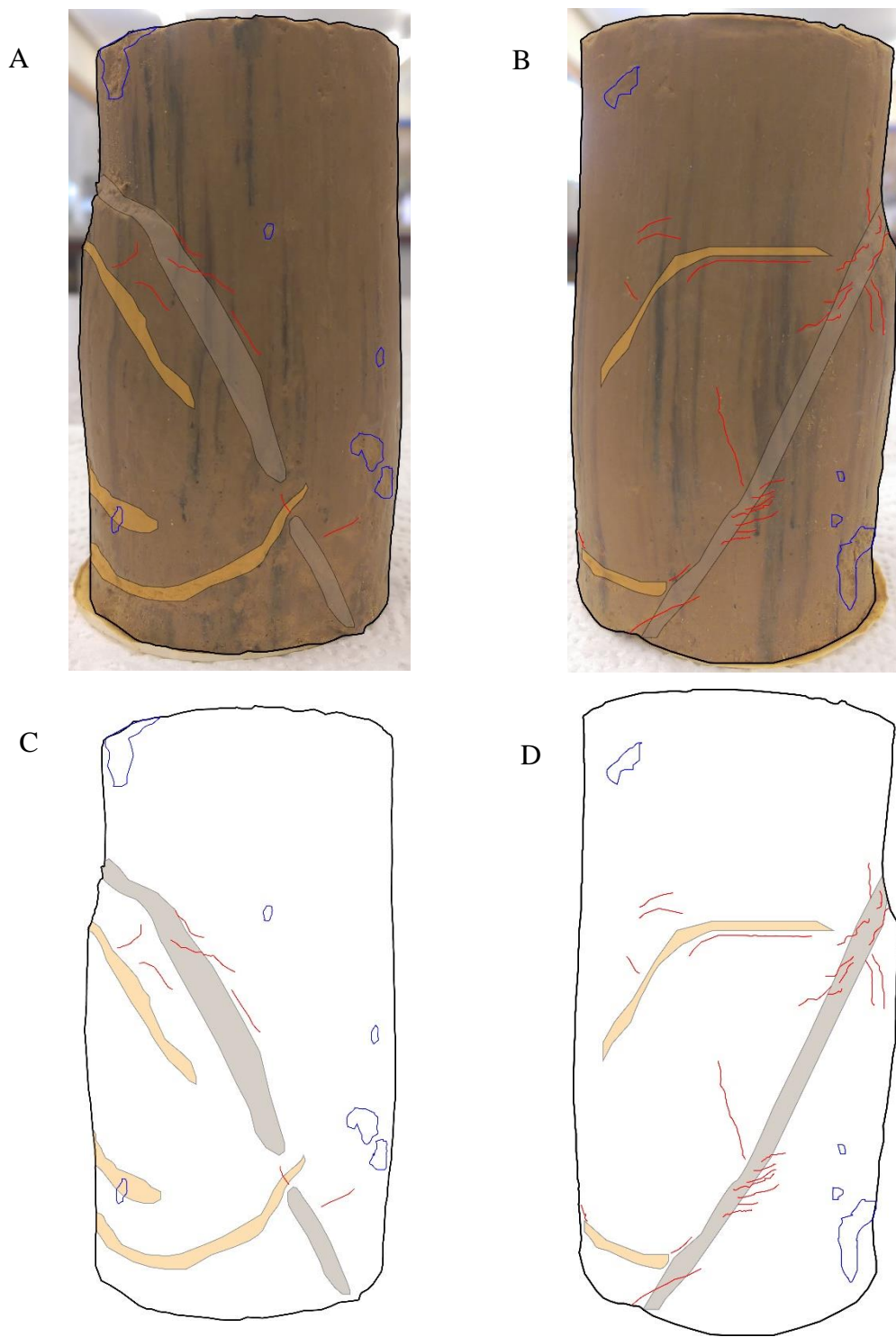


Figure 5.9(A & B) Failed triaxial specimens for the treated soil at 280 kPa, where grey denotes PSZ, Orange secondary shear zones, Red representing micro shears and blue depressions in the surface. (D & C) Failed tri-axial specimen sketches showing the drawn features

355 kPa confining pressure

At the confining pressure of 355kPa, the failure type changes, shifting from shear failure as was observed at the lower confining pressures, to a complex intermediate failure bordering barrel failure at this highest confining pressure. PSZ's propagate almost laterally along the sample aiding the barrel style shape form during failure (figure 5.10A, B), with numerous micro-shears evident above the shear surface and within the shear surface following failure of the sample. Furthermore, a secondary shear surface is observed to be developing to the bottom left of the sample with some micro-shears propagating away (Figure 5.10 C and D) . Secondary shear surfaces were forming along a shear like pattern with two separate shear areas potentially forming as the shearing process progressed. A significant note that has been observed across all samples is the streaking of manganese across the sample as it failed as opposed to concentrating along the failure zone as was observed in the failure for the untreated 355 kPa confining stress sample (Figure 5.7).

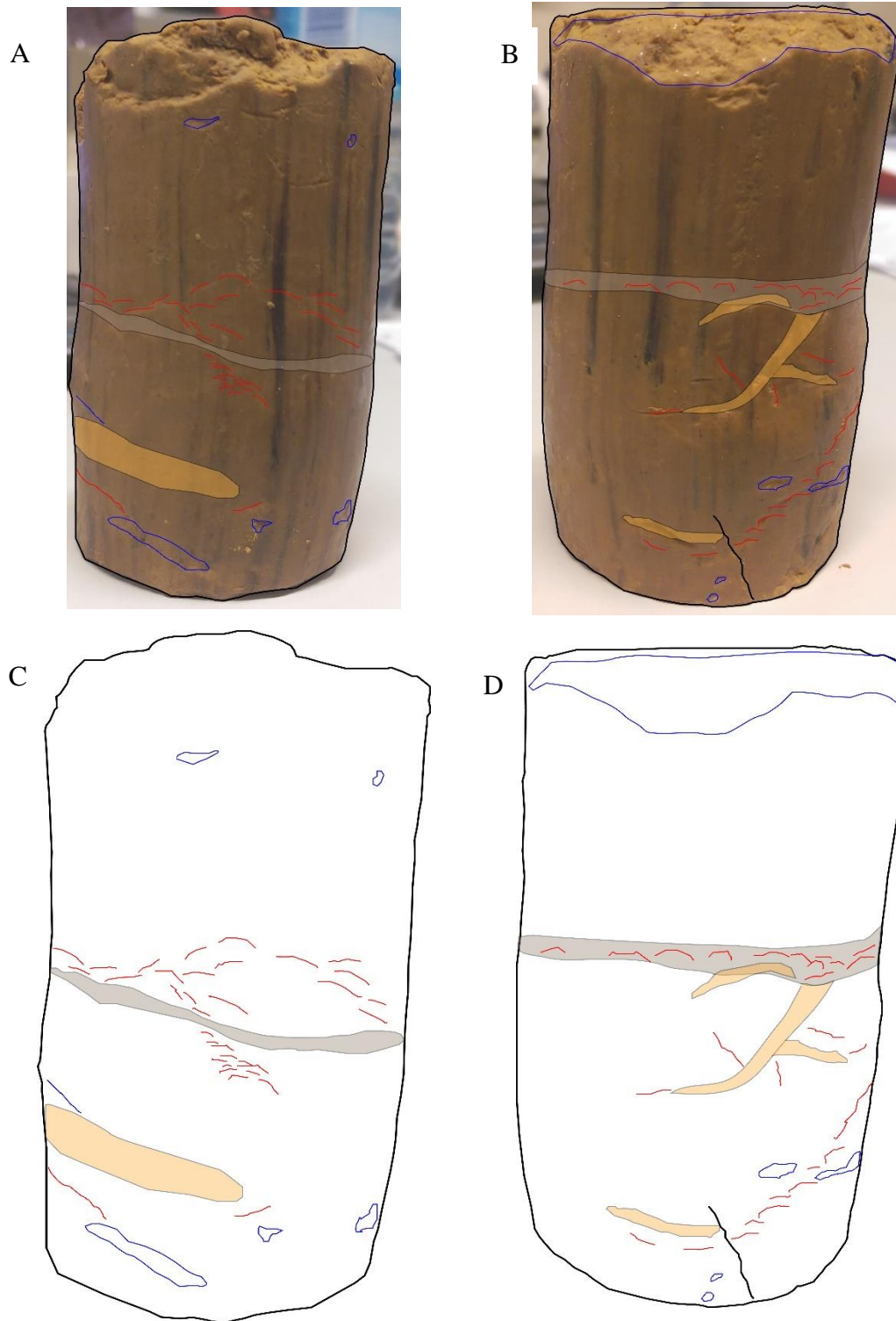


Figure 5.10(A & B) Failed triaxial specimens for the treated soil at 205 kPa, where grey denotes PSZ, Orange secondary shear zones, Red representing micro shears and blue depressions in the surface. (D & C) Failed tri-axial specimen sketches showing the drawn features

5.5 Thin Sections

Following sketching of samples, thin sections of the shear surfaces of each sample were taken. The thin sections were taken in two fashions for each confining pressure, with one thin section being taken perpendicular to the shear surface, and the second being at parallel to the PSZ. Thin sections allow the use of optical light microscopy as to identify minerals found within the soil itself, while also allowing for the identification of any smaller as micro and Riedel shears that may have propagated within the sample, similar to Mills (2016) study.

5.5.1 Component abundances and characteristics

Table 5.2. Mineral abundances observed across the thin sections produced for 205 and 280 kPa, mineral abundances have been estimated as point counting was not conducted due to the small size of the clay and silt minerals.

Component	Average Size (mm)	Shape (-)	Abundance (%)
Clay Minerals	-	-	80
Silt Minerals	<0.05	-	20
Lithics	0.4-0.6	sub-rounded	1
Quartz	<0.2	angular	1
Ilmenite	~0.2	platy-tabular	1
Magnetite	0.025	cubic	rare
Hypersthene	0.025	tabular	rare
Pyroxene	0.02	rounded	rare
Manganese	0.6+	sub-rounded	1

During observations of all the thin sections, abundances were approximated using visual estimates as no point counting was undertaken. It was determined that the thin sections were made up of approximately 96% groundmass with 4% made up of coarse minerals. The groundmass comprised of approximately 80% clay minerals and 15% silt sized minerals (0.02- 1mm), many which were highly weathered. The groundmass was noted as having a significant degree of weathering as indicated by the deep rust orange colour stain that permeated the slides. Identification of silt minerals

was difficult due to their small size and significant weathering, as such identification of these minerals was only determined through the usage of cross polarised light on the optical light microscope. Data is summarised below to allow for a greater indication if what minerals were present.

5.5.2 205 kPa confining pressure Thin Section

When examining the 205 kPa thin sections there was evidence of a homogenous rust/orange stained background, most likely a weathered iron oxide clay. There was positive identification of a number of quartz lithics found throughout the sample; these quartz crystals were highly fractured and evidently highly weathered. A factor to observe in this is the clustering and inclusion of the quartz crystals in close proximity to a light brown, fractured, amorphous unit which under light microscope was difficult to identify. Following advice from a mineralogist it was identified that this was most likely either a large, smooth clay inclusion that under pressure from the shear surface has presented in the fashion observed, or potentially a piece of weathered pumice that has large quartz crystals inclusions. Based upon the proposed depositional history of the Pahoia Tephra being an airfall tephra, and the distance of unit from likely eruptive source, I infer that it is most likely a clay inclusion. Further investigation with SEM was conducted to give an accurate determination.

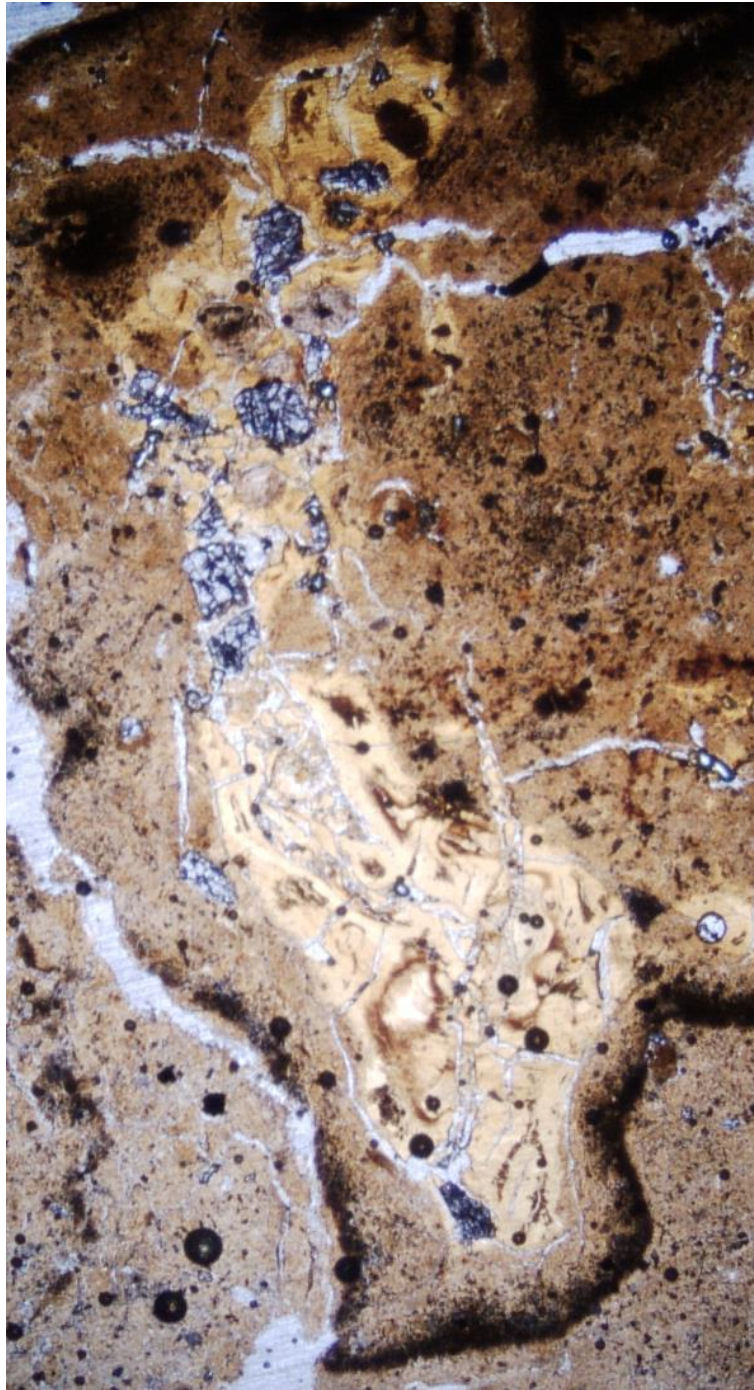


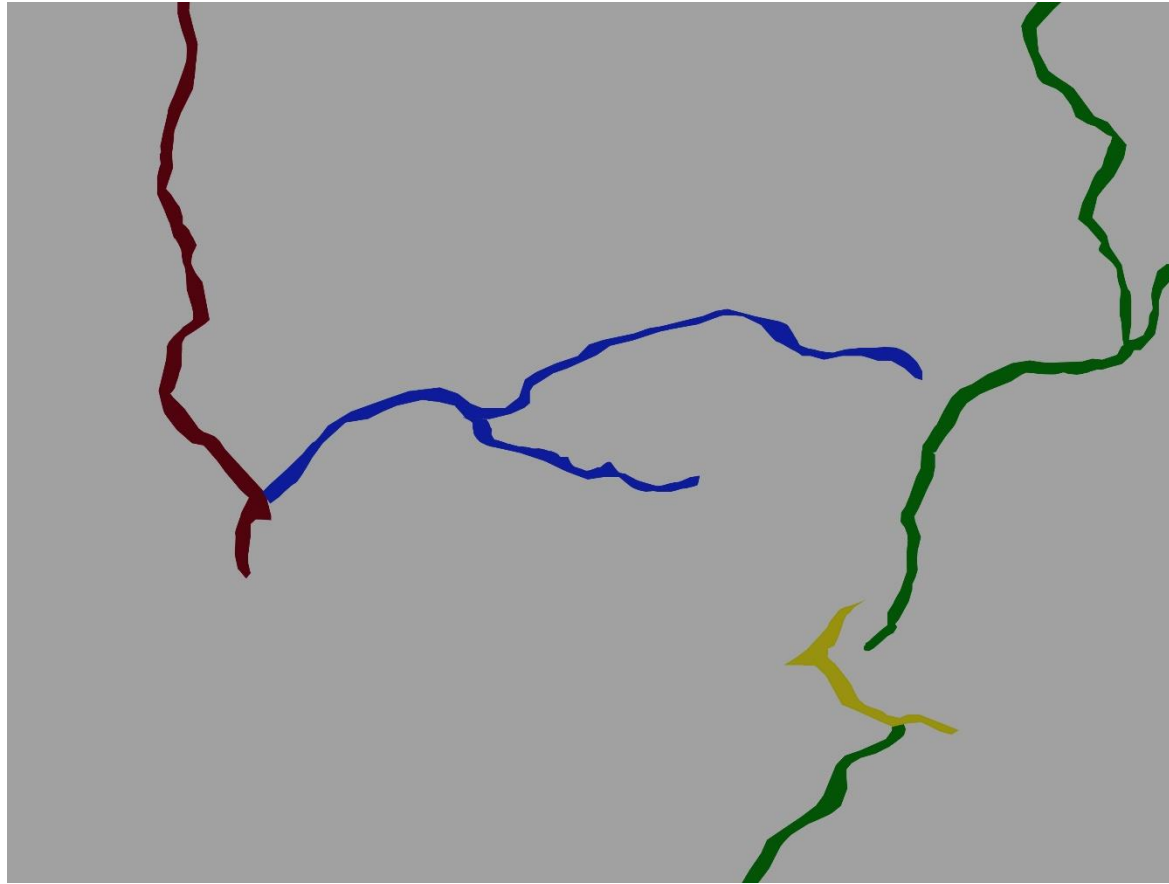
Figure 5.11. An amorphous unidentified object observed on the 205 kPa thin section, with inclusions within the crystal thought to be either quartz or zircon crystals.

Figure 5.11 shows another 1x magnification of the sample thin section in which we can observe the shear surface directly passing through a crystal as opposed to around the crystal. This indicates that whatever this crystal is, the background clay was of a greater strength to the crystal itself and as such the shear surface has progressed through it. This crystal was identified as a hypersthene crystal. In this same snapshot

of the thin section there are large dark coloured inclusions in close proximity to the hypersthene crystal. These are thought to be either ilmenite or manganese inclusions present within the background mass of the soil.

This thin section provides an ideal image to identify any Reidel shears that may have propagated through the sample across shear sections. Figure 5.12 A and B details each of these in detail, with the key factors in this image being identified as areas shaded in green being the (PSZ), red as a secondary shear zone acting, blue as the R' shears progressing between shear zones and yellow as stress fractures. In this figure it is evident that on the right hand side of the figure the PSZ has progressed from the top down, and progresses through the hypersthene crystal. The fracture then stops and re propagates a small distance below the termination of the initial part of the shear zone.

A



B

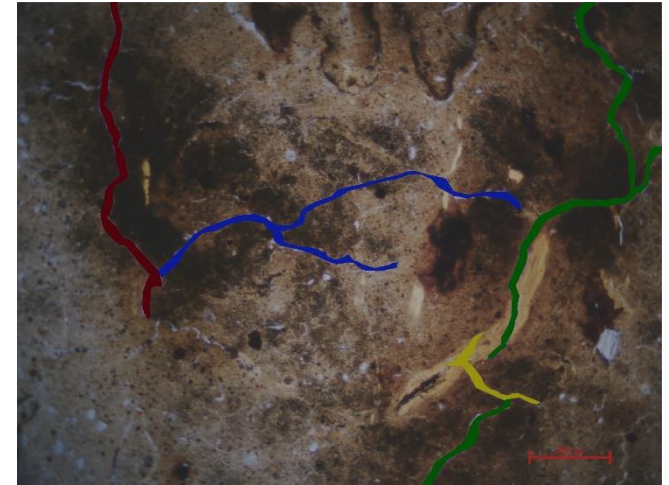


Figure 5.12. (A) Thin section at 205kPa with shears denoted on the sample. PSZ is represented as the green line, R'shear as blue, secondary conjugate shear as red and yellow as additional R shears. (B) Shears and shear direction overlain on thin section image.

5.5.3 280 kPa confining pressure Thin Section

Thin sections taken from the core tested at 280 kPa confining pressure were taken across and along the primary shear surface, and allowed for an insight into how the soil acted at a higher confining pressure following treatment. A key feature that was observed at this higher confining pressure was the evident inclusions and infilling beginning to occur both within the background groundmass and along fracture zones. Figure 5.13A displays this well, showing evidence of either fresh or relict fractures within the groundmass that have been infilled by a dark material, while figure 5.13B shows a fracture passing through a hypersthene crystal that has a dark, almost opaque, infilling into the fracture. This infilling was observed across a number of fractures within the slides, with it evident that this infilling was occurring globally within the sample and not locally within these particular shear zones. As with the 205kPa thin section, fractures once again appeared to progress directly through hypersthene crystals (Figure 5.13C), but it is also interesting to note that in places, where fractures directly interacted with other crystals variable results were observed. In some instances, fractures passed through the crystals, whereas in some instances the shear surface passed around the crystal, diverting the pressure around itself. When interacting with magnetite inclusions, the shear zone penetrated and fractured the crystal directly (Figure 5.13D).

Riedel shears were present once again in this sample as shown in figures 5.14A and B, with multiple R shears progressing at angles of approximately 61° from the PSZ across the sample and interacting with the secondary shear fracture.

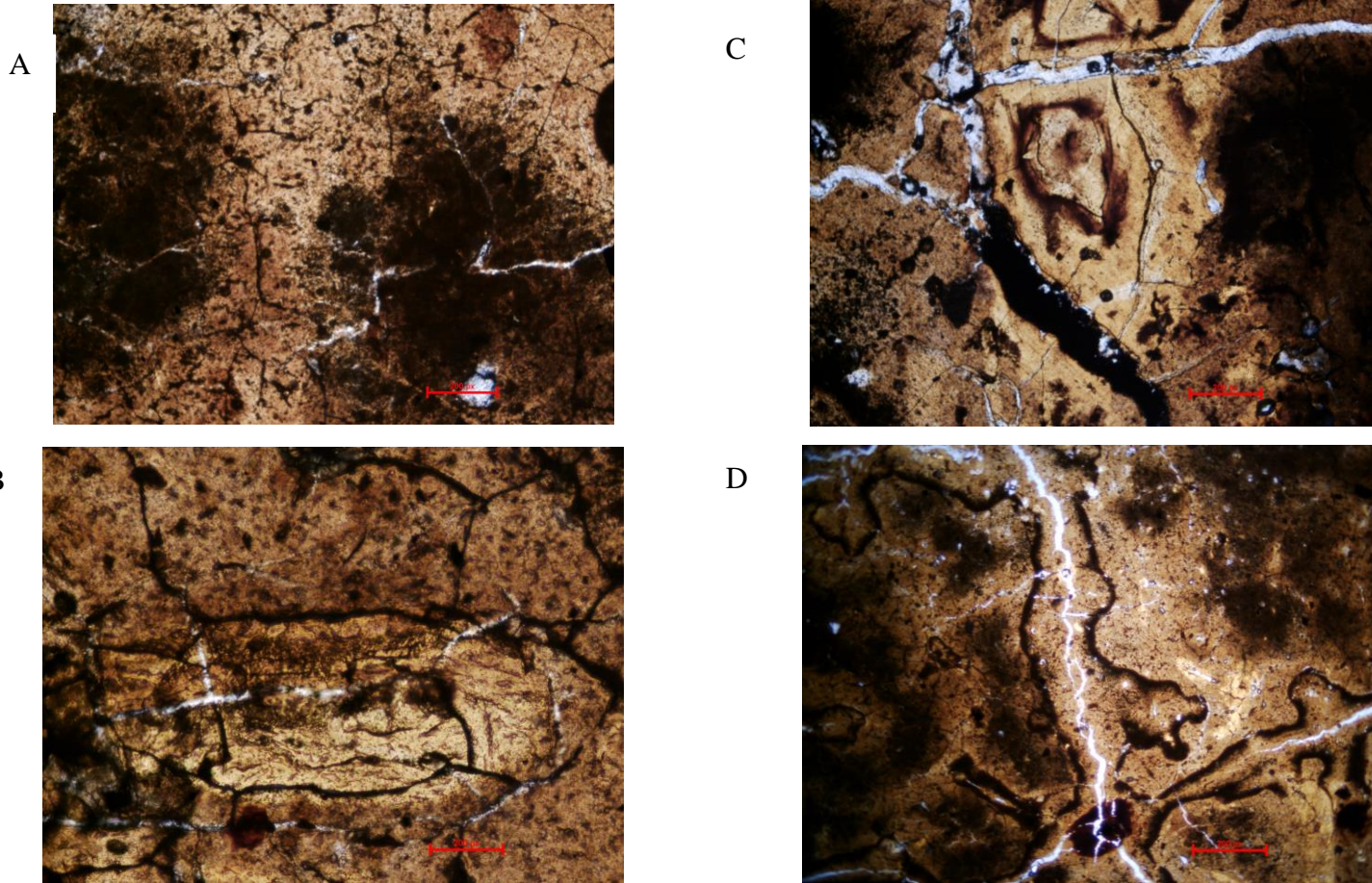
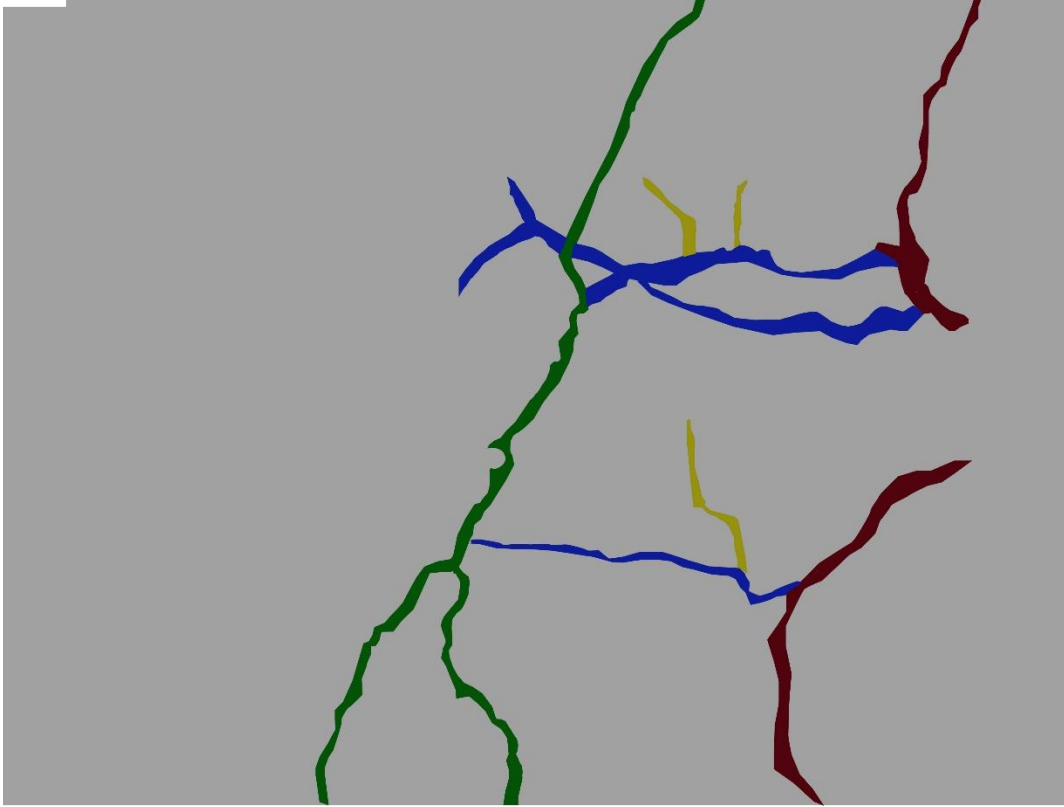


Figure 5.13(A) Relict or infilled fractures present in the 280 kPa thin section (B)Hypersthene crystal present in the 280 kPa thin section with shears passing through the crystal. (C)Infilling by an unidentified black substance in the shear zone of the 280 kPa thin section. (D) shear fracture passing directly through what is thought to be a magnetite crystal.

A



B

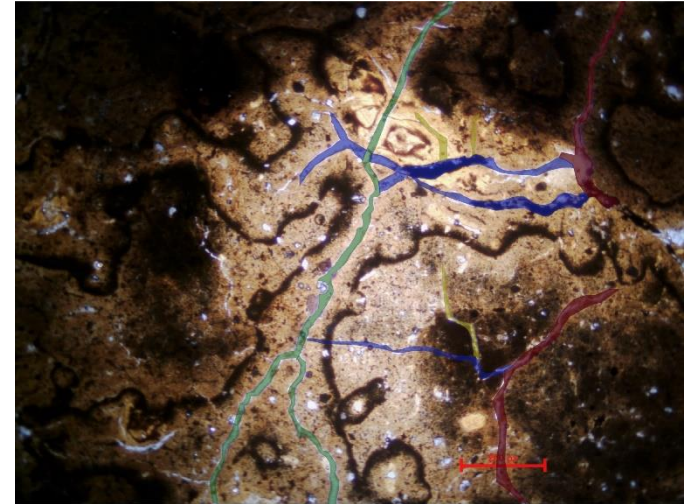


Figure 5.14 (A)Thin section at 280kPa with shears denoted on the sample. PSZ is represented as the green line, R'shear as blue, secondary conjugate shear as red and yellow as additional R shears. **(B)**Shears overlain on the slide are shown above.

5.5.4 355 kPa confining stress thin Section

For thin sections created for the soil core tested at 355 kPa confining stress, both thin sections were taken parallel to the primary shear zone. The thin sections themselves provided a good degree of information and allowed an insight into the way in which the treated soil acted at the highest confining pressure utilised in this study. In this instance quartz crystals were much more evident in a number of areas throughout the thin section (Figure 5.15A), though this could be due to variable spatial distribution inherent in the soil. A key point of interest that became evident in the thin sections was the presence of lithics within the PSZ and its interaction in accommodating some of the pressure incurred by the shear plane. Figure 5.15 B and C shows a lithic at the intersection of two larger hypersthene crystals, which, when examined at 10 times magnification shows scour marks present within the soil in close proximity to the lithic. As with 280 kPa confining stress, there is evidence of infilling of either fresh or relict fracture zones by an unknown dark substance, with this shown in the 355 kPa thin section (Figure 5.15 D), further investigation of these infillings with SEM was undertaken to determine what may have infilled these fractures. Another factor that was observed in the 355 kPa confining thin sections was the noticeable drop in total evident fracture zones, with fractures being far less pronounced and smaller in size. This was reflected well by the sample with PSZ less prominent when examining the soil cores following failure.

Reidel shears were far less prominent in the sample failed at 355 kPa confining stress, keeping with the overall thin section where there were fewer fracture zones visible. Within the sample it was evident of a single large shear that connected the PSZ and secondary shear band, with this band progressing at almost an exact 61° between shear zones. This lack of shearing is a fascinating insight into how the shearing has evolved and altered to prevent the formation of a primary shear failure.

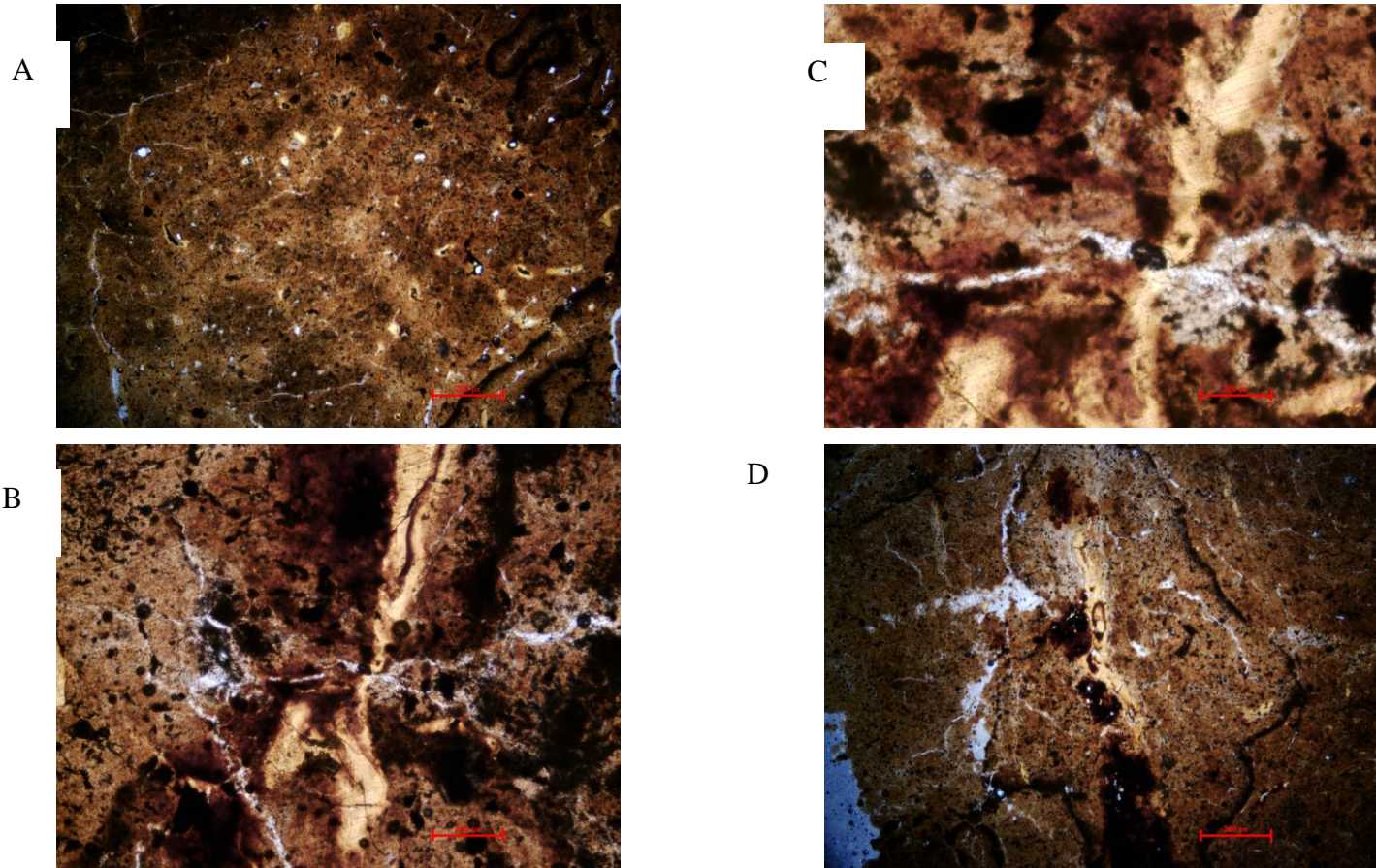
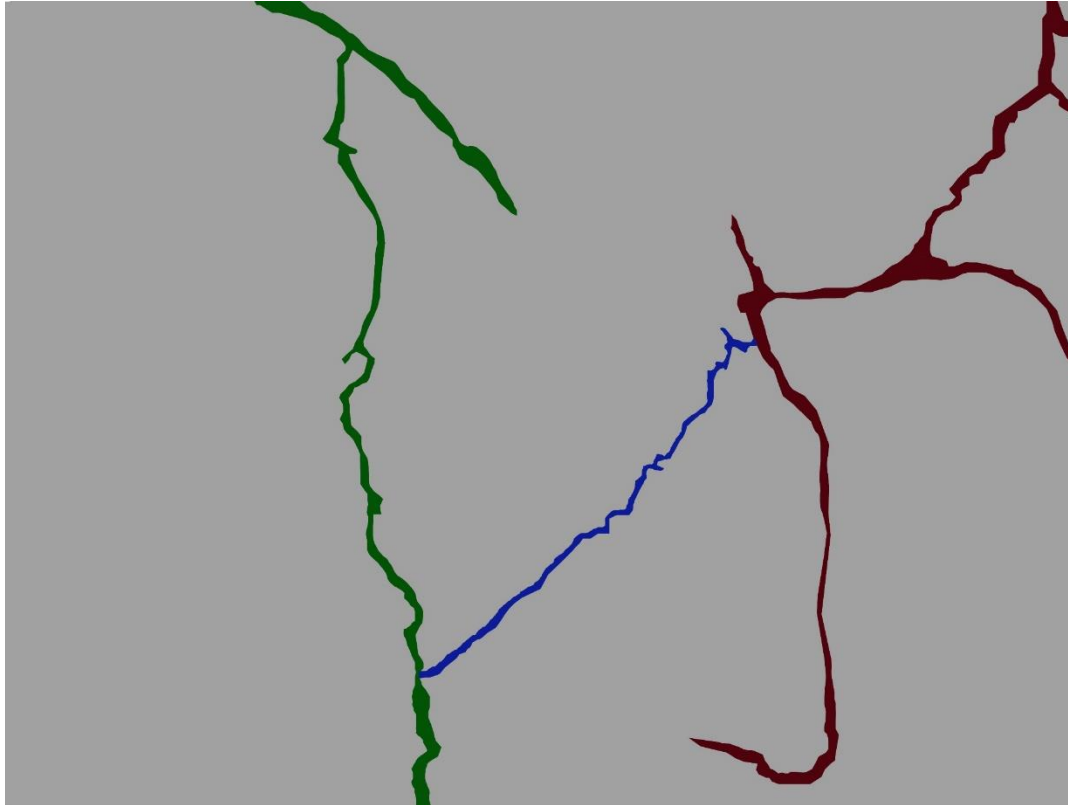


Figure 5.15. (A) Quartz crystals present in the 355 kPa thin section, crystals were much more distinct throughout the groundmass as this higher confining pressure. (B) A snapshot of the intersection of two shear fractures passing through an apparent weak point of a crystal, the intersection appears to have an indistinct black mass in the middle. (C) A higher magnification view of the fracture intersection shown in 5.15B shows a lithic wedged into the shear space between the two fracture. (D) Further dark infillings present in the 355 kPa thin section

A



B

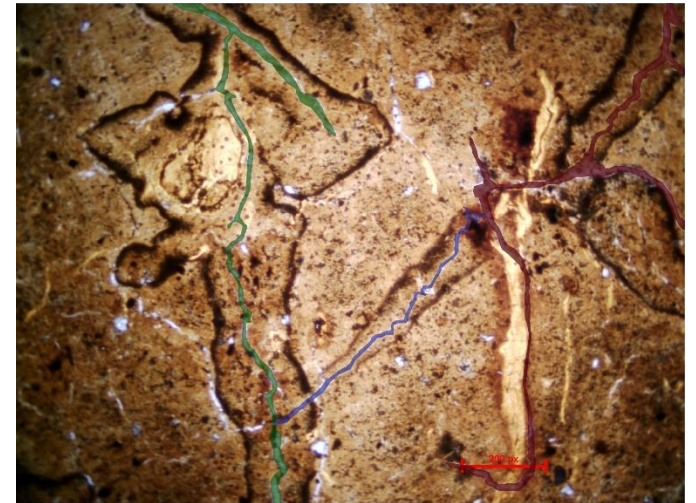


Figure 5.16. (A) Thin section at 355kPa with shears denoted on the sample. PSZ is represented as the green line, R'shear as blue, secondary conjugate shear as red. (B) Shears overlain on the slide image.

5.6 Summary of Chapter

From the data collected for this study it became evident that the application of K_2CO_3 to our soil cores has had a positive strengthening effect on the soil raising the effective stress of all treated soil cores when compared to soil cores by proportions exceeding 100%. Furthermore, pore pressure was also reduced at point of failure for all samples. This lower pore pressure is reflected in stress strain curves plotted for treated samples, with untreated samples exhibiting typical normally consolidated clay behaviour during testing, showing contraction before point of failure and showing a large degree of strain softening. In contrast to this treated samples showed stress strain curves that exhibited dilation as axial strain increased, before reaching a point of failure and undergoing significant contraction following failure. With this said the sample at 355 kPa confining pressure for treated samples exhibited behaviour more similar to the untreated samples. When sketching the failed treated soil core samples, the discrepancy between the stress strain curves that were plotted for the lower confining pressures (205,280 kPa) and highest confining pressure (355 kPa) becomes evident as the form of failure for this higher confining pressure shows failure to be a complex to barrel style failure, differing from the lower confining pressures that show shear failure.

Thin sections were taken and showed approximately 95% of the soil to be made up of clay and silt minerals, with the final 5% being made up of smaller proportions of other minerals. The thin sections themselves showed a variety of features with the most prominent of these being the progression of shear failures directly through hypersthene crystals as opposed to around them, indicating a stronger groundmass when compared to the hypersthene crystal itself.

CHAPTER 6

Scanning Electron Microscope Imagery

6.1 Introduction

This chapter will consider data collected using a Scanning Electron Microscope (SEM) thin section slides that, while under light microscopy, displayed features that were not discernible via regular light microscopy and as such need a greater degree of accuracy to gain the relevant information. From the electron microscope, a wealth of data has been gathered including images, measurements of element amount on a specific slide, together with point values and element distribution across specific areas selected. Back - scatter images showing elemental differences on slides to distinguish between areas of 'light' and 'heavy' elements allow for the examination of features not readily visible through using regular scanning electron imaging. All images were derived at 15.0kV power and with the stage at 15.0 mm

6.2 General Thin Section

When examining the SEM images, it is worth first starting with the lowest magnification. Figure 6.1 shows a sample of a thin section from 280 kPa confining pressure at 70 times magnification in regular SEM mode. The image shows approximately 3.7mm of sample. The image highlights a number of key features; both desiccation cracks and the actual fracture can be seen, with the larger darker grey coloured areas throughout the sample highlighting the infilled shear zones, while the black cracks throughout the sample (circled in orange) highlight the desiccation cracks present throughout sample. As would be expected, there are a large number of desiccation cracks present due to samples needing to be dried thoroughly prior to mounting onto a thin section slide. There is evidence of some minerals present in the upper-right part of the figure, circled in red, though at this scale mineralogy is indeterminate.

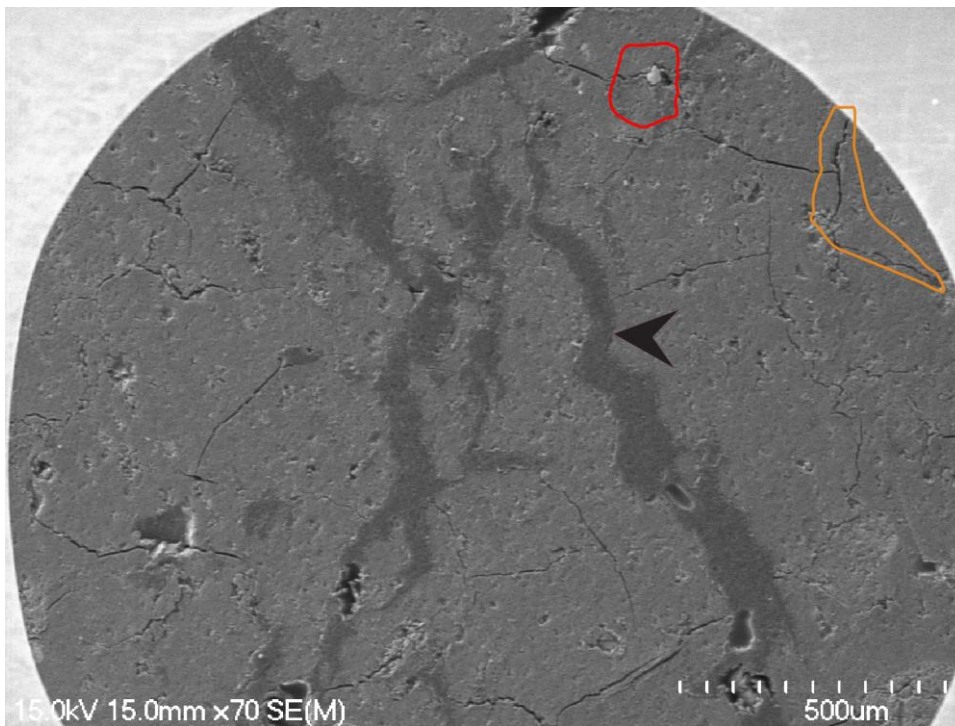


Figure 6.1. A normal SEM image of the 280 kPa thin section at the lowest possible magnification, desiccation cracks are denoted as circled in orange and indeterminate crystal circled in red.

6.3 Mineral Specifics (180x Magnification)

Figure 6.2 was taken using Back Scatter Electron (BSE) imaging to allow for accurate distinguishing between minerals dominated by heavy or light elements. The slide was the 355kPa thin section and shows a wide range of features. There is evidence of a large desiccation crack propagating from right to left across the upper portion of the figure. Approximately 3 or 4 differing minerals are present as well as the background clay mass. Minerals present were split into differing areas with each mineral given a corresponding number to allow for identification.

6.3.1 Mineral 1

Mineral 1 shown in figure 6.2, appears significantly weathered and potentially broken up in nature with a mixture of light and heavy elements present within the actual mineral itself. Element distribution measurements, shown in figure 6.2 show the mineral to be rich in both carbon and silicon with a distinctive lack of any other key elements present. This mixture of elements could indicate that the mineral is Silicon

Carbide or a mineral known as *Moissanite*, though due to the rare nature of this mineral this may not be the case.

6.3.2 Mineral 2

Mineral 2 was a lighter coloured, squarish mineral with element distribution indicating a high volume of iron present. Other elements appeared to not be present within the sample, or if present were sparing and did not register in sufficient amounts for the element detector. Small amounts of oxygen were present on the mineral indicating that the mineral may well be magnetite.

6.3.3 Minerals 3 & 4

Minerals 3 and 4 appear to be carbon based in nature, with distinctive increases in carbon shown on element distributions from figure 6.3. Furthermore, the distinctive lack of silicon, aluminium and oxygen present indicates that these dark coloured areas on the image are not made up of halloysite infilling. This darker colour and richness in carbon is most likely the resin used in thin section preparation.

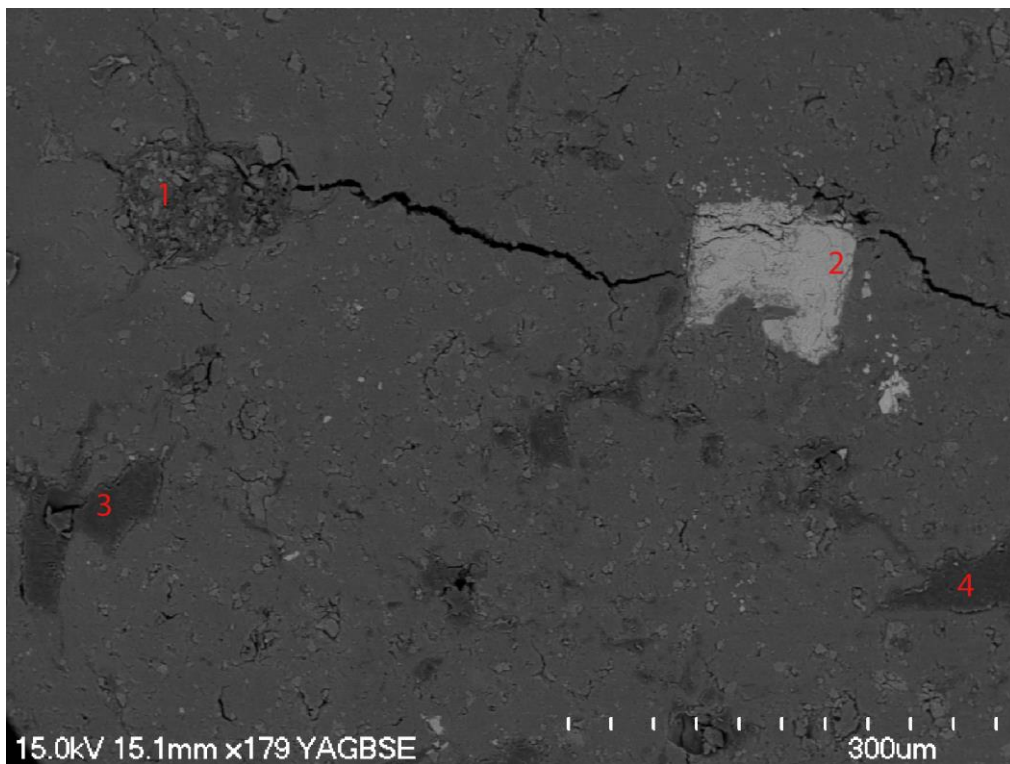


Figure 6.2. A BSE image taken of the 355 kPa thin section of 4 separate key features, each labelled in red for separate identification.

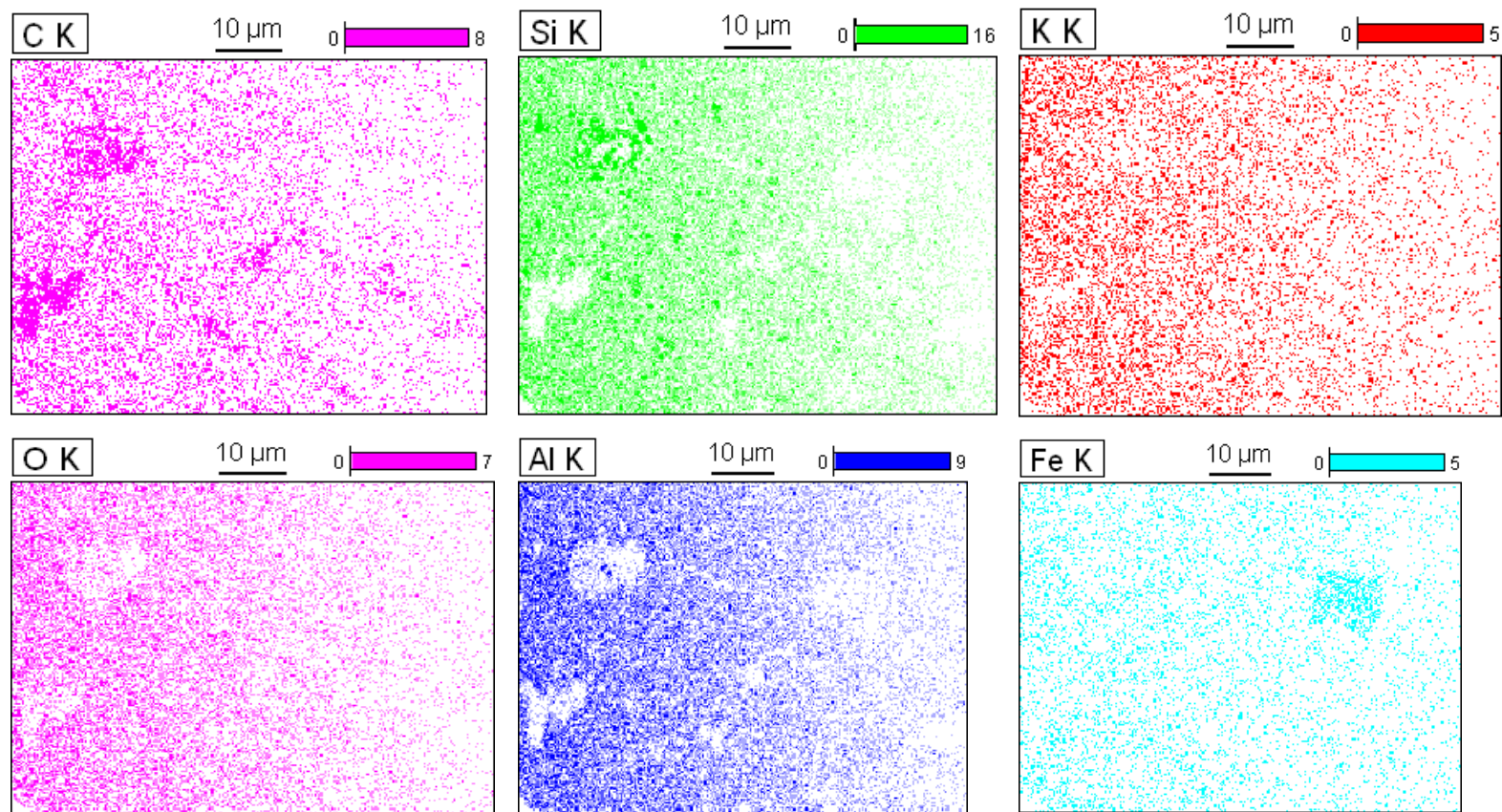


Figure 6.3. Element distribution graphs showing distribution of elements on the image of figure 6.2, elements are identified as points in differing colours with particular element identified in the top left of each image.

6.4 Infilling in Shears (180x magnification)

Figure 6.4 is from the 280kPa thin section showing multiple shear fractures using both normal SEM imagery and BSE imagery to highlight different minerals. Figure 6.4A and B shows a number of fractures that have been infilled with an unidentified compound. Furthermore, desiccation cracks can be observed spanning the sample, with the edges of these desiccation cracks appearing white on the image as they have become more charged under the Electron Microscope. To highlight differences between the infilling and the groundmass, and as such allow a better view of the shear fractures throughout the sample, BSE imagery (Figure 6.4B) was used. In this figure, the progression of shear fractures is much more pronounced as it progresses across the thin section in the image, not only this but the usage of BSE highlights a larger number of minerals than the regular SEM.

Element analysis of the area was conducted (Figure 6.5) and showed the infilling to be dominated by carbon, with few other elements identified in this infill, with the rest of the slide is dominated by silicon, aluminium, oxygen and potassium as would be expected by a halloysite rich groundmass. With this said, the BSE imagery used in Figure 6.5 shows the presence of areas that differ noticeably to the groundmass itself, Spot analysis was used to gather a greater degree of information on these areas to allow for specific analysis of these spots. Figure 6.6 shows the 6 spots defined for specific spot analysis, with points 1,5 and 6 being on lighter coloured areas in the BSE imagery, 2 and 4 on the infilling and 3 on the groundmass itself. The graphs in figure 6.6 show the dominant elements in each.

Point 1 was shown to be dominant in Ti, Fe, O and Mg, indicating that this mineral was most likely ilmenite. Point 5 appears to have collected some information on the background mass on top of the mineral itself with Al, Si and K detected, though it is similar to Point 1 and is most likely ilmenite as is the case with Point 6. Points 2 and 4 indicate the infilling to be dominated by C, with trace K and trace Cl found.

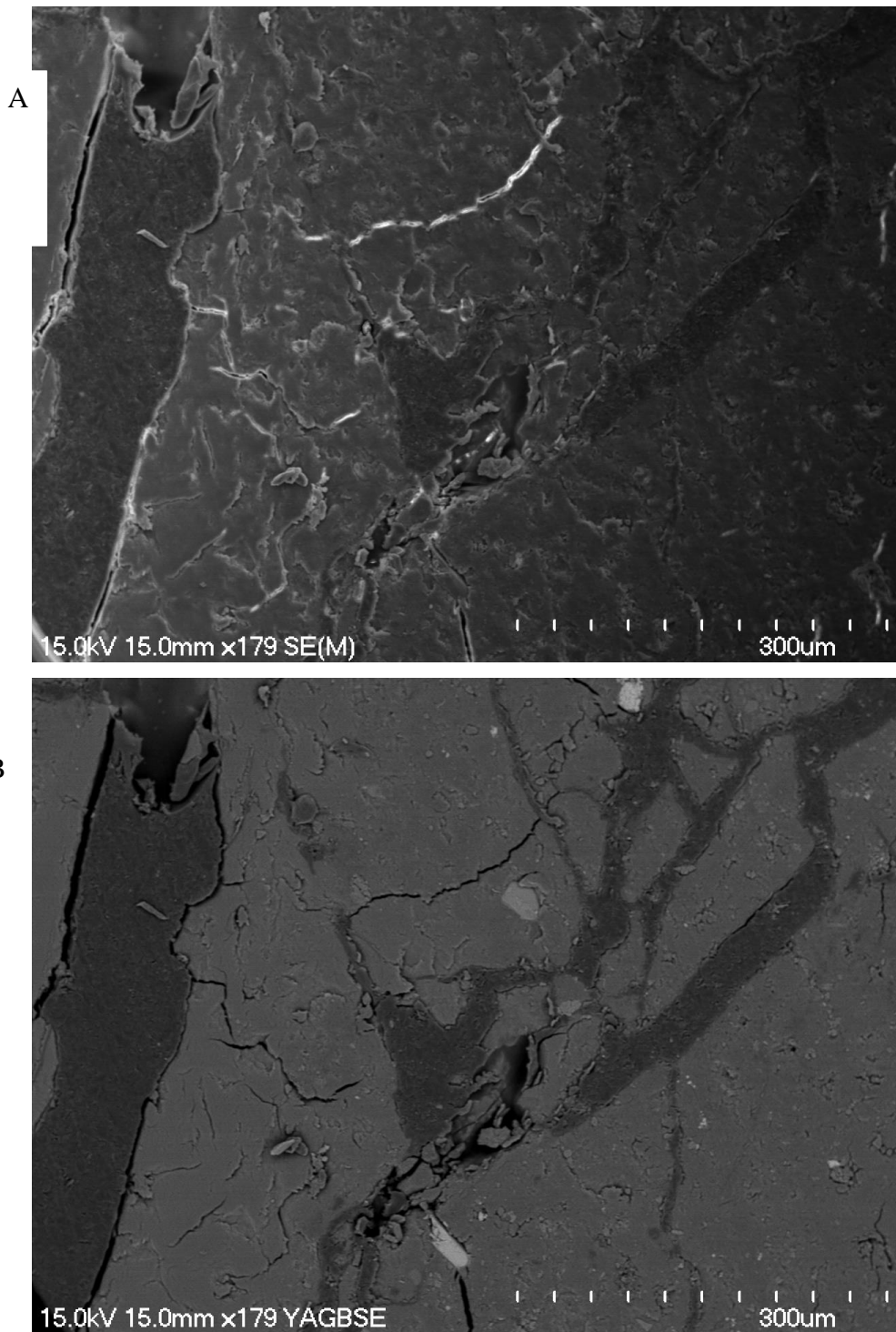


Figure 6.4. (A)An SEM image of the 280 kPa image showing infilled shears present within the thin section at 179 times magnification(B) A BSE image of infilled shears present on the 280 kPa thin section at 179 times magnification.

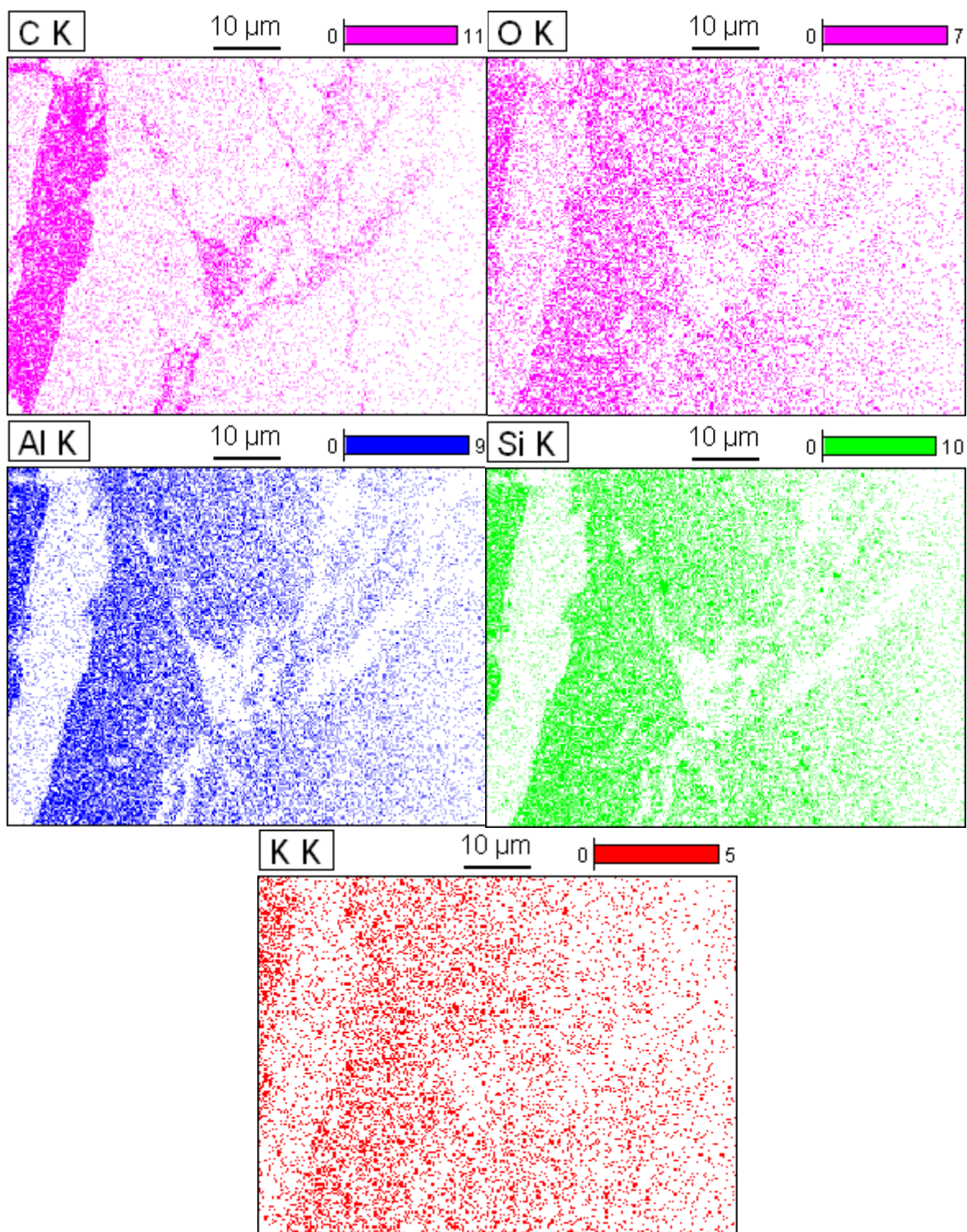


Figure 6.5. Element distribution maps for the images used in figure 6.4, with particular element for each distribution identified above each distribution box in the top left.

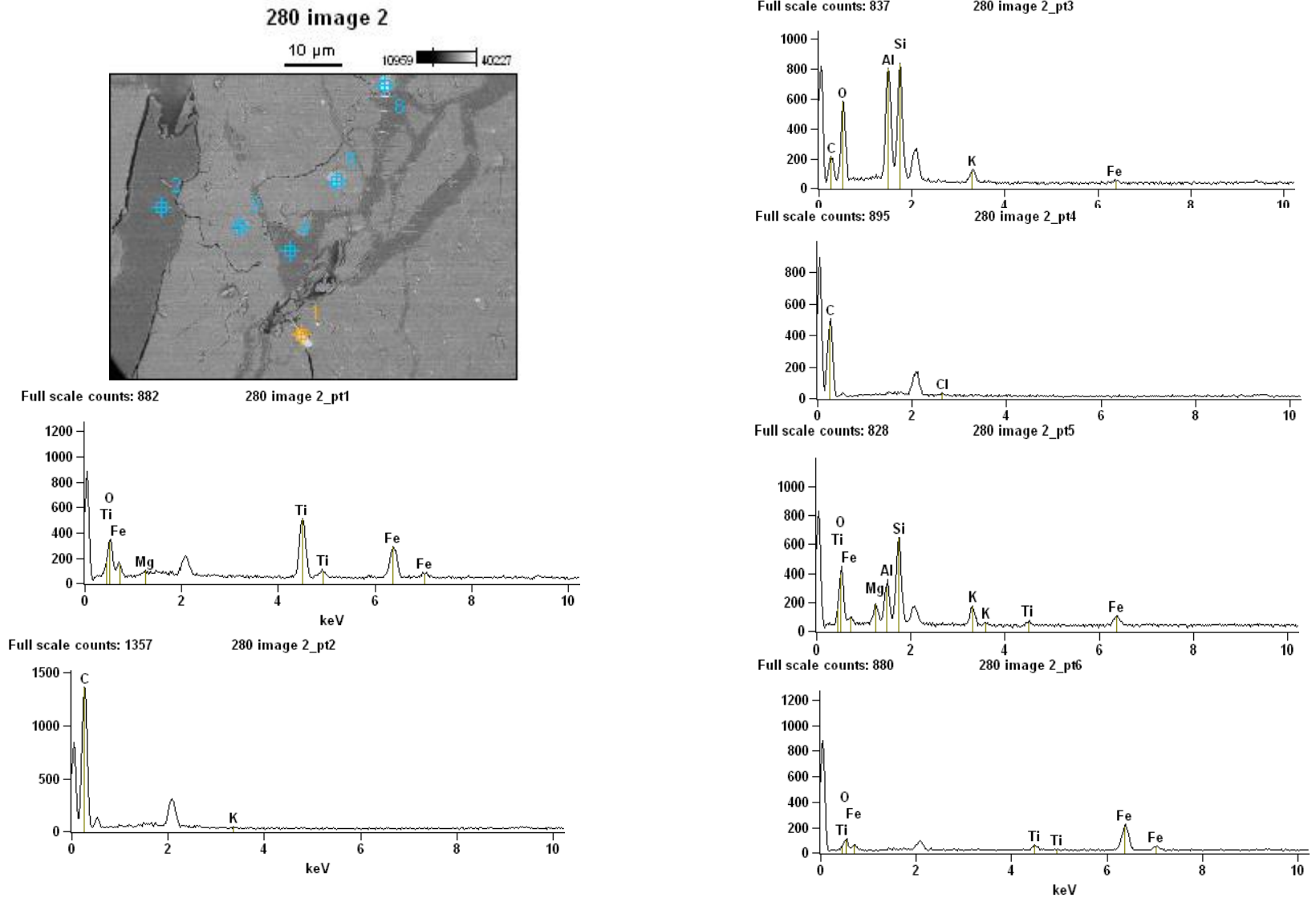


Figure 6.6. Point element distribution on the 280 kPa thin section, where specific points had element volumes graphed. Each point has its own graph produced as shown above, with particular point indicated in the title of each graph.

6.5 Shear Zone Alignment

The thin section taken at 280 kPa confining pressure allowed for the highly detailed image of the shear zone to be seen (Figure 6.7). The image was taken at the edge of the PSZ, with the bulk of the image being taken up by the material within the shear zone itself. Initial examination suggest that the material appears disordered, but upon further study 2 main fractures are present within the material, with the second fracture, running along the edge of the clay groundmass splitting into 4 separate fractures at varying points. This causes a slight alignment of the material within the shear zone (Figure 6.7).

Within the shear zone, we can see large pieces of smooth material, present with sharp edges that are much larger than the material surrounding it. To identify these element distribution analyses was undertaken (Figure 6.8). This showed that these large pieces of sharp material were silicon rich, and most likely volcanic glass of some form that had been incorporated into the PSZ during the formation of a shear band. Concentrations of aluminium and silicon in close proximity were also detected, as would be expected as the clay within the shear zone was compressed during shearing. Interestingly the clay appears to have compressed into small specific areas as opposed to spread and become well distributed throughout the shear zone. Of all the elements detected the one most of a surprise is that there was a large concentration of calcium detected at the upper left part of the image as well as throughout the area.

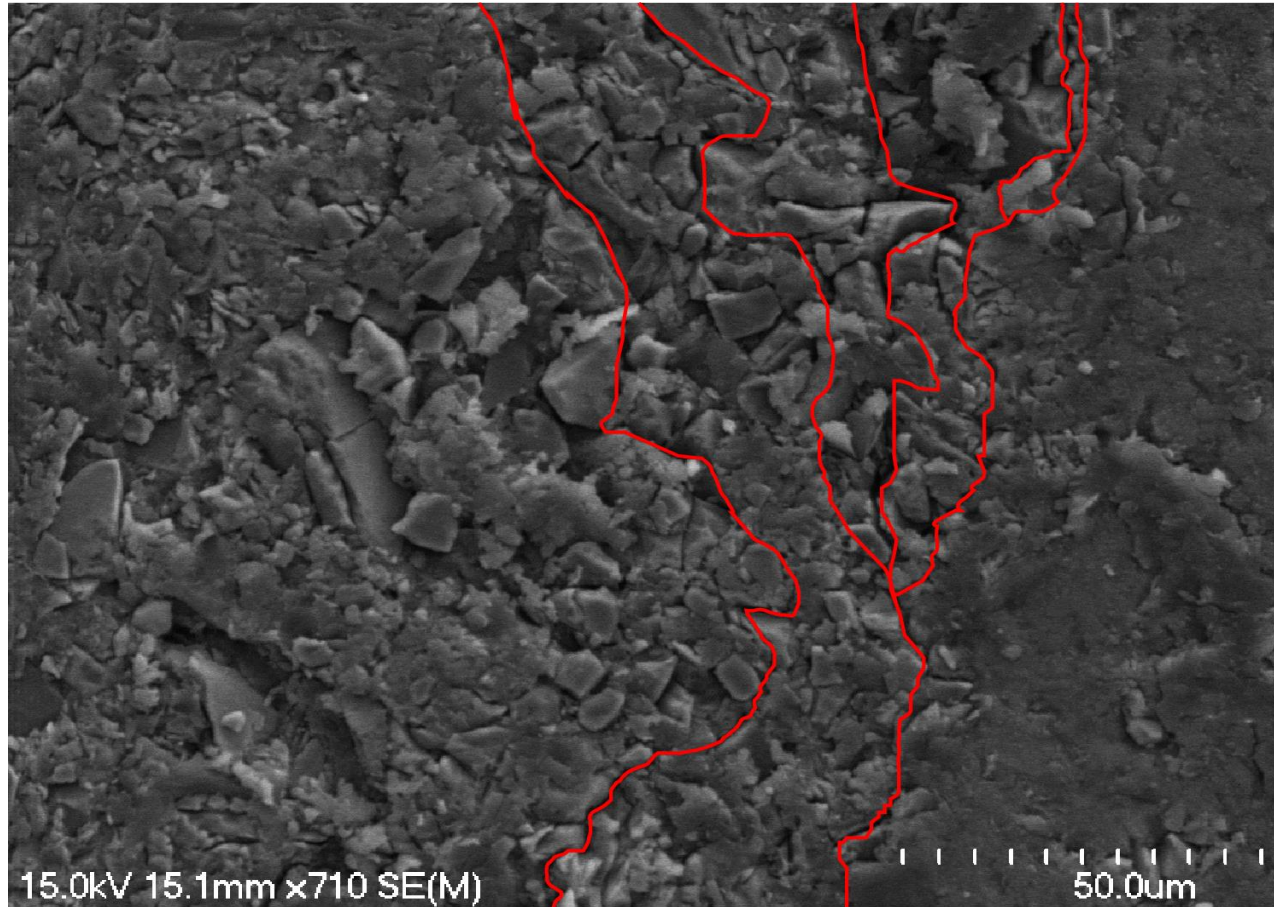


Figure 6.7. Taken at 710 times magnification of the 280 kPa thin section shear zone, propagation of alignments and fractures within the shear zone is indicated in the image above by the red lines.

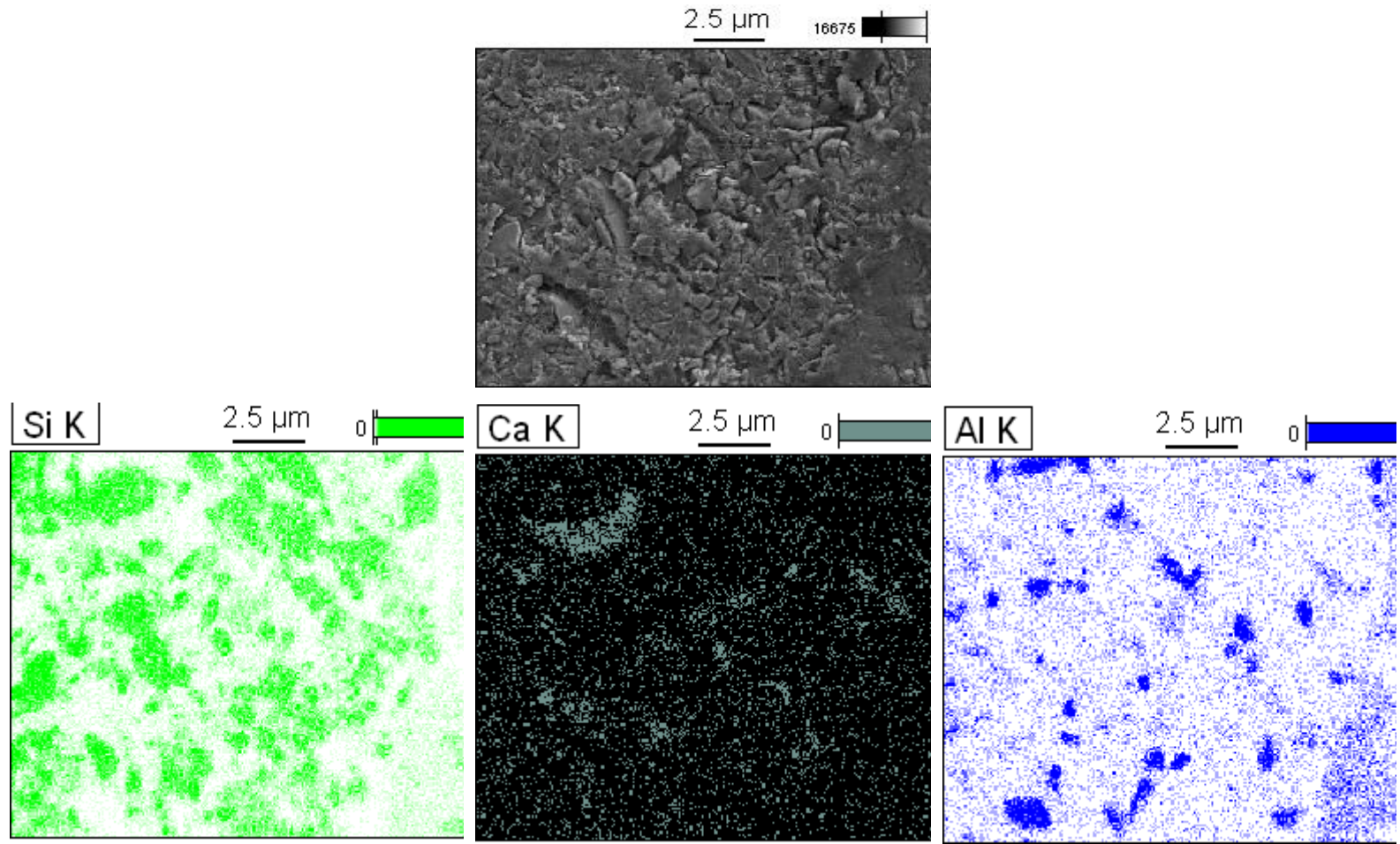


Figure 6.8. Element distribution maps for the image above taken for the shear zone of the 280 kPa thin section at 710 times magnification. Concentrations of calcium (middle image) can be seen above by the grey dots on a black background.

6.6 Surface Nodules

On the 280 kPa confining stress thin section, a clustering of bright nodular, circular and plate like objects were observed in close proximity to the PSZ. This was captured in figure 6.9A. The PSZ proceeded approximately 2 centimetres above the image taken, with the image captured at 1510 times normal magnification. The image itself shows a wide variety of features present on the clay surface. The background clay appears dark in the image. The two main prominent features that are evident on the clay surface are, firstly the bright, large nodules present on the clay surface, and second, the platy flakes that appear at various points across the image, stretching between the bright round objects in some instances. When undertaking element distribution imaging on the image as a whole, we can observe a deficiency in O, Al, Si and C. What we can observe is that these nodules present a spike in K. Areas within the shear zone displayed higher concentrations of Si. These are visible as large plate objects, noticeably larger than the nodules and clay groundmass around it, indicating that these are most likely portions of volcanic glass. To better distinguish these features, and gain a better explanation of what these nodules may be, a more detailed analysis was undertaken at a much higher magnification.

6.7 Nodules

The nodules were examined at both 15,000 times magnification (Figure 6.9B) and 40,000 times magnification (Figure 6.9C) using BSE imaging to gain a better contrast and present the nodules in higher detail. When examined at these higher magnifications it becomes more apparent that these nodules are made up of a number of smaller parts that have fused together along specific planes. Measurement of these nodules according to a scale of 3.00um indicates that these nodules are approximately 0.3mm in size. When examining at the highest magnification it is apparent that whatever the nodules are, desiccation cracks are present on the surface, with the shape being roughly spheroid in nature.

The highest magnification also indicates that these larger nodules are connected to the groundmass at specific points with desiccation present on this groundmass similarly to these larger nodules. A point element analysis was undertaken (Figure 6.9D) with 7 specific points identified. Points 1,2 and 7 were taken of the clay groundmass,

while points 3,4,5 and 6 were taken on the nodules themselves. As expected points 1,2 and 7 all displayed element graphs representative of halloysite, being rich in silicon and aluminium, with a small peak observed for potassium (Figures 6.10) Surprisingly for points 3,4 and 5 the results were consistent and displayed similar results. The results indicated that these nodules were incredibly rich in potassium, but also displayed peaks in silicon, aluminium and oxygen though not to the same degree as potassium. Initial indications suggest that these large nodules may well be large amalgamations of halloysite clay.

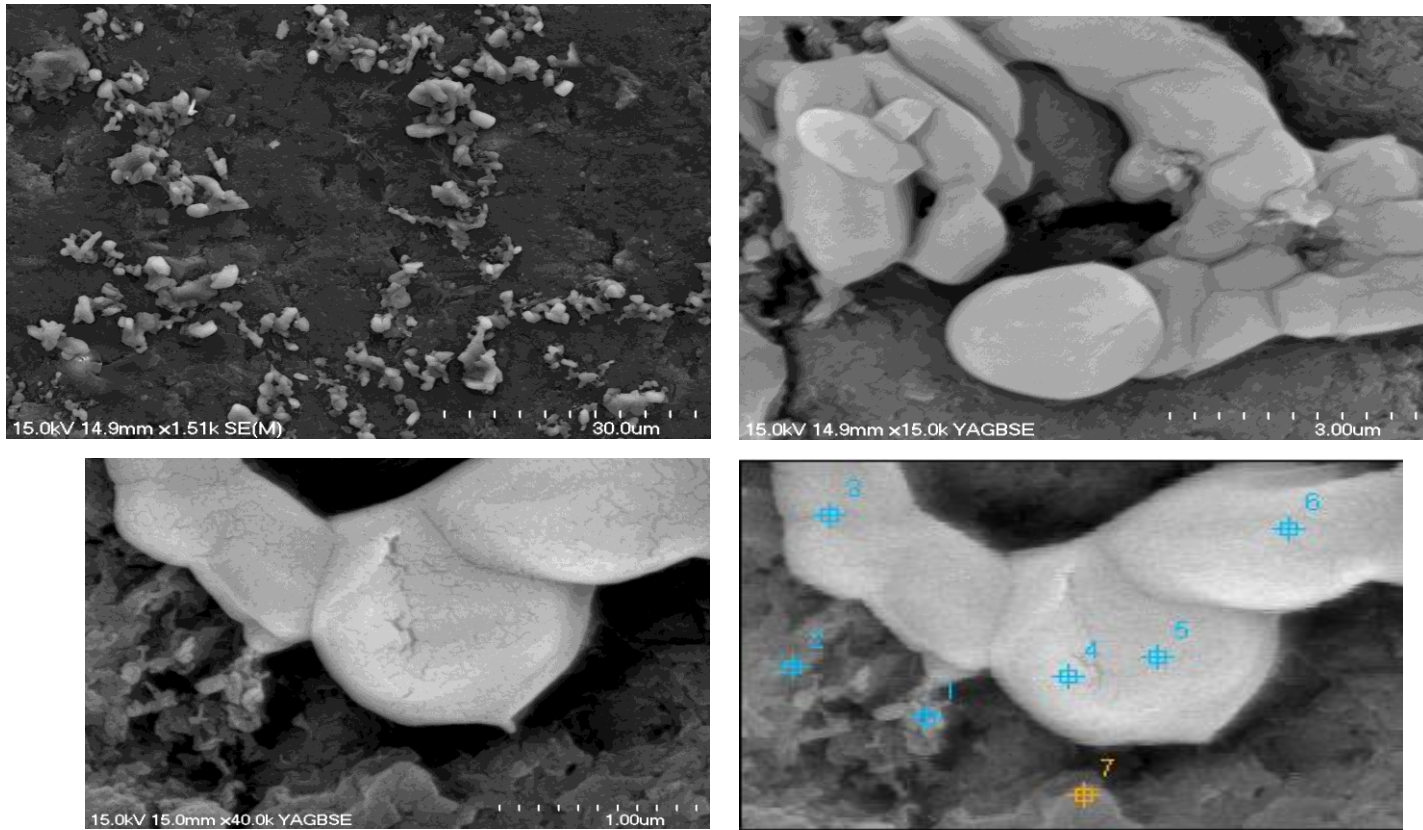


Figure 6.9(A) Taken at 1500 times magnification of the 280 kPa thin section in regular SEM bright circular nodules can be observed propagating on the clay shear surface, with plate like flecks present. **(B)** A BSE taken at 15,000 times magnification of one of the nodules, at this higher magnification it can be seen that these nodules are connected to each other and made up of numerous smaller nodules that have bonded together. **(C & D)** Taken as a BSE image at 40,000 times magnification an extreme close up of the nodule reveals the circular concave shape of the nodules, with desiccation cracks evident, the right hand image shows the points at which point element measurements have been mad

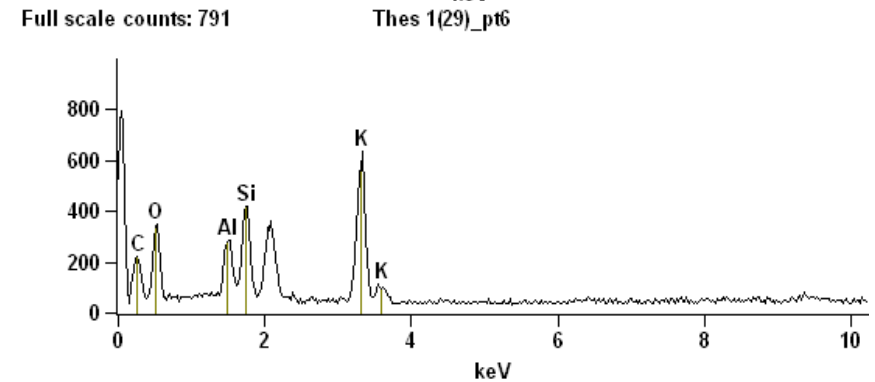
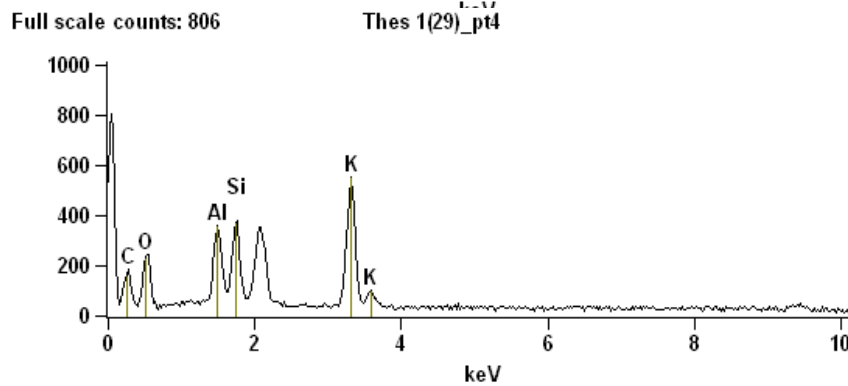
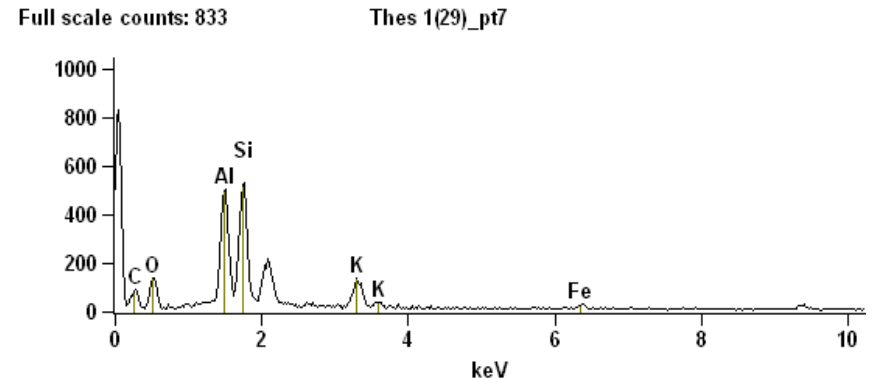
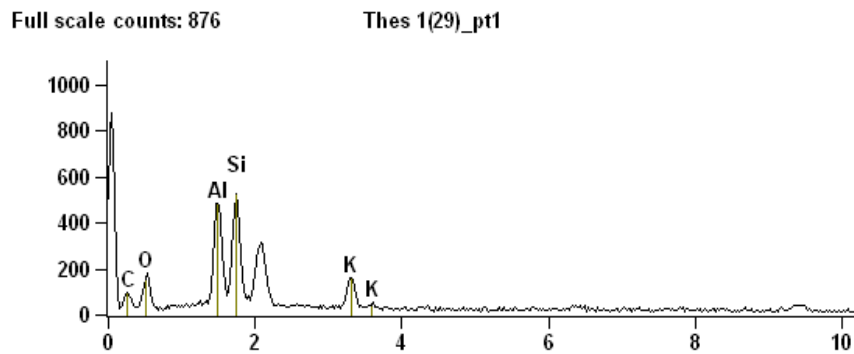


Figure 6.10. Point element analysis graphs for points 1,4,6 and 7 for image 6.9D. Points 1 and 7 show typical treated halloysite clay measurements with peaks measured for silicon and aluminium, whereas points 4 and 6 show peaks similarly for halloysite for silicon and aluminium, but differences are observed as there is a significant peak in potassium for these two points, with potassium measured as the highest proportion of element present at these points.

6.8 Fractured Crystals

Figure 6.11 was taken on the 205kPa thin section and shows a low magnification (200x) image of a crystal found within the clay groundmass (Figure 6.11). When examining the crystal in wider context we can observe that it is a large and hexagonal in shape with cracks propagating through the sample in an up-down fashion, with some form of cleavage observed from a distance. When examined closer up it become apparent that there are hundreds of thin layers of material pushed together making up the crystal surface, with a noticeable relief present on the surface, furthermore the close up of the surface highlights the fact that there are plenty of broken edges present on the surface of the mineral, with a number of recesses into the mineral crystal present on the surface. Based on the shape and distinctive features present on the crystal it is inferred that this is a highly weathered orthoclase crystal present in the groundmass, with the cracking present in the crystal itself most likely attributed to pressure placed on the sample during shearing and not as a result of desiccation.

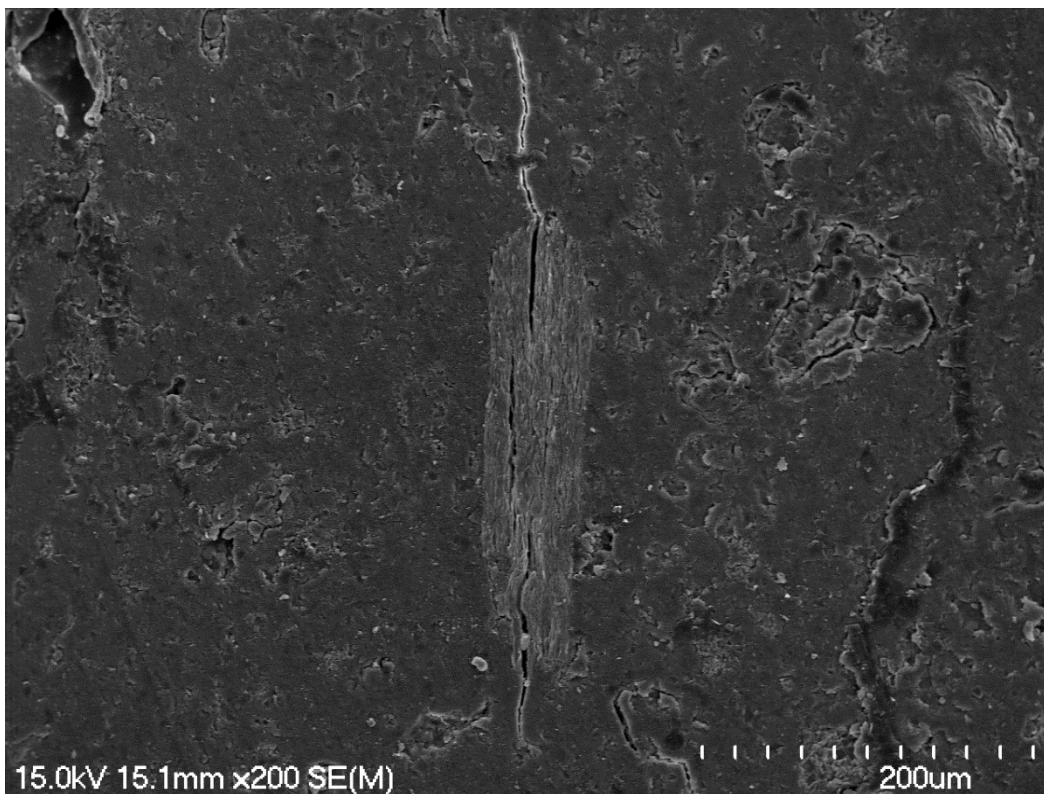


Figure 6.11. A possible orthoclase crystal with fracture propagating through the crystal at 200 times magnification taken in normal SEM

6.9 Crystal identification

Identifying certain crystals through usage of an optical microscope proved to be difficult due to the varying thickness of thin sections during creation as a result of the varying hardness of the slide. Furthermore, in more than one instance crystals were highly fractured as a result of interaction with shear zones and have had a shear propagate through the crystal resulting in a greater degree of fracturing occurring to the mineral crystal.

The crystal Figure 6.13 was found within the 205 kPa thin section. It is a crystal with charged edges present and fractures crossing throughout the mineral. To the right of the crystal it was evident there was a shear zone that had been infilled by an unknown substance. A broad-spectrum analysis was performed and the elements present were graphed (Figure 6.12). This broad analysis showed a large proportion of iron and carbon present (50.5% and 27.2% respectively), with a distribution of potassium, silicon, aluminium, titanium and oxygen spread across the area.

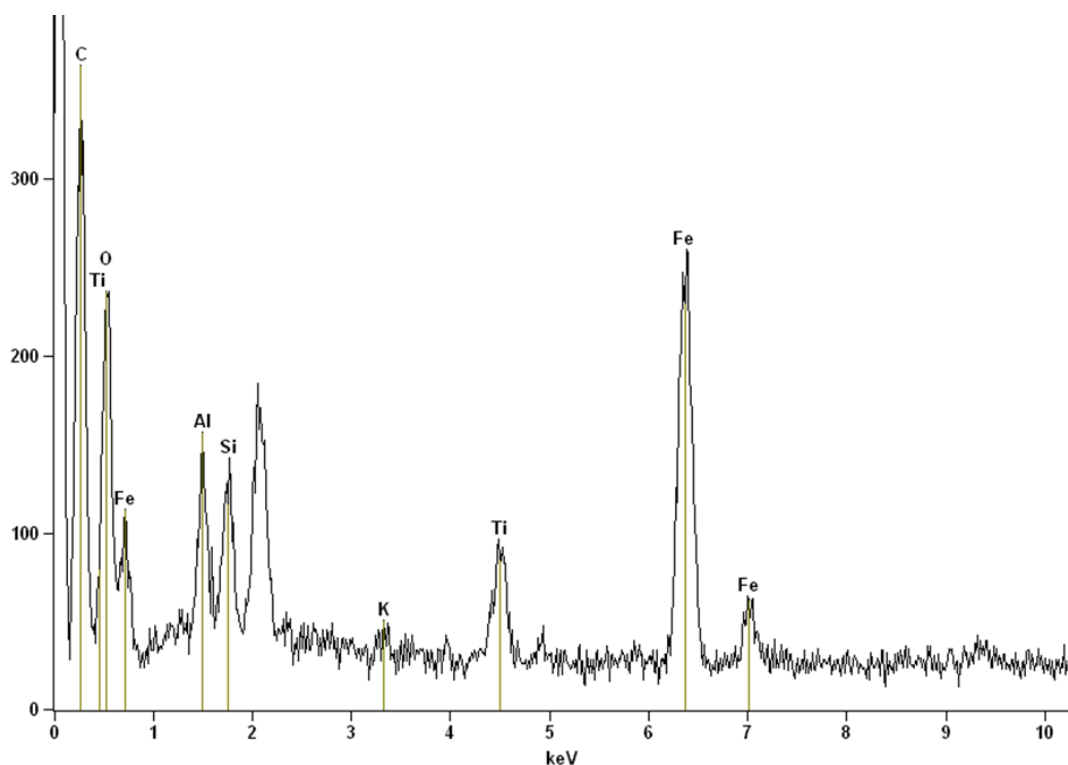


Figure 6.12. An element distribution graph for the crystal present in figure 6.14 with peaks measured for multiple elements.

When focussing on the mineral itself at a greater degree of magnification identification of the mineral via visual methods was not possible, as such an element map was created for the mineral. These were displayed in figure 6.13. These images show element distribution of the mineral surface. As can be seen the primary elements present were Titanium, Iron and Silicon with other elements not detected in sufficient quantities to be plotted. This does not mean that Oxygen and other elements are not present within the sample, instead it shows that these elements are not present in a sufficient number to be plotted onto the distribution image. Based upon the large volume of Iron and Titanium found within the sample as it is postulated that this mineral in particular is an ilmenite crystal.

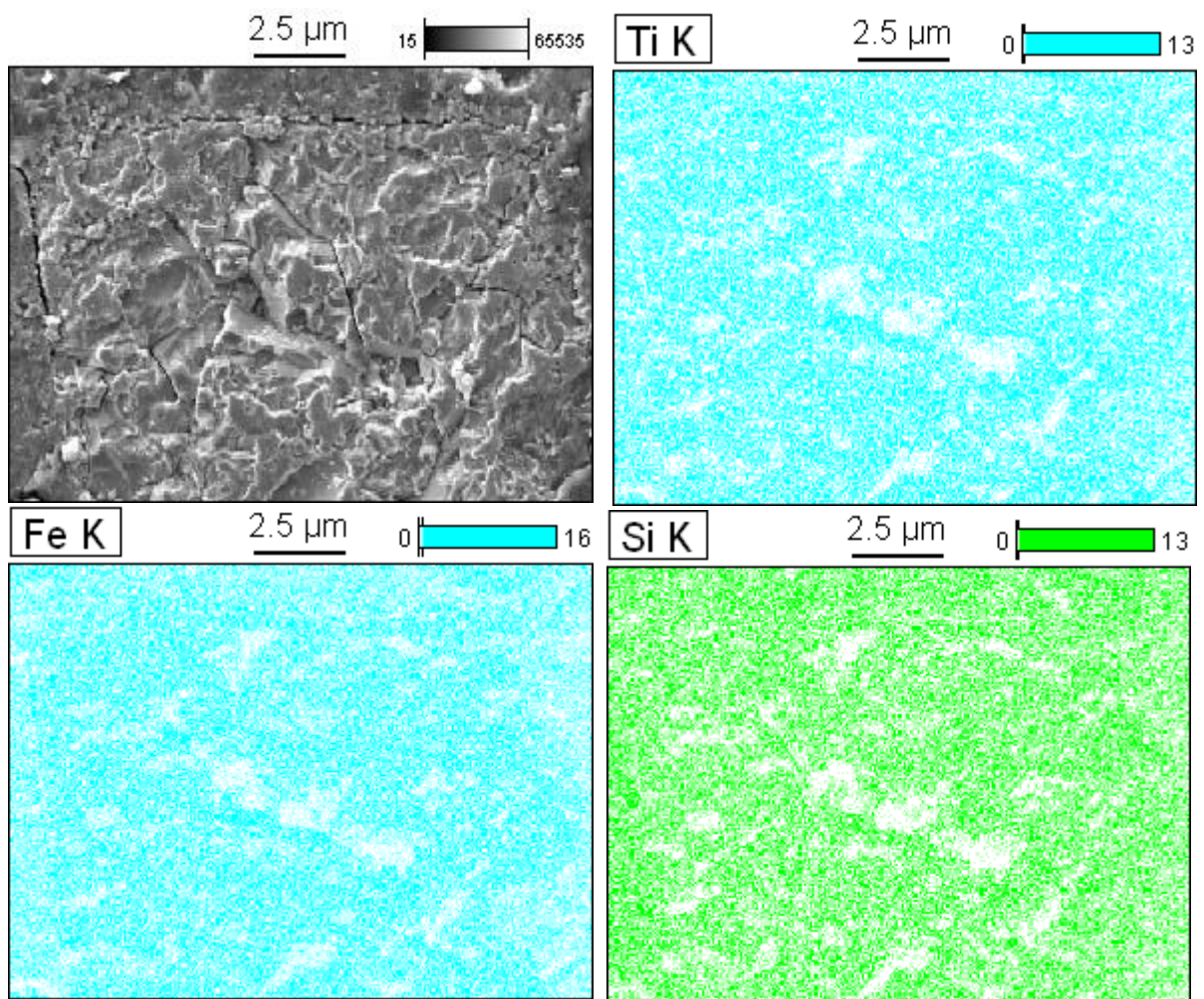


Figure 6.13. An element distribution map for titanium, iron and silicon present for the image shown in the top left corner.

6.9.1 Unidentified crystal

On the 355kPa thin section it was noted when examining in low magnification the presence of a large unidentified object, this object was further examined in higher magnification. The object itself can be observed in figure 6.14A and B below. As it can be seen it is a 'mug' shaped object with numerous indentations and textures on the surface, appearing to be curling around on itself with a flat base. SEM and BSE imagery were both taken to observe any significant changes in element weighting on the object in comparison to the background mass, at approximately 4500 times magnification. BSE imagery showed little variance in its imagery (Figure .6.14B), merely producing a slightly sharper image. To better determine the potential make-up and assist in identification of the object element distribution was conducted on the sample. These element distributions can be observed in figure 6.15. Some key elements that were observed were for one Carbon, this was evidently highly present in the background mass of the image- with this being potentially attributed to the epoxy resin. The object itself displayed a distinctive and identifiable concentration of both Sodium (Na) and Chlorine (Cl), with some Potassium (K) identified on it. Accumulations of Silicon (Si) could be observed at the base of the object as well as specific points around the object, these potentially being quartz crystals or volcanic glass found in close proximity to the object. In attempting to identify the object itself the element distribution suggests an object having a high concentration of both Na and Cl, indicating the potential for it to be a Sodium Chloride crystal, though considerably weathered.

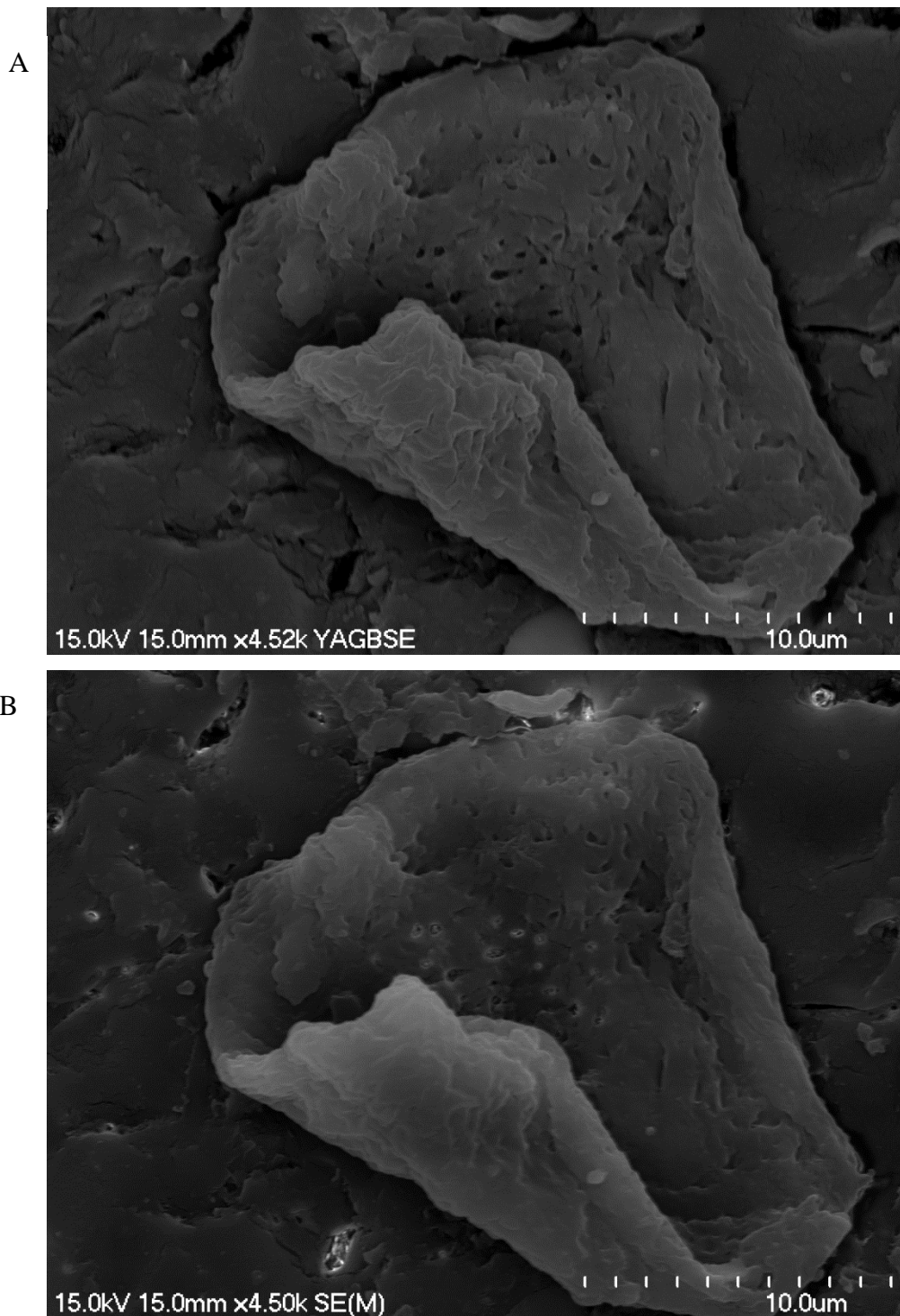


Figure 6.14(A) A BSE image of what is thought to be a weathered NaCl crystal found in the 355 kPa thin section. **(B)** An SEM image at 4500 times magnification of what is thought to be a NaCl crystal.

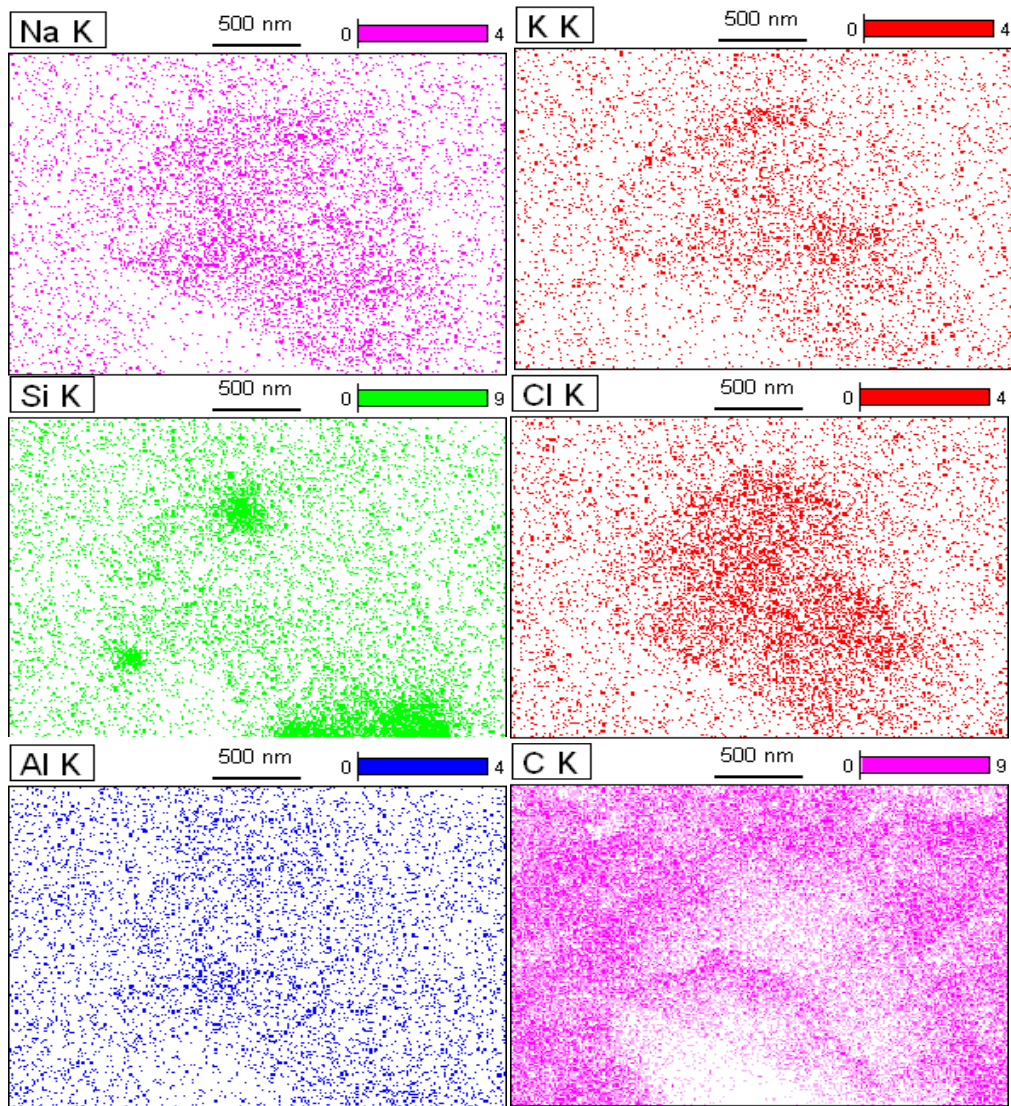


Figure 6.15. An element distribution chart for a variety of elements detected on the image of figure 6.14. Concentrations of Na and Cl are heavily evident on the crystal itself.

6.10 Summary

Usage of SEM and BSE imagery along with element point and distribution analysis allows a wealth of information to be derived from our thin section slides on a larger scale. By utilising this higher magnification imagery we are able to observe crystals closely and determine how they may have interacted during shear. Furthermore, we are able to examine in great detail how soil and material within a shear zone has acted during shearing while under stress, and whether traits such as mineral and soil alignment has occurred during shearing. Element distribution allows for the identification of minerals, such as NaCl where they have weathered beyond usual distinguishable nature.

Chapter 7

Discussion

7.1 Chapter Outline

In this chapter, all the results gathered during the course of this study will be discussed in order to explain the factors that have caused the results that I have observed. The failures that have occurred recently during the writing of this thesis will also be discussed with potential failure mechanisms, cause of these failures and the parameters that may have had a negative effect on the slopes prior to failure discussed before being summarised in the final paragraph.

7.2 Geo-mechanical properties

To begin with it is necessary to review my sampling techniques and examine whether or not these were of a sufficient standard for the study and for future potential studies that may occur. As stated, the necessity of properly sampling and storing samples during the course of study on soil of a sensitive nature is paramount due to the rapid loss of sensitivity in soil following removal from its *in-situ* state if improperly stored (Lessard & Mitchell, 1985; Rochelle *et al.*, 1986a). In this regard, and from all the samples collected, it is of my belief that all steps undertaken while field sampling were conducted in a fashion that ensured that field moisture was maintained and if any loss of sensitivity occurred at all in the samples it was negligible.

The only factor that could potentially be altered for future studies is, instead of the use of standard stainless steel corers as were used in this study, for future use plastic soil corers may potentially be used instead. It is noted that stainless steel, though stable for the most part, does interact with salt solutions, and as such during the treatment process there is the noted potential for the interaction of the soil cores to react while immersed in the salt solution (Suttcliffe *et al.*, 1972). With this said, the reaction amount is considered negligible for the purposes of this study, so has had no effect on the results produced.

7.2.1 Atterberg Limits

A key aspect of any study involving sensitive soils is determining the Atterberg limits of the soil. These limits give us a strong underpinning for any changes or manipulations a person may wish to make to the soil. From the table we can see that even when comparing the data of Moon (Personal communication, 2016), Mills (2016) and the baseline data for distilled water in this study the results are varied. Liquid Limit ranged from 66 (Mills, 2016) to 100 (Moon, 2016) with 92 measured in this study. In contrast to this the plastic limits (PL) of Moons (2016) and Mills (2016) results were much closer together in value (53 and 41), which is significantly lower than the results produced in this study (78.2).

One potential reason for the variability between the results produced across these three studies could possibly be linked to spatial variability in soil make-up, with it a well-established result in literature the discrepancies within soil over a short area (Nielsen *et al.*, 1973; Phoon & Kulhawy, 1999). With this said, it is my belief that this potential reasoning can be discounted as the local variability is believed to be relatively low, with all soil collected for the three studies taken from within 2 meters of each other. Instead there are two strong possibilities that could potentially explain the results observed.

First, focusing on the Liquid Limit variability we can see that the results produced in this study and Moons (2016) personal communication are consistent, while Mills (2016) study produced a Liquid limit divergent to those of this study. I propose that the reasoning for this difference can be attributed to the presence of halloysite in its dehydrated 7Å form within Mills (2016) study, as the low values of both the liquid and plastic limits are strongly in keeping with those of previous studies on dehydrated halloysite (Selby, 1982; Selby, 1993). This is not to say that errors were made in Mills (2016) study during testing, the more likely explanation is the soil has undergone some drying process during sampling, transport and storage.

When focusing on the Plastic Limits we can see that the PL of this study were significantly higher in comparison to those derived in the previous studies. Though Mills (2016) results may have been skewed due to the presence of an excess of 7Å halloysite, the PL of said study was much closer to that derived by Moon (2016). The discrepancy between those studies and the result of this study may well be founded in operator error. It is highly likely that due to the subjective nature of

the methodology used in deriving the Plastic limits, mistakes may have been made during this study resulting in anomalously high results being produced. The consistency of the results produced during this study for PL before and after treatment indicates a consistent error being reproduced across all samples and results tested.

The minimal change in PL after treatment may reflect the fact that measurement of the plastic limit was derived from soil taken after a single addition of salt treatment to the soil paste. This could indicate that the soil has had insufficient amounts of salt ions and time to affect the plastic limit in an appreciable way. To adjust this, it is suggested that for any further research conducted the methodology for measuring plastic limit is altered with the sample utilised for measuring the plastic limit taken from the final sample after liquid limit has been reached and potentially exceeded as this would allow sufficient time and treatment of a sample. That way any changes that have occurred to the soil can be appropriately observed.

7.2.2 Atterberg Limits - Treatments How they Worked out

For the initial parts of this study when determining the salt that would be of most use, 3 salts were chosen to be used as these showed most promise of influencing a potential rheologically positive result. Potassium Chloride (KCl) was chosen due to its use in Norway in a long term trial of stabilising a landslide in sensitive soil and the positive results produced by this trial in the stabilisation of the slope (Helle *et al.*, 2015; Helle *et al.*, 2017), as well as further studies conducted in Italy in stabilising a similar sensitive-soil derived slope (De Rosa *et al.*, 2016). Potassium Hydroxide (KOH) was used due to a combination of the fact that throughout literature a strong link had been derived between the pH of halloysite rich soils and their propensity to take up ions, and furthermore the strong affination of halloysite to readily intercalate potassium ions (Packham, 1965; Theng & Wells, 1995). Potassium Carbonate (K_2CO_3) was chosen for a number of reasons.

First of these is due to the relation between K_2CO_3 and $CaCO_3$, with K_2CO_3 being of a similar nature to conventional lime, with the key difference being the differing cation within the compound. It is well known throughout literature the positive rheological effect that lime has on clays when treated (Locat *et al.*, 1990), it was perceived that though a differing cation is utilised the effect of the salt may have a similar positive effect on the soil. Furthermore, the intercalation of K_2CO_3

into the halloysite crystal lattice was well established in the literature, with a number of researchers indicating the growth of the halloysite crystal lattice from 10.1Å to 13.6Å following treatment with K_2CO_3 (Garrett & Walker, 1959; Wada, 1959; Carr *et al.*, 1978). Figure 7.1 details the normal arrangement of a single halloysite unit, with the upper aluminol sheet and full halloysite unit shown at the top of the diagram. The figure displays the hypothetical arrangement of associated water present within halloysite in its 10.1Å arrangement.

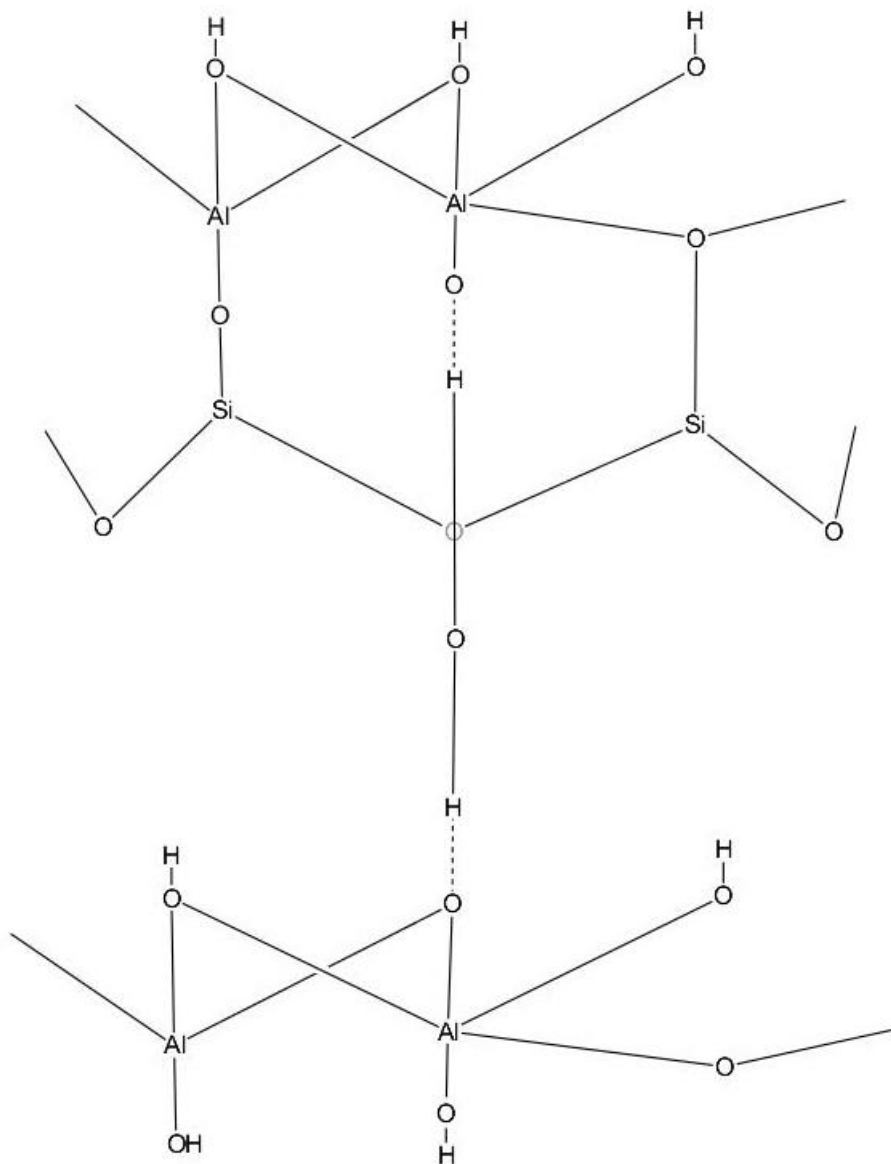


Figure 7.1. A concept sketch of how water intercalates into the halloysite crystal basal space. The H₂O unit forms temporary hydrogen bonds with the hydrogen deficient hydroxyl groups on the aluminol sheets and actively intercalates.

7.2.2.1 - Potassium Chloride Treatment

KCl was arguably the treatment of least effectiveness in producing positive results for the study. When looking at the results in further detail we can see that the LL was reduced to 79%, PL lowered to 75% and activity reduced to 0.28 when compared with baseline values.

Evidently the usage of KCL following results such as these was discounted from the study for further use, as it definitively provided evidence of weakening of the soil paste as can be observed by the reduced Liquid Limit following treatment of the soil. Though removed as a potential further soil treatment it is important to examine why the treatment was unsuccessful. One prominent attribute that can be examined here is the effect of the KCl treatment on the pH of the soil, with both measurements used for measuring the pH producing a reduction in pH from baseline.

This is significant as pH when examining soils rich in halloysite can be used as a key indicator of whether the clay colloid surface is likely to take up ions. The point of zero charge (PZC) measured on the clay surface is the measured potentiometric charge on the surface of each clay particle and indicates whether the clay surface is positively charged whereupon there is an excess of Hydron ions (H^+) on the clay surface, neutral, where the clay surface has the ideal number of hydroxyl bonds to the inner aluminol groups, or negatively charged where the clay surface has exposed bound oxygens that are deficient in a H^+ ion. Theng & Wells (1995) paper indicates that at lower soil pH for halloysite the clay surface is positively charged and as such has an excess of H^+ ions bonded. At these lower pH's the soil will actively look to release these H^+ ions where possible and return itself to a state of neutrality, this is due to the chemical instability created by the excess of H^+ ions present on the clay surface.

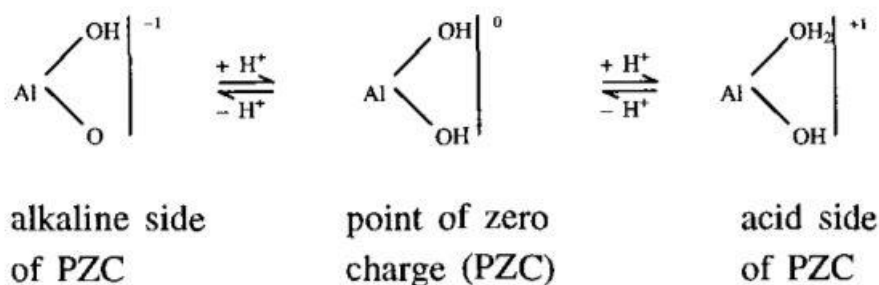
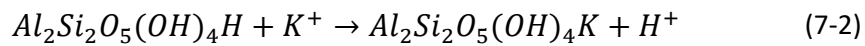
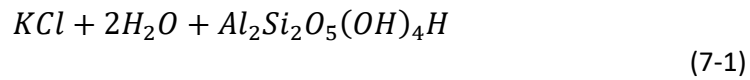


Figure 7.2. Sourced from Theng & Wells (1995), showing how the Aluminol sheet in halloysite changes its charge dependant on the soil pH.

Figure 7.2 details this difference on the clay surface as a result of the excess of H^+ ions present. A potential hypothesis for the resultant drop in pH is the change in number of hydron ions present in solution. This derives from the concept that pH is a direct measurement of whether a solution has a larger volume of H^+ (usually in the form of hydronium or H_3O^+) or OH^- groups present. A larger volume of H^+ indicating a decrease in pH and the inverse for an increase in pH. How this occurs can potentially be explained in equation 7.1 and 7.2 below.



The equation details firstly the dissociation of potassium chloride (KCl) in water, and following this the interaction with water. It is worth noting that though the natural equation of halloysite is only $Al_2Si_2O_5(OH)_4$ for the purpose of expressing the presence of the additional H^+ on the surface of the halloysite that occurs due to the positive surface charge present on the clay naturally as a result of its low pH an additional H ion is added to the end of the molecular make-up. It is necessary to note that it is only bonded with weak hydrogen bonding onto the clay's surface. Furthermore, another point to make note of is the fact that though this equation shows a representation of the potential interaction with KCl during treatment, the likelihood of this exchange of ions on the clay surface of K^+ replacing the H on the clay surface is likely to be stunted as a result of the positively charged clay surface, with the positive charges on the surface repelling the K^+ ions when they come in to contact with the surface.

With this said, the large diffusion gradient that will occur in close proximity to the clay surface as a result of the large number of K^+ ions per ml of water means that there will be some exchange of this form occurring (Tan, 2010). Tan (2010) indicates that these ions have to overcome a double diffuse layer (Figure 7.3) whereupon ions are required to overcome the energy to bind with the OH groups bound to the Al ions of the crystal lattice. This indicates that the ions present within solution need to have a significantly high energy when coming into contact with the clay surface to overcome the electrostatic repulsion. This activation energy required highly unlikely to be achieved due to the heat required to provide sufficient energy causing a dehydration of the halloysite. As a result this can only be achieved by

saturation of the double diffuse layer by an excess of ions, and as such forcing the transfer of ions the creation of an incredibly large osmotic gradient.

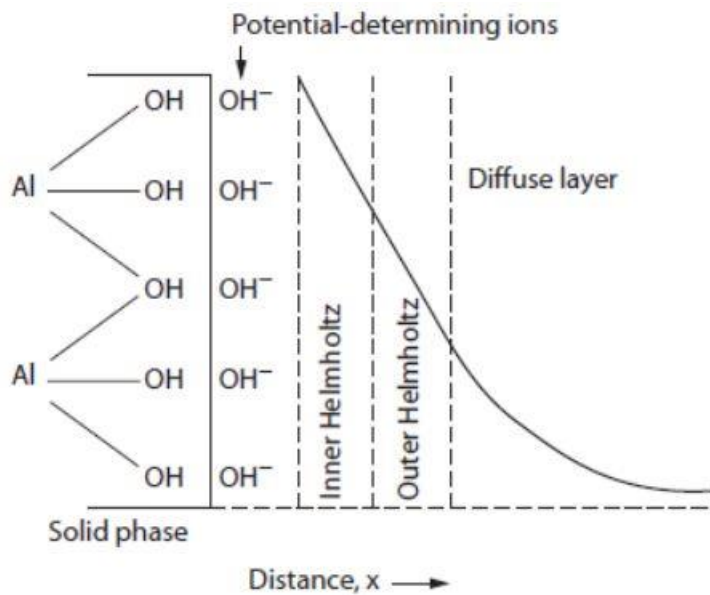


Figure 7.3. Sourced from Tan (2010), the diagram above represents the hypothetical inner and outer hemholtz layers that ions have to overcome to bond.

Regarding the lowering of pH of KCl treated samples, it is hypothesised that to some degree on the very outer edges of each halloysite clay particle some exchange of H⁺ on the clay surface and K⁺ in solution does occur, resulting in the release of either 1 or 2 H⁺ ions into solution. This increase in H⁺ ions, though they may react with any anions in solution at a later point, form the basis of a conjugate acid within the reaction, and as a result cause the drop in pH that we can observe following the treatment of the soil. It can be stated with relative confidence based on the data of previous literature that the K⁺ ions in this instance will not have intercalated into the crystal lattice, as we would expect a growth in the size of the basal spacing of the clay following treatment, a trait which was not observed in the work conducted by Garret and Walker (1959) and Wada (1965). Why this occurs has not been explained in literature, though it can be hypothesised that due to the low pH of the clay with the KCl treatment, the electrostatic repulsive nature of the clay surface is too great for the K⁺ ions present in solution to overcome.

7.2.2.2 Potassium Hydroxide Treatment (KOH)

The results that were produced following the KOH treatment were unexpected and were the opposite of what I had anticipated. As can be observed in the treatment of KCl, the effect of pH on the likelihood of an ion to intercalate and

thus increase the measurable rheological strength is well stated throughout literature (Garrett & Walker, 1959; Wada, 1959; Carr *et al.*, 1978; Theng & Wells, 1995), with the higher the pH the more likely the ion is to intercalate within the clay and interact with the clay surface. KOH is a strongly basic compound and readily dissociates due to its alkaline nature, with a natural pH of 10.8.

The compound readily reacts with both organic and inorganic compounds to form various hydroxyl complexes. Due to the basic nature of the ion it was thought that the treatment would indeed increase the measurable Atterberg limits of the soil. The results though showed a differing trend, with the liquid limit showing a decrease from the baseline from 93% to the measured 84% moisture content, a decrease of 9%. With this said though the soil pH had markedly increased from the natural soil pH of around 5 to pH of 8.03 - 8.32 using the differing methods. The treatment had evidently increased the soil pH to a point that had made the PZC of the soil surface negative, with the soil itself being weakly alkaline. This established through previous studies conducted on the PZC of halloysite (Theng & Wells, 1995; Joussein *et al.*, 2005). Though evidently on the negative side of the PZC the soil still showed a decrease in the liquid limit.

Literature indicates that KOH does not directly intercalate into the crystal lattice, but certainly interacts with the clay surface at these neutral pH values. Carr *et al.* (1978) indicate that following treatment with KOH halloysite crystals will exhibit expansion across the C axis, resulting in disordering of the clay. They also showed that following treatment the treated halloysite, once dehydrated, will completely rehydrate from its 7Å form to its 10Å form, though did not elaborate on this point. This rehydration indicated that the inter-layer halloysites had a distance of 3.1Å between each tetrahedral and octahedral space, showing that the distance between layers following treatment is identical to that of the natural distance between layers in this inter-layer space where the clay's hole water usually resides (Figure 2.2A and B).

The disordering described by Carr could potentially arise from the edge interactions of KOH and the clays themselves, with the KOH replacing the hole water on these edges with the slight increase in basal spacing observed (2.9Å for water and 3.1Å for KOH) possibly accounting for this. Figure 7.4 shows a molecular view of the water interaction in between the clay layers, with each KOH only able to interact with a single H deficient OH group on the aluminol surface. On top of the Silanol surface of the clay the KOH is unable to interact with the inner

OH group. This interaction most likely only occurs on the broken edges of each Halloysite unit and as a result sparingly releases the excess OH groups accounting for the slight increase in pH to approximately 8.

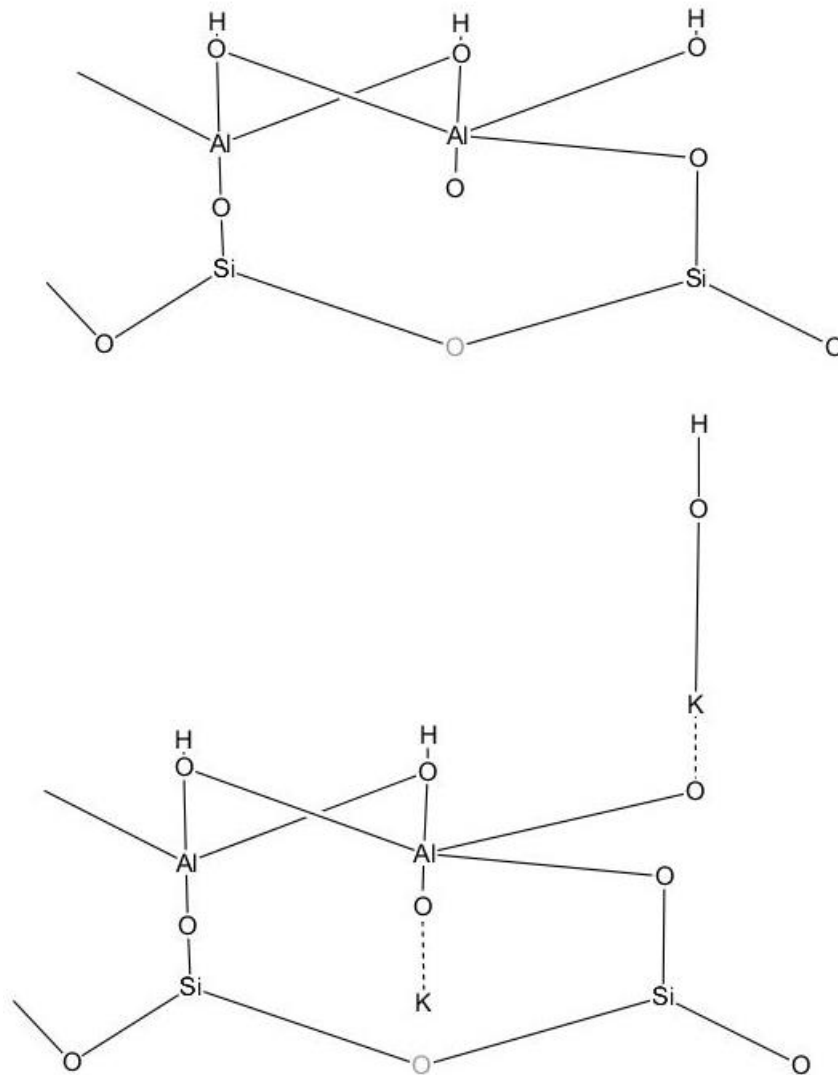


Figure 7.4. A hypothetical concept sketch of the chemical bonding and ionic bonding that will occur when KOH interacts with the aluminol sheet of halloysite.

7.2.2.3 Potassium Carbonate (K₂CO₃) Treatment

Prior to the usage of K₂CO₃ as a treatment it had become evident that previously tried K⁺ based treatments had been unsuccessful. However, it became apparent that K₂CO₃ had produced positive results, with a measurable positive rheological change within the soil paste. Liquid limit increased from 92.3% to 92.6% moisture content following treatment and plastic limit was also slightly affected with a drop in plastic limit from 78.2 to 73.4 resulting in an increase in overall plasticity. The largest change that was measured for the K₂CO₃ treatment was the pH, with both the soil paste and air dry methods recording a significant increase in soil pH from the baseline results to 10.3 and 10.4. This increase in pH of approximately 5 pH units indicates a significant release of OH⁻ groups into solution following treatment of the paste with K₂CO₃.

The treatment of the halloysite rich clay with K₂CO₃ showed that there has been significant interaction between the solute and the clay itself, a factor which is well established in literature with multiple authors indicating the propensity for K₂CO₃ to readily intercalate into the halloysite crystal lattice itself (Garrett & Walker, 1959; Wada, 1959; Carr *et al.*, 1978). K₂CO₃ enters the space usually occupied by water between the upper silanol of one halloysite unit and the lower aluminol unit of another clay (Figure 2.2B), various authors indicate a growth of halloysite from 10.1Å to 13.6Å following mixing with K₂CO₃, with the salt itself accounting for approximately 6.1Å in growth of the basal space following intercalation into the inter crystal space.

This 6.1Å growth in basal space accounts for the replacement of water within the basal space by K₂CO₃, with the halloysite growth from the dehydrated form (Garrett & Walker, 1959; Wada, 1959; Carr *et al.*, 1978; Theng & Wells, 1995). A key factor in the maintaining of the rheological strength following treatment, even with expansion of the clay size could be attributed to the way in which the potassium carbonate has intercalated into the intra-clay basal layer where water usually resides. Figure 7.5 shows a sketch drawing of the method in which the compound may have intercalated between the layers.

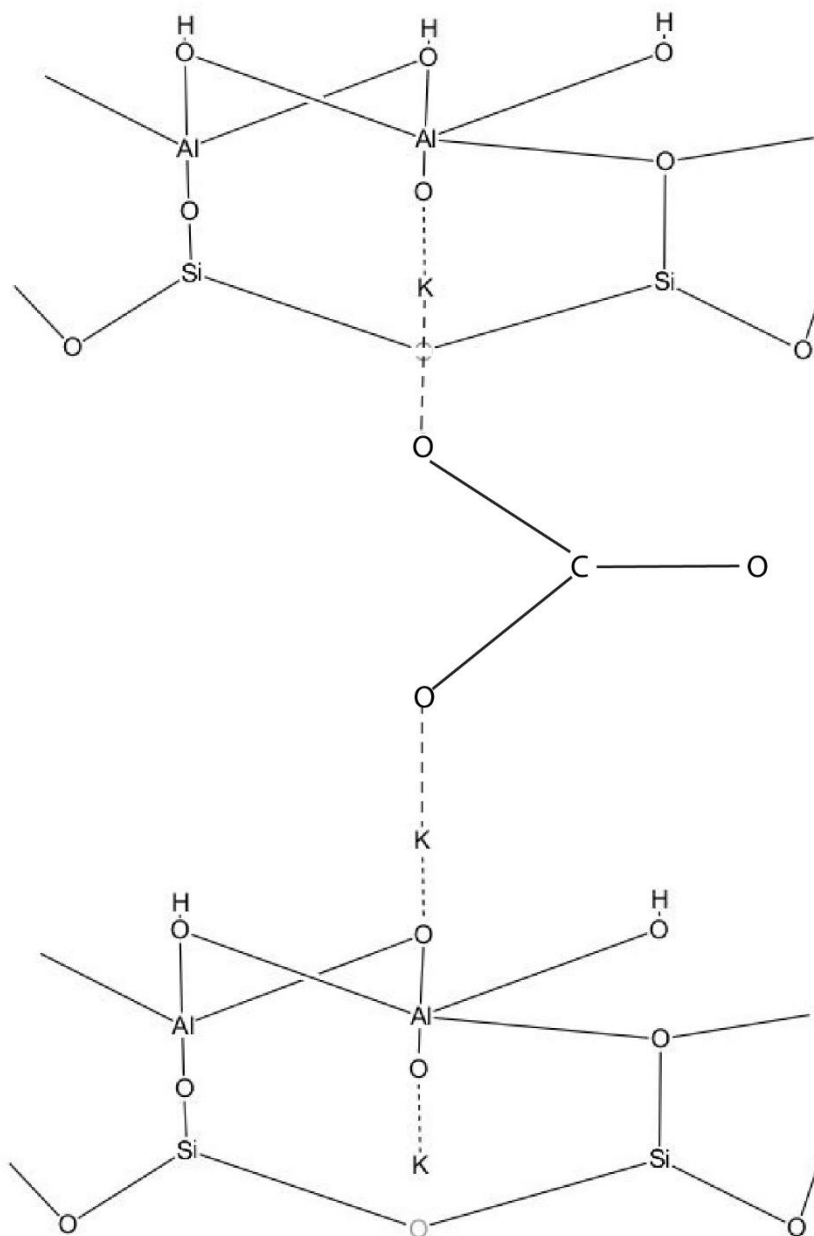


Figure 7.5. A hypothetical concept sketch of the way in which K_2CO_3 intercalates into the halloysite crystal lattice, and subsequently forms temporary ionic bonds with the hydrogen deficient aluminol oxygens.

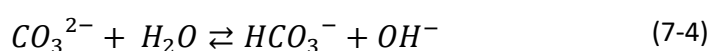
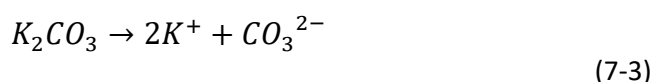
The molecular sketch shows that the two K^+ ions interact with the aluminol layers of two differing halloysite units. One fits into the hexagonal recess known to be present on the silanol surface (Joussein *et al.*, 2005). The K^+ interacts with the inner hydroxyl group connected to one of the Aluminium ions making up the aluminol layers, forming a temporary bond with the inner oxygen. It is important to

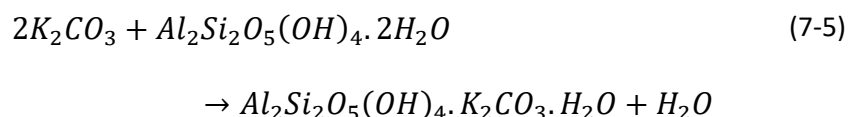
note that the K^+ ion, while in solution is dissociated from the carbonate group, so as such is bonded in a fashion that allows the ion to change which anion it shares its electron with, this allows the K^+ of the K_2CO_3 ion to interact with the inner oxygen of the aluminium sheet.

The expansion comes about as a result of the presence of the carbonate molecule within the inter-layer space with strong repulsion occurring between the oxygen ions of the carbonate molecule and the oxygens bonded to the silicon ion of the silanol layer. With the inter-layer space taken up by the carbonate the other K^+ ion is taken on by the exposed oxygen found on the upper aluminol surface of the lower halloysite unit, forming a strong bond, with the potassium sharing electrons with both the hydrogen deficient hydroxyl and carbonate groups. This exposed oxygen is deficient in a hydrogen as a result of the lower pH induced by the presence of the strong base of K_2CO_3 , causing the PZC of the clay in this instance to be negative (Theng & Wells, 1995). K^+ is favoured to bind with the exposed oxygen over water in this instance due to the significantly larger valence produced by K^+ ions when compared with H^+ ions.

To determine whether intercalation occurs would require a number of tests that lay outside of the scope of this thesis. These tests include the usage of Infrared spectroscopy, ICP-MS testing and X-Ray Diffraction testing to determine basal spacing size.

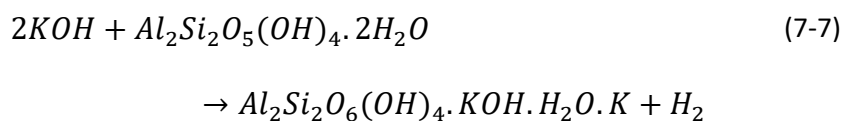
With all of this examined it is important to consider the potential reasoning as to why the pH of the mixture was higher when treated with K_2CO_3 in contrast to being treated with KOH as both are strong bases, and actively de-protonate compounds when placed in solution. The key factor as to why one treatment results in a significantly larger volume of OH^- ions released into solution to increase the pH may have basis in the interaction between the salts and the conjugate acids and conjugate bases they form. Equation 7.3 details the dissociation of K_2CO_3 and the various conjugate bases and acids it forms as a result when interacting in solution with water and then halloysite





As is expressed in equation 7.5 we can observe that as the treatment progresses following interaction with the Halloysite clay mineral itself, the K_2CO_3 actively intercalates into the clay basal space, resulting in the forcing of a single H_2O out of the clay into solution. Equation 7.4 shows the equilibrium produced when K_2CO_3 is dissociated in water, with the alkalinity increased as the CO_3^{2-} ions deprotonate water and produce an excess of OH^- ions. By intercalating into the halloysite basal space, an excess of water is present within the surrounding solution, as such this causes an imbalance in equation 7.4, with the left side of the equation having an additional H_2O ion. As such to maintain the equilibrium of the reaction, the reaction will tend to the right to remove this additional H_2O , resulting in an excess of OH^- ions present in solution, producing the drop in pH that we observe for the sample.

In contrast to this it is necessary to examine why the KOH treatment did not produce a pH as high as K_2CO_3 did. Equation 7.7 displays the steps between the dissociation of KOH in water and its interaction with halloysite itself as was applied to K_2CO_3 initially above



As we can observe from equation 7.6, initially KOH breaks down into a more strongly basic solution as there is an excess of OH^- ions in solution following the introduction of KOH into water. When interacting with halloysite we can see a release of the water that is replaced on the clay edges by the KOH molecule. As such we are left with a single K^+ ion. This weakly basic ion then looks to form a strong conjugate base, and as a result of the excess OH^- ions present it reforms KOH in solution. While there is the presence of a strong base in KOH the effectiveness

of this base is reduced due to the large number of water (H₂O) molecules present at the end of the treatment, which reduces the overall pH essentially diluting the strength of the basic KOH and accounting for the lower pH that we observed.

7.2.3 Ion Uptake Curves

Ion uptake by halloysite is a factor examined by Wada (1959) in significant detail, and further elaborated on by Carr *et al* (1985) in later work, with researchers examining how many ions were taken up by the halloysite clay when treated with a variety of salts. Wada (1959) found that 200-300 mmol of salt ions in solution per 100 grams of clay were adsorbed onto the clay surface and as such intercalated into the crystal lattice of the clays themselves. This amount accounts for approximately 2 molecules of salt taken up per unit cell of halloysite. This value was revised in further research to approximately 14 mmol of salt ions per 100g of clay taken up (Wada, 1965). With this we can estimate the potential number of ions that will likely be taken up during the course of this treatment.

When examining the clay cores in this study the average weight of all clay cores prior to treatment was approximately 460 grams of soil, this value taking into account the weight of the steel soil corers. From this we can estimate that based on a value of approximately 63% of the soil (with a margin of error of 4%) from the sampling site being made up of clay (Mills, 2016), 290 grams of soil per 460 grams of each core is directly made up of halloysite in some form. If we apply the measurements derived from Wada (1959, 1965) of only 14 mmol of salt per 100g of clay, a total of 40.6 mmol of salt will be taken up in total within the clay itself. The data collected of the varying conductivity of the solutes during treatment for 3 soil cores in each bucket allows us to map the changing and final volumes of ions taken up into the soil cores themselves, albeit with a number of assumptions.

The data collected for the conductivity changes of the treatment solution, shown in figure 4.6 in chapter 4 indicates that approximately 4×10^{17} ions of K⁺ were taken up by the total soil within the soil cores of each treatment bucket. This is calculated from the change in overall conductivity of the solution during the treatment period. When converted to the molar equivalent we apply Avogadro's number to derive the molar value from the number of ions which allows us to produce a value of 0.4 moles of K⁺ taken up in total by the 3 soil cores. Following this we can determine how much is taken up per gram of clay. To achieve this, we sum the average weight of clay for 3 soil cores (290g the average, thus 870 grams

is the total weight of clay) meaning $0.4/870$, which produces a value of 0.001379 moles of K^+ taken up per gram of clay present in the soil, or 1.38 mmol of ions per gram of soil. From this we can expand it to have it in keeping with the units used by Wada to produce a value of 138 mmol/100g of clay. This indicates that during treatment the soil took up significantly more ions than would have been expected, in the order of 100 mmol greater than predicted based upon Wada's (1959, 1965) studies. This discrepancy could well be founded in differences in the morphology of the clay, with differing sources of clays globally producing a wide range of cation exchange capacities (CEC) dependant on location. This indicates that prediction of ion uptake is an incredibly challenging task to accomplish as discussed by previous authors (Riviere, 1948; Garrett & Walker, 1959; Wada, 1959, 1965; Carr *et al.*, 1978; Joussein *et al.*, 2005).

7.2.4 Concluding

To summarise the data collected from chapter 4 it can be concluded that the change to liquid limits for the soil following treatments can be regarded as a reliable result, which shows that of all the treatments K_2CO_3 is the salt showing most promise for future treatment. The reasoning behind the success of K_2CO_3 is thought to be linked to the increase in the pH that the salt induced following treatment, which forced the clay surface to become negatively charged, which as a result of the positively charged nature of the K^+ ions in solution allowed for intercalation of the K_2CO_3 salt into the halloysite inter-layer space, resulting in an expansion of the basal size from 10.1\AA to 13.6\AA . We can state with confidence that salt was successfully taken up by the cores based upon the drop-in conductivity measured for the treatment solutions, showing that per 100 grams of clay approximately 138 mmol of salt were taken up.

7.3 Tri-axial data

The data that was collected on the soil cores being run through static tri-axial test produced a wide variety of results with distinctive features. When examining the baseline (no treatment) tri-axial data it can be observed that deviator stress at the point of failure was relatively low for all samples, ranging from 151 kPa for the sample at lowest confining pressure (205 kPa), to 313 kPa for the highest. When comparing this to the data collected in Mills' (2016) study, we can see that my results are noticeably lower across all 3 confining pressures compared with those

collected for similar confining pressures. As expected both pore pressure and axial strain pressures increased as tri-axial strain increased, with the degree of strain softening increasing similarly as well with increasing confining pressure. The point of failure as a percentage of axial strain though reduced as the confining pressure increased with strain at failure dropping from 1.63% to 1.53% and then 1.09% for the highest confining pressure.

Stress strain plots for these untreated samples, shown in in Chapter 5, show the progression of relatively gentle failure curves as the confining pressure increases on sample, with reduction of deviator stress following failure being minimal for the 205kPa confining pressure, and relatively small for 280 kPa confining pressure. The sample at highest confining pressure showed the greatest degree of deviator stress relief following failure(strain softening), with pressures dropping a significant amount (41%) following failure. It is also important to note that for the two pore pressure curves plotted on these stress strain plots, pore water pressure (PWP) peak occurred noticeably after the axial strain peak, with PWP for both samples still increasing even though the axial strain and deviator stress reduced following failure of the sample.

In contrast to this we can examine the results produced following treatment of the soil with the K_2CO_3 solute for 3-4 weeks. In this case it is noticeable that the axial strain at failure (q) is higher for all samples than that of the untreated samples measuring 343 kPa , 424 kPa and 386 kPa for the 3 confining pressures in increasing order respectively. It is worth noting that though axial strain peak increases between the lower and middle confining pressures, the highest confining pressure produces a peak deviator stress less than that of the middling treated confining pressure. In contrast to this we can observe an increase in PWP across the board, with PWP pressure peak increasing as confining pressure increases, with the highest PWP (170 kPa) measured for the highest confining pressure. Axial strain at point of failure increases as the confining pressure increases progressing from 0.78% for the lowest confining pressure to 1.11% for the highest confining pressure. Furthermore, the range of deviator stresses at point of deviator stress peak were far less varied than the baseline values only varying by 81kPa between highest and lowest confining pressures, compared to 162kPa for the untreated samples.

7.3.1 Comparison of Treated and Untreated

The treatments have had a pronounced positive effect on the soils during tri-axial testing producing increases in peak deviator stress of various magnitudes for each confining pressure. For the lowest confining pressure there was an increase in peak deviator stress of 227% between untreated and treated samples. It is worth noting that due to errors with the PWP sensor during testing the PWP at point of failure for the untreated 205kPa sample is inaccurate and thus has been discounted at this stage. For the intermediate confining pressure (280 kPa) a 187% increase in peak deviator stress was observed, while simultaneously observing a decrease of 87% in PWP at its peak. The highest confining pressure (355 kPa) had an increase of 124% for peak deviator stress and similarly and 87% decrease in peak PWP. Axial strain at failure for all treated samples was lower than for untreated counterparts for all but highest confining pressure were only minimal change of was observed at point of failure.

The data presented at this point all indicates that treatment of the sensitive soil has had a resoundingly positive effect on the soil itself and has comprehensively raised the peak shear strength of the soil by an average of 186% across the three confining pressures, while also accounting for an 87% reduction in PWP.

7.3.2 Shear Strength Increase

To accurately determine whether there has indeed been a shear strength increase it is important to examine both the peak stress values determined from tri-axial, as well as the cohesion and friction angles of the soil. Cohesion and friction angle together describe shear strength (Table 7.1). There are two values given for treated soils: one calculated for all measured values; and the second ('adjusted') discounting the results determined at highest confining pressure. This value has been reported due to the nature of failure in the final sample, as explained in Chapter 5. For the treated soils the sample at 355kPa confining pressure did not shear in a normal fashion and instead underwent a barrel/complex failure style, with no distinctive shear surface visible. This lack of a distinctive shear surface appears to have led to an anomalous result being produced for the peak deviator stress and hence a $>10^\circ$ reduction in friction angle.

Table 7.1. Effective stresses measured for both untreated and treated soils, measuring effective friction angle, and effective cohesion.

	Φ' (°)	C' (kPa)
Untreated Soil	19.3	26.6
Treated Soil		
Original	12.9	123.5
Adjusted	28.2	58.4

For the untreated soils, cohesion of 26.6 kPa, and a friction angle of 19.32° was measured, the friction angle is lower than that measured in Mills (2016) study but cohesion is almost identical (Φ' =31 and C'=26). When compared to Moon (2016) the friction angle is within the range for halloysite (Φ' =19-41 and C'=12-18). Comparison with adjusted values for treated samples shows an increase in effective cohesion, as well as an increase in effective friction angle, with Φ' increasing to 28.24° and c' to 58.40 kPa. This shows a general increase in strength of the soil in terms of both friction angle and cohesion. This indicates that the treatment we have applied has had a significant impact on the soil itself and has increased effective shear strength significantly.

How this occurs can be linked back to the factors examined in the earlier sections of this discussion with regards to the intercalation of K₂CO₃ into the halloysite crystal lattice itself, and the effect that the salt itself has on the basal spacing of the clay. Cohesion within soils can be linked to the degree of cementing within the soil. This is affected by how close and compacted the soil particles are with each other, with increasing cohesion indicating increased compaction within the soil and as result increased soil shear strength required to overcome the interparticle forces that hold the soil together (Kemper & Rosenau, 1984).

Within our soils we can see that the treatment of the soil has had a significant impact on the soil's cohesiveness, by increasing the soil effective cohesion 220%. This indicates that the soil is more comprehensively cemented, as such indicating that the soil particles are more stable and connected, and hence requiring more energy to break the interparticle forces. As indicated in the literature review the usage of K₂CO₃ in treating soil leads to an expansion of the basal spacing of the

halloysite clay from 10.1Å to 13.6Å (Garrett & Walker, 1959; Wada, 1965; Carr *et al.*, 1978).

This expansion causes a direct increase in cohesion as the sample is required to occupy the same space as previously, but must accommodate for the wide-scale increase in clay size. The drop in PWP can be potentially attributed to the pore spaces available following the basal space expansion after treatment with K_2CO_3 . As the basal space is increased, following treatment it allows for more accommodation of the fluctuating and increasing PWP as the deviator stress increases. Furthermore the introduction of treatment with the solute has increased the attractive forces present within the interparticle forces, having achieved this through increasing the level of primary valence bonding between the each halloysite crystal, as a result increases our cohesion as it increases the amount of energy required to break these chemical bonds (Mitchell, 1994).

This occurs as the water present within the basal space in the form of associated water is directly displaced by K_2CO_3 , as the hydrogen deficient hydroxyl group will preferentially form a temporary ionic bond with the K^+ ions present as opposed to the H^+ ions of the water present. As a result this water is displaced from the clay, which, forces an expansion of the clay basal space. As the axial strain increases on the soil, pore pressure slowly rises, in which we observe dilation of the sample before contraction at point of failure, this expansion of the basal space allows for the temporary accommodation of water into the clay basal space, of which is accommodated until point of failure before being forced out following failure.

7.3.3 Stress Paths

For the lowest confining pressure of the untreated samples a stress path could not be drawn as the PWP sensor failed, resulting in inaccurate and wildly incorrect results being produced for the sample at 205 kPa. When comparing the stress paths of both untreated and treated soils we can observe that the soils characteristically contracted and underwent shrinkage following failure. The degree of shrinkage and as to whether a soil will contract or dilate in consolidated clays is linked to consolidation ratios, effective confining pressures and void ratios. Mitchell and Soga (2003), laid out framework for clays undergoing shearing and how these clays at differing consolidation states will change their contraction and dilation as a result of pore pressure changes within the soil. Figure 7.6 details this,

depicting the change in pore water pressure as a soil progresses during shearing. The diagram indicates that for normally and slightly consolidated clays, similar to those we are dealing with in this study, soils will undergo significant positive pore water pressure changes during shearing, resulting in water being forced out of the sample as shearing continues. This positive change in PWP causes a reduction in volume of the sample when reaching its critical state, resulting in contraction of the soil, as indicated by a shift to the left on a stress path plot.

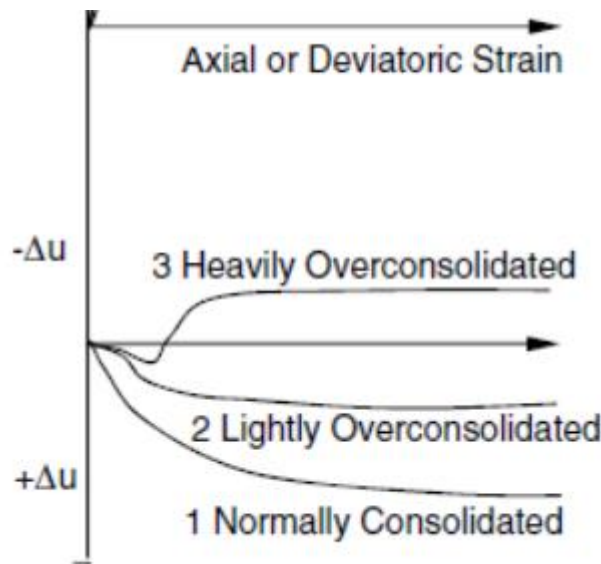


Figure 7.6. Sourced from Tan (2010), the figure above indicates whether pore pressures will become positive or negative under axial strain conditions for clays.

Of the samples tested, the treated samples were the only runs that appeared to adhere to a single critical state line as the confining pressures increased, with the degree of contraction changing as confining pressure increased. It is important to note that, untreated samples appeared to fail in a relatively ductile fashion, and underwent significant contraction before peak deviator stress was even reached for both intermediate and highest confining pressures (280 & 355 kPa).

In contrast, the treated samples tend to the right, in a more dilative fashion before reaching peak deviator stress and failing, before undergoing significant contraction. The treated sample at 355 kPa does not show this same trend, with contraction of the sample occurring prior to peak deviator stress. This difference can be attributed to the change in failure style, shifting from a brittle failure as occurring in the previous samples to a more ductile failure, as is observed in the barrel style failure of the sample described in chapter 5. This dilation of samples prior to failure further indicates that as the pore water pressure within the sample

increases as the sample is undergoing shearing, there is a degree of accommodation space present, with the pore water pressure causing an expansion in volume, before reaching a critical point at the critical state line and undergoing noticeable contraction to a state less than that of its starting size. The concept of which was further expanded in the previous sub section.

7.4 Failure Types, Thin Sections and SEM

When examining my soil cores, I observed the bulk of the soil cores experienced shear failure of some sort, with distinctive shear bands observed for all but the highest confining pressure for the treated sample. This formation of shear failure is expected, with previous studies indicating the link between clay content and the propensity for a soil to undergo a specific form of failure.

7.5 Thin Sections

The distributions of minerals within prepared thin sections were well defined, with minerals observed all consistent with those observed in rhyolitic tephra (Stoops, 2003). Furthermore, data gathered in this study show similarity to those seen in Mills (2016) study, with the largest difference being observed in the Manganese seen within the thin sections, with our study showing close to 5% manganese in treated, where in contrast Mills (2016) found that manganese was rare in the thin sections. This increase in manganese could be linked to the increase in pH of the soil following treatment, with manganese known to precipitate out of solution at pH's of 9 and higher (Aomine & Wada, 1962).

As indicated in chapter 5, for the 205 kPa treated thin section results were derived from the thin section running perpendicular to the thin section. This was since thin sections were less thick and allowed for clearer observation of minerals and fracturing features under optical light microscope. As anticipated across all confining pressures weathered quartz, and othered weathered minerals were observed. The degree of weathering for these minerals fits well with the proposed depositional status of the Pahoia tephra, with multiple studies indicating that the sensitive layer, targeted in this study, is made up of reworked tephra undergoing multiple changes in a potentially fluvial environment- leading to the degree of weathering we observe in the minerals in this study (Wyatt, 2009; Moon, 2016).

On numerous occasions across the thin sections, the propagation of fractures through minerals as opposed to the clay itself was observed across all confining pressures. When propagating within soil, shear fractures often fail along a band where pore water pressure has concentrated, generally causing fractures to pass through the softer material, along the path of least resistance (Gylland *et al.*, 2013; Gylland *et al.*, 2014). In this instance, the shear propagating through crystals is a fascinating point, as it indicates that the path of least resistance while the samples were undergoing shear was not the treated groundmass when reaching these crystals, but instead created pressure along specific points on minerals, with the pressure sufficient enough to cause fracturing of the crystals. The fact that the crystals, which in this instance were generally hypersthene and ilmenite, which all have a hardness well in excess of that of clay had shears propagate through indicates that the clay fabric around the crystals has a higher resistance to these shear fractions. Though these crystals do have relatively well-developed cleavage which could account for the propagation of failures through them

7.5.1 Riedel Shears

Within our thin section samples some riedel shears were observed. Mills (2016) predicted that for samples from Omokoroa, to determine the angle of R and R' shears, they would lie at an angle of $45^\circ \pm \Phi/2$. With this in mind, she predicted that angles of R' would be 61° and 29° for R, this based upon a friction angle of 31° . Treated samples in this study in contrast derived a Φ of 12° for unadjusted and 28° for adjusted results. Due to the formation of barrel failure in the highest confining pressure sample (355 kPa confining pressure), a friction angle of 28° was used to determine the angles of R and R'. By applying the equation for working out these shears we can determine that $R'=59^\circ$ and $R=31^\circ$. Within our samples we observe what are thought to be R' shears progressing at an angle of approximately 60° from the primary displacement discontinuity (PDS), and in some instances, we observe the propagation of R shears at differing times. As expected, R' shears present during certain forms of shearing, and propagate to eventually form the PDS. For the highest confining pressure, an R' shear presents at approximately 50° angling across the sample to the secondary shear running parallel to the PSZ. This angle differs as it accounts for the change in failure style of the highest confining pressure. When including this result in calculating friction angle for treated samples, the resultant

Φ is 12° , which when applied to the calculation for determining R' angles presents an R' that will propagate at 51° .

7.6 Scanning Electron Microscopy

Usage of Scanning Electron Microscope imagery allowed for further confirmations of mineral types present within the clay, allowing for confirmation and validation of the results presented in the mineral component abundances within the clay. SEM allowed for the identification of another mineral that was not observed during thin section examination, potentially due to its small size, and fractured nature. Furthermore, highly weathered salt crystals were observed propagated on the surface of the clay, much to the surprise of myself. Issues were indeed arisen as the discrepancy of what had infilled the fracture surface did present at times, with elemental point analysis and distribution analysis indicating a high carbon fraction present within the fracture zones, further research and conference with SEM technicians indicated that this high carbon response was most likely a result of the resin utilised during creation of the shear samples, resulting in an excessive response of carbon when undergoing elemental analysis.

Direct analysis and observation of the shears themselves was possible as magnification of the shear zones was attained on a number of occasions. An example of this is figure 6.7. In the figure, the border between an infilled shear fracture and clay groundmass is present. When magnified to 710x magnification, the infilling of the shear fracture can be observed in a high quality. Within this shear zone multiple portions make up the somewhat chaotic and disordered fracture zone. Large pieces of volcanic glass are present within the clay groundmass, with an alignment of the material appearing to occur.

As illustrated in the figure smaller shear fractures that have propagated even through the larger shear fracture are highlighted causing an ordering and alignment of minerals along a variety of directions, which, once highlighted becomes highly evident. This alignment of clay minerals and volcanic glass during failure is a trait that has been theorised and observed in failures of illitic northern hemisphere clays, though not in halloysite rich clays (Gylland *et al.*, 2013; Gylland *et al.*, 2014; Torrance, 2014). Elemental analysis of the shear zone provided further unexpected results. Results of aluminium, silicon and potassium through the shear zone was expected as these make up the key components of the treated halloysite and volcanic glass that can be observed throughout the shear zone. The key divergence from our

elemental analysis was a concentration of calcium detected near the top of the selected area of the thin section.

This calcium concentration was an unexpected occurrence, with it naturally at low concentrations within the soil, any Ca in the system, due to the incredibly high volume of K^+ ions that would have been present in solution during treatment would have displaced the Ca present within the soil, resulting in a deficiency on Ca. The excess of Ca observed could potentially be explained by the dissolution of volcanic glass within the shear zone. As the pwp increases, and focuses along the shear surface, causing localised spikes in pressure (Locat *et al.*, 2011; Gylland *et al.*, 2013; Gylland *et al.*, 2014).

The localised spike in pore water pressure, as well as the high deviator and confining stresses resulted in the dissolution of some of the weakest and most weathered volcanic glass. Silicates, when faced with high pressure solutions (pore water in this instance) as well as high external pressures show a tendency to dissolve into solution, which, in the case of volcanic glass, results in the accelerated breakdown of the mineral components, producing an excess in calcium we observe on the surface (Correns, 1949). With this said the reality of this occurring within the real world are not known as literature is not extensive on the subject, with further research into this subject required.

CHAPTER 8

Conclusion

Landslides in the Bay of Plenty region are widespread and numerous, with the source of these failures often grounded in the presence of a sensitive soil of some kind that fails under high pore water pressures and leads to large retrogressive landslides. These sensitive soils are generally sourced from rhyolitic tephra falls, which has led to them becoming rich in halloysite clays. Based upon the work of Moum *et al* (1970), methods have been adapted to see if the application of a potassium based salt to a particular halloysite rich sensitive soil will increase the shear strength to an effective level to mitigate against landsliding.

Treatment of sensitive soil from the landslide at Bramley Drive, Omokoroa, with a variety of salts provided a wealth of data on the interaction of a halloysite rich clay soil and salt solutions. During the course of this study it was observed that both KCl and KOH salt solutions have a net negative rheological effect on the strength of the sensitive soil paste, producing a reduced liquid limit in both instances and a more dispersive paste overall. In contrast to this, treatment with K_2CO_3 results in an improvement (increased PI) in the behaviour of the soil paste.

K_2CO_3 treatment was then applied to intact halloysite rich soil cores taken from the base of the landslide at Bramley Drive. Tri-axial testing indicates a significant increase in shear strength following treatment of the soil, with increases in shear strength ranging between 227% and 124%. On top of an increase in shear strength, treatment has a pronounced effect on pore water pressure development within the soil exhibited a drop of 80%, with stress strain curves indicating dilation of treated samples prior to failure. This implies that the treated soil cores have in some fashion accommodated the increasing pore water pressures as axial strain increased, before failing and undergoing contraction.

Accommodation of pore water pressure is thought to be achieved in a number of ways. The application of K_2CO_3 to the soil produces an increase in soil pH following application of the salt solution. This shift of pH to more alkaline, results in the halloysite clay surface becoming increasingly negatively charged, promoting intercalation of the K_2CO_3 salt into the halloysite basal space. Temporary ionic bonds form between the hydron deficient hydroxyl groups and positively charged potassium ions (K^+) ionically bonded to the carbonate ion,

allowing for the formation of a stable intercalation of the K_2CO_3 ions into the clay basal space. In literature, this process is inferred to expand the halloysite basal space from 10.1Å to 13.6Å.

As such I hypothesise that as the K_2CO_3 salt intercalates into the halloysite basal space, it displaces a water molecule from the halloysite basal space into solution, and as a result forces the clay to expand. This forced expansion occurs following treatment means the clay expands within the soil body, eliminating pore space, leading to an increased cohesion and friction angle of the clay. This in turn increases the surface area the clay particles have to interact with one another, which, as a result increases the energy requirement for overcoming the resistance the clay interparticle friction imparts as a result of the increased cohesion, and decrease in pore space. Furthermore, this expansion and displacement of water leaves 'empty' space in the halloysite basal space, meaning that as pore pressure rises prior to failure, the clay can accommodate some of this pore pressure increase by taking up the water into the basal space, appearing as dilation on the p' q' stress path plot.

Analysis of shear surfaces indicated discrete shear failures developed for samples while under tri-axial strain. These observations of discrete shear failure support the work conducted by Mills (2016) and Briaud (2014) of localisation of shear bands during stress application to a soil body, with grain re-alignment and consequent locally excessive high pore pressures leading to enhanced fracture progression. The reduced pore pressures observed in treated soils as a result of the clay expansion is a key determinant in the increased effective strength I see in the treated clay. SEM imaging indicated further that the treatment of the soil with K_2CO_3 in some instances leads to potassium rich clays binding together to form larger clay aggregates, which may have a direct influence on the clay strength as bonding of the treated clays occurs on a scale much larger than initially believed.

The successful application of this salt in increasing the undisturbed peak shear strength of a halloysite rich soil as exhibited during the course of this study may have widescale implications in stabilisation of halloysite rich sensitive soil landslides both here in New Zealand and on a global scale.

The research conducted in this study produced a number of fascinating results and opened a number of avenues of further research that could potentially be conducted. This study has shown that though treatment of halloysite from the Pahoia Tephra from Bramley Drive in Omokoroa with K_2CO_3 does not effectively increase the liquid limit, treatment of the undisturbed soil cores increases the

effective strength of the soil by significant margins. Though the methods and forms of salt used in this study deviated from those used by Moum *et al* (1970) in their study, the successful nature of treatment in this study opens a number of avenues for potential application to the sensitive soils found both within the Omokoroa Peninsula and halloysite rich sensitive soils on a global scale. Some recommended key factors for further research include:

1. Examining the interface between the lower Pahoia tephra and ignimbrite to examine how the two differing soil layers interact when under differing confining pressures and situations through bi axial and tri axial testing. The interaction between the two layers is not well understood. By gaining an understanding of how these two layers interact under potential land sliding conditions it poses the potential to allow for an effective remedial treatment to be better applied.
2. Examination of whether K_2CO_3 effectively intercalates into the halloysite crystal lattice following treatment via methodologies outlined in this thesis. This could be achieved through X-ray Diffraction, ICP-MS or infra-red spectroscopy methods. By applying these methods, an effective hypothesis and understanding could be developed to give a greater understanding of how K_2CO_3 interacts with the clay.
3. Further testing of soil of a similar nature from Bramley Drive or the Omokoroa Peninsula that shows sensitivity. Due to active landsliding and the inability to collect further specimens, the triaxial test programme planned for this research had to be curtailed. Further testing under a range of treatments and stress conditions is required to confirm the observations made in this study. This will add credence to the potential application of the methodologies used in this study on a larger scale to prevent further failures occurring in the soils of the Omokoroa Peninsula.

References

- Alexander, L., Faust, G., Hendricks, S., Insley, H., & McMurdie, H. (1943). Relationship of the clay minerals halloysite and endellite. *American Mineralogist*, 28(1), 1-18.
- Aomine, S., & Wada, K. (1962). Differential weathering of volcanic ash and pumice, resulting in formation of hydrated halloysite. *American mineralogist*, 47, 1024-1048.
- Bailey, S. (1990). Halloysite-a critical assessment. *Sciences Geologiques-Memoires*, 86, 89-98.
- Bernander, S. (2011). *Progressive landslides in long natural slopes: formation, potential extension and configuration of finished slides in strain-softening soils*. thesis, Luleå tekniska universitet.
- Berthier, P. (1826). Analyse de l'halloysite. *Ann. Chim. Phys*, 32, 332-335.
- Boettinger, J., & Graham, R. (1995). Zeolite occurrence in soil environments: An updated review. *Natural zeolites*, 93, 23-37.
- Boulangier, R. W., & Idriss, I. (2006). Liquefaction susceptibility criteria for silts and clays. *Journal of geotechnical and geoenvironmental engineering*, 132(11), 1413-1426.
- Bradfield, R. (1923). The nature of the acidity of the colloidal clay of acid soils. *Journal of the American Chemical Society*, 45(11), 2669-2678.
- Briaud, J.-L. (2013). *Geotechnical engineering: unsaturated and saturated soils*. John Wiley & Sons.
- Bridley, G. (1961). Kaolin, serpentine, and kindred minerals. *X-ray Identification and Crystal Structures of Clay Minerals*. Mineralogical Society of London, 51-131.
- Carr, R., Chaikum, N., & Patterson, N. (1978). Intercalation of salts in halloysite. *Clays Clay Miner*, 26(2), 144-152.
- Chadwick, O. A., Gavenda, R. T., Kelly, E. F., Ziegler, K., Olson, C. G., Elliott, W. C., & Hendricks, D. M. (2003). The impact of climate on the biogeochemical functioning of volcanic soils. *Chemical Geology*, 202(3), 195-223.
- Chapman, H. (1965). Cation-exchange capacity. *Methods of soil analysis. Part 2. Chemical and microbiological properties(methodsofsoilanb)*, 891-901.
- Chorover, J., DiChiaro, M. J., & Chadwick, O. A. (1999). Structural charge and cesium retention in a chronosequence of tephritic soils. *Soil Science Society of America Journal*, 63(1), 169-177.

- Churchman, G. (1973). Dehydration of the washed potassium acetate complex of halloysite. *Clays and Clay Minerals*, 21, 423-424.
- Churchman, G. (2000). The alteration and formation of soil minerals by weathering. *Handbook of soil science*, 3-76.
- Churchman, G., & Carr, R. (1975). The definition and nomenclature of halloysites. *Clays and Clay Minerals*, 23(5), 382-388.
- Churchman, G., Davy, T., Aylmore, L., Gilkes, R., & Self, P. (1995). Characteristics of fine pores in some halloysites. *Clay Minerals*, 30(2), 89-98.
- Correns, C. W. (1949). Growth and dissolution of crystals under linear pressure. *Discussions of the Faraday society*, 5, 267-271.
- Cruden, D. M., & Varnes, D. J. (1996). Landslides: investigation and mitigation. Chapter 3-Landslide types and processes. *Transportation research board special report*(247).
- Cunningham, M. J. (2012). *Sensitive rhyolitic pyroclastic deposits in the Tauranga region: mineralogy, geomechanics and microstructure of peak and remoulded states*. Masters thesis, University of Waikato, Hamilton, New Zealand.
- De Rosa, J., Pontolillo, D. M., Di Maio, C., & Vassallo, R. (2016). Chemical Clay Soil Improvement: From Laboratory to Field Test. *Procedia Engineering*, 158, 284-289.
- Douglas, M. (1947). The nomenclature of the halloysite minerals. *Mineralogical Magazine*, 28(196), 36-44.
- Garrett, W., & Walker, G. (1959). The cation-exchange capacity of hydrated halloysite and the formation of halloysite-salt complexes. *Clay Minerals*, 4(22), 75-80.
- Giese, R. (1988). Kaolin minerals; structures and stabilities. *Reviews in Mineralogy and Geochemistry*, 19(1), 29-66.
- Grim, R. E. (1968). Clay mineralogy. International series in the earth and planetary sciences. *McGraw-Hill, New York*.
- Gulliver, C., & Houghton, B. (1980). *Omokoroa Point land stability investigation*. Tonkin & Taylor.
- Gylland, A. S., Jostad, H. P., & Nordal, S. (2014). Experimental study of strain localization in sensitive clays. *Acta Geotechnica*, 9(2), 227-240.
- Gylland, A. S., Rueslåtten, H., Jostad, H. P., & Nordal, S. (2013). Microstructural observations of shear zones in sensitive clay. *Engineering Geology*, 163, 75-88.

- Harrison, J. L., & Greenberg, S. S. (1962) Dehydration of fully hydrated halloysite from Lawrence County, Indiana. In *9th National Conference on Clays and Clay Minerals* (pp. 374-377): Citeseer.
- Harvey, C. C. (1997). Exploration and assessment of kaolin clays formed from acid volcanic rocks on the Coromandel Peninsula, North Island, New Zealand. *Applied clay science*, 11(5), 381-392.
- Harvey, C. C., & Murray, H. H. (1990). GEOLOGY, MINERALOGY AND EXPLOITATION OF HALLOYSITE CLAYS OF NORTHLAND, NEW ZEALAND. *Clay Miner. Soc. Spec. Pub.*(1), 233-248.
- Hatrack, A., Howarth, A., Galloway, J., & Ramsay, G. (1982). Report of Committee to Inquire into the Failure of the Ruahihi Canal. *Ministry of Works and Development, Wellington, New Zealand*.
- Helle, T. E., Aagaard, P., & Nordal, S. (2017). In Situ Improvement of Highly Sensitive Clays by Potassium Chloride Migration. *Journal of Geotechnical and Geoenvironmental Engineering*, 143(10), 04017074.
- Helle, T. E., Nordal, S., Aagaard, P., & Lied, O. K. (2015). Long-term effect of potassium chloride treatment on improving the soil behavior of highly sensitive clay—Ulvensplitten, Norway. *Canadian Geotechnical Journal*, 53(3), 410-422.
- Hughes, I. (1966). *Mineral changes of halloysite on drying*. New Zealand Pottery and Ceramics Research Association.
- Hvorslev, M. J. (1961). *Physical components of the shear strength of saturated clays*. Army Engineer Waterways Experiment Station Vicksburg Ms.
- Jacquet, D. (1990). Sensitivity to remoulding of some volcanic ash soils in New Zealand. *Engineering Geology*, 28(1-2), 1-25.
- Joussein, E., Petit, S., Churchman, J., Theng, B., Righi, D., & Delvaux, B. (2005). Halloysite clay minerals—a review. *Clay minerals*, 40(4), 383-426.
- Keam, M. J. (2008). *Engineering geology and mass movement on the Omokoroa Peninsula, Bay of Plenty, New Zealand*. thesis, University of Auckland.
- Kemper, W., & Rosenau, R. (1984). Soil cohesion as affected by time and water content. *Soil Science Society of America Journal*, 48(5), 1001-1006.
- Kirkman, J., H. (1977). Possible structure of halloysite disks and cylinders observed in some New Zealand rhyolitic tephtras. *Clay Minerals*, 12, 199.
- Kluger, M. O., Moon, V. G., Kreiter, S., Lowe, D. J., Churchman, G. J., Hepp, D. A., Seibel, D., Jorat, M. E., & Mörz, T. (2017). A new attraction-detachment model for explaining flow sliding in clay-rich tephtras. *Geology*, 45(2), 131-134.

- Lessard, G., & Mitchell, J. K. (1985). The causes and effects of aging in quick clays. *Canadian Geotechnical Journal*, 22(3), 335-346.
- Locat, A., Leroueil, S., Bernander, S., Demers, D., Jostad, H. P., & Ouehb, L. (2011). Progressive failures in eastern Canadian and Scandinavian sensitive clays. *Canadian Geotechnical Journal*, 48(11), 1696-1712.
- Locat, J., Berube, M.-A., & Choquette, M. (1990). Laboratory investigations on the lime stabilization of sensitive clays: shear strength development. *Canadian Geotechnical Journal*, 27(3), 294-304.
- Locat, J., & St-Gelais, D. (2014). Nature of Sensitive Clays from Québec. In *Landslides in Sensitive Clays* (pp. 25-37). Springer.
- Lowe, D. J., & Churchman, G. J. (2016). Tales of the unexpected: halloysite delivers surprises and a paradox.
- Manderson, T. P. (2017). *Causes of diurnal ground movements at Omokoroa, New Zealand*. thesis, University of Waikato.
- Marshall, C., & Krinbill, C. (1942). The Clays as Colloidal Electrolytes. *The Journal of Physical Chemistry*, 46(9), 1077-1090.
- McCraw, J. (1967). The surface features and soil pattern of the Hamilton Basin.
- Mehmel, M. (1935). Ueber die struktur von halloysit und metahalloysit. *Zeitschrift für Kristallographie-Crystalline Materials*, 90(1-6), 35-43.
- Mills, P. (2016). *Failure mechanisms in sensitive volcanic soils in the Tauranga Region, New Zealand*. thesis, University of Waikato.
- Mitchell, J. K. (1994). Fundamentals of soil behaviour. *Soil Use Management*, 10(2), 94.
- Moon, V. (2016). Halloysite behaving badly: geomechanics and slope behaviour of halloysite-rich soils. *Clay Minerals*, 51(3), 517-528.
- Moon, V. G. (2017). Unpublished
- Moon, V. G., Cunningham, M. J., Wyatt, J. B., Lowe, D. J., Morz, T., & Jorat, M. (2013). Landslides in sensitive soils, Tauranga, New Zealand.
- Moon, V. G., de Lange, W. P., Garae, C., Morz, T., Jorat, M., & Kreiter, S. (2015) Monitoring the landslide at Bramley Drive, Tauranga, NZ. In *12th Australia New Zealand Conference on Geomechanics: ANZ 2015 Changing the Face of the Earth-Geomechanics and Human Influence*.
- Morgenstern, N., & Tchalenko, J. (1967). Microscopic structures in kaolin subjected to direct shear.
- Moum, J., Sopp, O., & Loken, T. (1970). Stabilization of undisturbed quick clay by salt wells. *Norwegian Geotechnical Institute Publ.*

- Nagasawa, K., & Miyazaki, S. (1975) Mineralogical properties of halloysite as related to its genesis. In *Proceedings of the International Clay Conference* (pp. 257-265).
- Ndayiragije, S., & Delvaux, B. (2004). Selective sorption of potassium in a weathering sequence of volcanic ash soils from Guadeloupe, French West Indies. *Catena*, 56(1), 185-198.
- Nielsen, D., Biggar, J., & Erh, K. (1973). Spatial variability of field-measured soil-water properties. *California Agriculture*, 42(7), 215-259.
- Noro, H. (1986). Hexagonal platy halloysite in an altered tuff bed, Komaki city, Aichi prefecture, Central Japan. *Clay Minerals*, 21(3), 401-415.
- Norrish, K. (1995) An unusual fibrous halloysite. In *Clays Controlling the Environment. Proceedings of the 10 th International Clay Conference* (pp. 275-284): CSIRO Publishing, Melbourne, Australia.
- Packham, R. (1965). Some studies of the coagulation of dispersed clays with hydrolyzing salts. *Journal of Colloid Science*, 20(1), 81-92.
- Panda, A. K., Mishra, B. G., Mishra, D. K., & Singh, R. K. (2010). Effect of sulphuric acid treatment on the physico-chemical characteristics of kaolin clay. *Colloids and Surfaces A: Physicochemical and Engineering Aspects*, 363(1), 98-104.
- Parfitt, R. (1990). Allophane in New Zealand-a review. *Soil Research*, 28(3), 343-360.
- Phoon, K.-K., & Kulhawy, F. H. (1999). Characterization of geotechnical variability. *Canadian Geotechnical Journal*, 36(4), 612-624.
- Quantin, P., Gautheyrou, J., & Lorenzoni, P. (1988). Halloysite formation through in situ weathering of volcanic glass from trachytic pumices, Vico's volcano, Italy. *Clay Minerals*, 23(4), 423-37.
- Quinn, P., Hutchinson, D., Diederichs, M., & Rowe, R. (2011). Characteristics of large landslides in sensitive clay in relation to susceptibility, hazard, and risk. *Canadian Geotechnical Journal*, 48(8), 1212-1232.
- Riviere, A. (1948). On the base exchange capacity of halloysites: Summary in. *Clay Miner. Bull*, 1, 121.
- Robertson, I. D., & Eggleton, R. A. (1991). Weathering of granitic muscovite to kaolinite and halloysite and of plagioclase-derived kaolinite to halloysite. *Clays and Clay Minerals*, 39(2), 113-126.
- Robertson, R., Brindley, G., & Mackenzie, R. (1954). Mineralogy of kaolin clays from Pugu, Tanganyika. *American Mineralogist*, 39(1-2), 118-138.
- Rochelle, P. L., Leroueil, S., & Tavenas, F. (1986a). The causes and effects of aging in quick clays: Discussion. *Canadian Geotechnical Journal*, 23(3), 407-408.

- Rochelle, P. L., Leroueil, S., & Tavenas, F. (1986b). A technique for long-term storage of clay samples. *Canadian Geotechnical Journal*, 23(4), 602-605.
- Rosenqvist, I. T. (1953). Considerations on the sensitivity of Norwegian quick-clays. *Geotechnique*, 3(5), 195-200.
- Rosenqvist, I. T. (1977) A general theory for quick clay properties. In *Proc. Third European Clay Conference, Oslo* (pp. 215-228).
- Selby, M. (1993). Rock-slope processes. *Hillslope Material and Processes*, 320-355.
- Selby, M. J. (1982). Hillslope materials and processes. *Hillslope materials and processes*.
- Skempton, A. (1964). Long-term stability of clay slopes. *Geotechnique*, 14(2), 77-102.
- Skempton, A. (1966) Some observations on tectonic shear zones. In *1st ISRM Congress: International Society for Rock Mechanics*.
- Skempton, A. W., & Northey, R. D. (1952). The sensitivity of clays. *Geotechnique*, 3(1), 30-53.
- Smalley, I., Ross, C. W., & Whitton, J. (1980). Clays from New Zealand support the inactive particle theory of soil sensitivity. *Nature*, 288(5791), 576-577.
- Stoops, G. (2003). *Guidelines for analysis and description of soil and regolith thin sections*. Soil Science Society of America Inc.
- Sudo, T. (1953). Particle shape of a certain clay of hydrated halloysite, as revealed by the electron microscope. *Mineralogical Journal*, 1(1), 66-68_1.
- Suttcliffe, J. M., Fessler, R. R., Boyd, W. K., & Parkins, R. N. (1972). Stress Corrosion Cracking of Carbon Steel in Carbonate Solutions. *CORROSION*, 28(8), 313-320.
- Tan, K., & Bartlett, R. J. (1994). Principles of soil Chemistry. *Soil Science*, 157(5), 330.
- Tan, K. H. (2010). *Principles of soil chemistry*. CRC press.
- Tavenas, F. (1984) Landslides in Canadian sensitive clays—a state-of-the-art. In *Proceedings of the 4th International Symposium on Landslides, Toronto, Ont* (pp. 16-21).
- Tavenas, F., Chagnon, J.-Y., & Rochelle, P. L. (1971). The Saint-Jean-Vianney landslide: observations and eyewitnesses accounts. *Canadian Geotechnical Journal*, 8(3), 463-478.
- Taylor, T. a. (1980). *Omokora Point Land stability Investigation*. Report Prepared by Tonkin & Taylor for Tauranga County Council (n.z). Tauranga 54p.

- Taylor, T. a. (2011). *Bramley Drive Landslip Hazard Assessment*. Tauranga. 18p.
- Tazaki, K. (1979). Micromorphology of halloysite produced by weathering of plagioclase in volcanic ash. *Developments in Sedimentology*, 27, 415-422.
- Terzaghi, K. (1944). *Ends and means in soil mechanics*. Harvard University.
- Thakur, V. (2007). Strain localization in sensitive soft clays. *NTNU, Trondheim*.
- Thakur, V., Degago, S., Oset, F., Aabøe, R., Dolva, B., Aunaas, K., Nyheim, T., Lyche, E., Jensen, O., & Sæter, M. (2014). Characterization of post-failure movements of landslides in soft sensitive clays. In *Landslides in Sensitive Clays* (pp. 91-103). Springer.
- Theng, B., & Wells, N. (1995). The flow characteristics of halloysite suspensions. *Clay Minerals*, 30(2), 99-106.
- Torrance, J. K. (1983). Towards a general model of quick clay development. *Sedimentology*, 30(4), 547-555.
- Torrance, J. K. (1992). Discussion on sensitivity to remoulding of some volcanic ash soils in New Zealand, by D. Jacquet. *Engineering Geology*, 32(1-2), 101-105.
- Torrance, J. K. (2014). Chemistry, sensitivity and quick-clay landslide amelioration. In *Landslides in Sensitive Clays* (pp. 15-24). Springer.
- Wada, K. (1959). Oriented penetration of ionic compounds between the silicate layers of halloysite. *American Mineralogist*, 44(1-2), 153-165.
- Wada, K. (1965). Intercalation of water in kaolin minerals. *The American mineralogist*, 50(7-8), 924-941.
- Wesley, L. (1973). Some basic engineering properties of halloysite and allophane clays in Java, Indonesia. *Geotechnique*, 23(4), 471-494.
- White, R. E. (2013). *Principles and practice of soil science: the soil as a natural resource*. John Wiley & Sons.
- Wyatt, J. B. (2009). *Sensitivity and clay mineralogy of weathered tephra-derived soil materials in the Tauranga region*. Masters thesis, University of Waikato, Hamilton, New Zealand.